Pump Two-Phase Performance Program
Volume 4: Comparison of Steady-State Versus Transient Test Results

---

NP-1556, Volume 4
Research Project 301

Final Report, September 1980

Work Performed by

COMBUSTION ENGINEERING, INC.
C-E Power Systems
1000 Prospect Hill Road
Windsor, Connecticut 06095

Authors
W. G. Kennedy
M. C. Jacob
J. C. Whitehouse
J. D. Fishburn
G. J. Kanupka

Project Manager
D. F. Streinz

Prepared for

Electric Power Research Institute
3412 Hillview Avenue
Palo Alto, California 94304

EPRI Project Manager
K. A. Nilsson

Water Reactor System Technology Program
Nuclear Power Division

DISTRIBUTION OF THIS DOCUMENT IS UNLIMITED

DISCLAIMER

This report was prepared as an account of work sponsored by an agency of the United States Government. Neither the United States Government nor any agency thereof, nor any of their employees, makes any warranty, express or implied, or assumes any legal liability or responsibility for the accuracy, completeness, or usefulness of any information, apparatus, product, or process disclosed, or represents that its use would not infringe privately owned rights. Reference herein to any specific commercial product, process, or service by trade name, trademark, manufacturer, or otherwise does not necessarily constitute or imply its endorsement, recommendation, or favoring by the United States Government or any agency thereof. The views and opinions of authors expressed herein do not necessarily state or reflect those of the United States Government or any agency thereof.

DISCLAIMER

Portions of this document may be illegible in electronic image products. Images are produced from the best available original document.

ORDERING INFORMATION

Requests for copies of this report should be directed to Research Reports Center (RRC), Box 50490, Palo Alto, CA 94303, (415) 965-4081. There is no charge for reports requested by EPRI member utilities and affiliates, contributing nonmembers, U.S. utility associations, U.S. government agencies (federal, state, and local), media, and foreign organizations with which EPRI has an information exchange agreement. On request, RRC will send a catalog of EPRI reports.

Copyright © 1980 Electric Power Research Institute, Inc.

EPRI authorizes the reproduction and distribution of all or any portion of this report and the preparation of any derivative work based on this report, in each case on the condition that any such reproduction, distribution, and preparation shall acknowledge this report and EPRI as the source.

NOTICE

This report was prepared by the organization(s) named below as an account of work sponsored by the Electric Power Research Institute, Inc. (EPRI). Neither EPRI, members of EPRI, the organization(s) named below, nor any person acting on their behalf: (a) makes any warranty or representation, express or implied, with respect to the accuracy, completeness, or usefulness of the information contained in this report, or that the use of any information, apparatus, method, or process disclosed in this report may not infringe privately owned rights; or (b) assumes any liabilities with respect to the use of, or for damages resulting from the use of, any information, apparatus, method, or process disclosed in this report.

Prepared by
Combustion Engineering, Inc.
Windsor, Connecticut

EPRI PERSPECTIVE

PROJECT DESCRIPTION

This final report under RP301 documents the findings of an experimental research effort to develop a data base on reactor coolant pump single- and two-phase performance behavior. Tests were performed on a geometrically scaled model of an actual reactor coolant pump. Both steady-state and transient blowdown tests were performed over sufficiently large ranges of thermal-hydraulic operating conditions and typical pump performance parameters to cover calculated hypothetical loss-of-coolant accident (LOCA) conditions.

PROJECT OBJECTIVES

Current analytic pump models used in LOCA analyses are based on a limited amount of experimental data. The goals of this project were (1) to establish a sufficiently large data base of steady-state and transient pump performance data to substantiate, and ultimately improve, analytic pump models currently used for reactor coolant pump LOCA analysis; and (2) to obtain data on pump characteristics under two-phase transient blowdown conditions to aid the evaluation of reactor coolant pump overspeed.

PROJECT RESULTS

The pump data base collected in this project is considered sufficiently large and diverse to cover a significant range of pump performance of primary importance to LOCA analysis. Initial evaluation of the test results indicates that pump rated head and torque degrade significantly under two-phase flow conditions. Pump free-wheeling speed (pump motor power off) is closely coupled to the volumetric flow rate through the pump during a blowdown transient. The maximum free-wheeling speed observed was near twice the rated speed for a discharge break equal to the flow area of the pump. For smaller size discharge breaks, the peak speed observed was less than twice the rated speed. With electric power to the pump drive motor on throughout the blowdown, however, the pump speed was maintained at an almost constant value.

Additional reduction and analysis of this data base is required before it can be used to support the development of an improved analytic model for pump two-phase performance.

This final report consists of eight volumes, as presented in the table of contents in the first volume. Volumes 1, 2, 3, 4, and 7 present the results and conclusions, as well as substantial discussion and description, of the entire project and the test data. Volumes 5 and 6 present the tabulated test data in computer printout and graphic format, which will be useful for further analyses. Volume 8 contains a description of the data processing methods. Volumes 2 through 8 are available from the Research Reports Center* upon request.

Kjell A. Nilsson, Project Manager
Nuclear Power Division

---

*Research Reports Center
P.O. Box 50490
Palo Alto, CA 94303
(415) 965-4081

ABSTRACT

The primary objective of the C-E/EPRI Pump Two-Phase Performance Program was to obtain sufficient steady-state and transient two-phase empirical data to substantiate and ultimately improve the reactor coolant pump analytical model currently used for LOCA analysis. A one-fifth scale pump, which geometrically models a reactor coolant pump, was tested in steady-state runs with single- and two-phase mixtures of water and steam over ranges of operating conditions representative of postulated loss-of-coolant accidents. Transient tests were also run to evaluate the applicability of the steady-state-based calculational models to transient conditions.

This project has produced test data which can appropriately be utilized for reactor coolant pump modeling in LOCA analyses. The steady-state test data show general coherence of the test results and overall pump performance trends for a model pump that should be representative of a reactor coolant pump to the extent that scaling laws apply. Both head and torque data correlate well in the form of homologous curves. Two-phase head degradation curves are approximately comparable to head degradation curves obtained in other test programs. Two-phase torque degradation curves have also been developed. The collected data should be useful for analytical model development.

Volume IV: Comparison of Steady-State vs
Transient Test Results

CONTENTS

ILLUSTRATIONS

ILLUSTRATIONS (Cont'd.)

ILLUSTRATIONS (Cont'd.)

ILLUSTRATIONS (Cont'd.)

TABLES

Section 1

PURPOSE AND METHOD OF COMPARING STEADY-STATE AND TRANSIENT PERFORMANCE

Analytical models incorporating currently available pump test data are used to calculate pump performance in transient flow situations occurring during NSSS LOCA's. Existing pump calculation models assume quasi-equilibrium conditions and use steady-state formulations with no time derivative terms except for angular accelerations, $d\omega/dt$, which is set up as a dependent variable applied for calculating speed changes. Also, the input performance data for these calculational models is generally taken from steady-state pump tests.

Pump performance is generally described in terms of pump head and hydraulic torque for a given set of operating conditions, i.e., speed, volumetric flow rate, pressure level, fluid density and void fraction. The question of whether the pump performance is the same no matter if these operating conditions occur in steady-state or in the course of a transient is addressed in this report. It is important that the transient tests covered a span of break sizes producing a range of transient rates comparable to the range encountered in LOCA analysis. It was not intended or practicable, however, to have the transient tests duplicate whole time-histories of NSSS LOCA blowdowns. The geometry and blowdown flow characteristics of the test loop, outside of the test section at the pump, were different than for an NSSS. Also, it was not attempted to define the detailed hydraulic characteristics of the loop by test measurements.

What is most significant in checking the test results is to see whether the steady-state data which was obtained for incorporation into and use by the calculational models predicts the same performance as measured during a transient test for a given set of operating conditions even when those conditions were varying rapidly in the transient test.

Thus, the method employed here to compare steady-state and transient performance data consists of the following steps:

1. Select sets of operating conditions of interest which occured at various times during the test blowdowns.

2. For each of these times, list the pump speed, volumetric flow rate, suction pressure, density and void fraction determined from the transient measurements.

3. List the associated transient pump heads and torques.

4. For the same sets of operating conditions, determine what pump heads and torques are indicated by the steady-state test data. The part of the operating range in which a particular comparison falls may have been covered directly by steady-state tests in the same range, or the steady-state input may be derived by scaling from other operating conditions through the use of flow similarity relationships such as the homologous ratios which have been discussed in Volume II, Section 5.1.

5. Compare the resulting steady-state and transient heads and torques. Compare any differences with accuracy requirements and measurement uncertainties. If significant differences are found see whether they correlate with severity of the transients as indicated by $d\alpha_F/dt$ or other rates of change of conditions.

Items 3 and 4 constitute transient performance "snapshots" as detailed in Section 2.

It should be mentioned that the methods used and evaluations performed in this project are preliminary. Many different approaches can be taken, and these data can be analyzed in much more detail than the scope of this project allows.

Section 2

COMPARISON OF SAMPLES

Two sample blowdowns producing a range of operating conditions of interest to LOCA analysis and for comparison with steady-state performance data were Tests 1319 and 1351. As described in Volume III, both Test 1319 and Test 1351 were forward flow blowdowns with full-sized (6 inch diameter) breaks. For Test 1319 the rotor was allowed to free-wheel with the pump motor power off during the test. For Test 1351 the pump power was not turned off during the transient thereby maintaining the pump speed at a relatively constant value for this test. Both tests produced good ranges of operating conditions, significant transient rates, and flow conditions favoring interpretation of transient flow measurements. Since Test 1319 was a free-wheeling blowdown, the pump speed varied in a manner similar to the volumetric flow rate. As a result, a smaller range for the homologous flow-to-speed ratio ν/α_N was obtained for this test in comparison to the ν/α_N-range for Test 1351, during which the pump speed was held constant at a speed ratio, $\alpha_N = 0.75$.

Snapshots of the transient pump conditions were extracted from the Test 1351 data as follows. Figure 2-1 shows the smooth curve of suction leg void fraction vs time drawn manually through the machine-plotted gamma densitometer data shown in Figure 2-2. The void fractions selected for making comparisons of transient and steady-state performance are marked in Figure 2-1. The corresponding times are also indicated. These same times are marked on smooth curves drawn through data for the other operating conditions as shown in Figures 2-3 to 2-16. The values of the various operating parameters, as read from the smoothed curves at the designated times, are listed in Table 2-1. Data for the pump head and hydraulic torque were treated in the same fashion, as shown in Figures 2-17 to 2-20. The resulting derived values of the homologous performance parameters are also listed in the table. A refinement and check of the graphical snapshot procedure was included for the 0.20 void fraction point where several of the curves were very steep. For these curves the process was

TEST 1351/1000 PSIA PON FWD BD
VOID FRACTION BEAM 2 GD SUCTION
PLOT No. 16

SMOOTH CURVE DRAWN MANUALLY THROUGH MACHINE PLOT OF
20 POINTS/SEC DATA (SEE SAME PLOT No., NEXT PAGE)

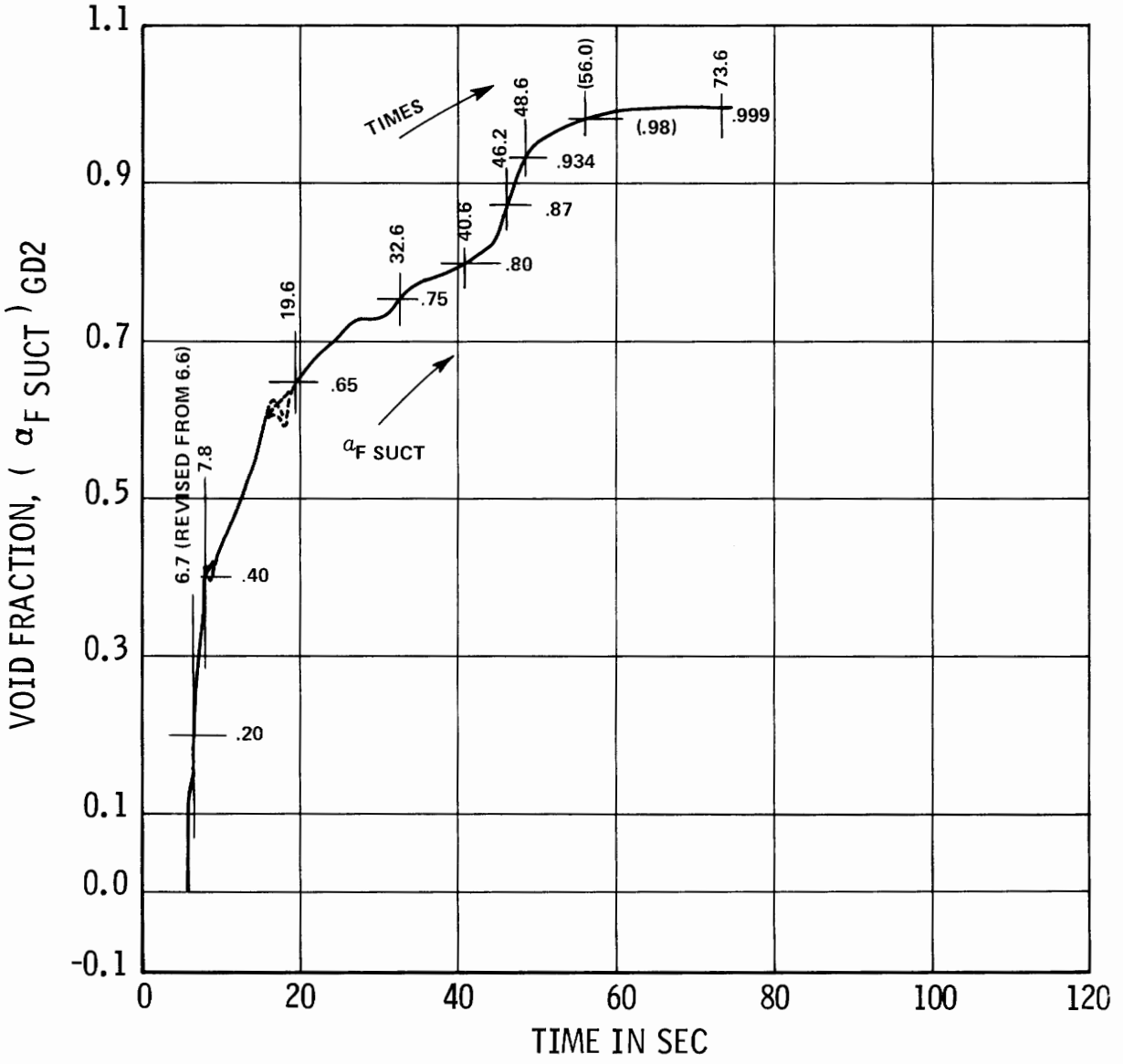

Figure 2-1. Test 1351, Smoothened Curve of Upstream Void Fraction vs Time

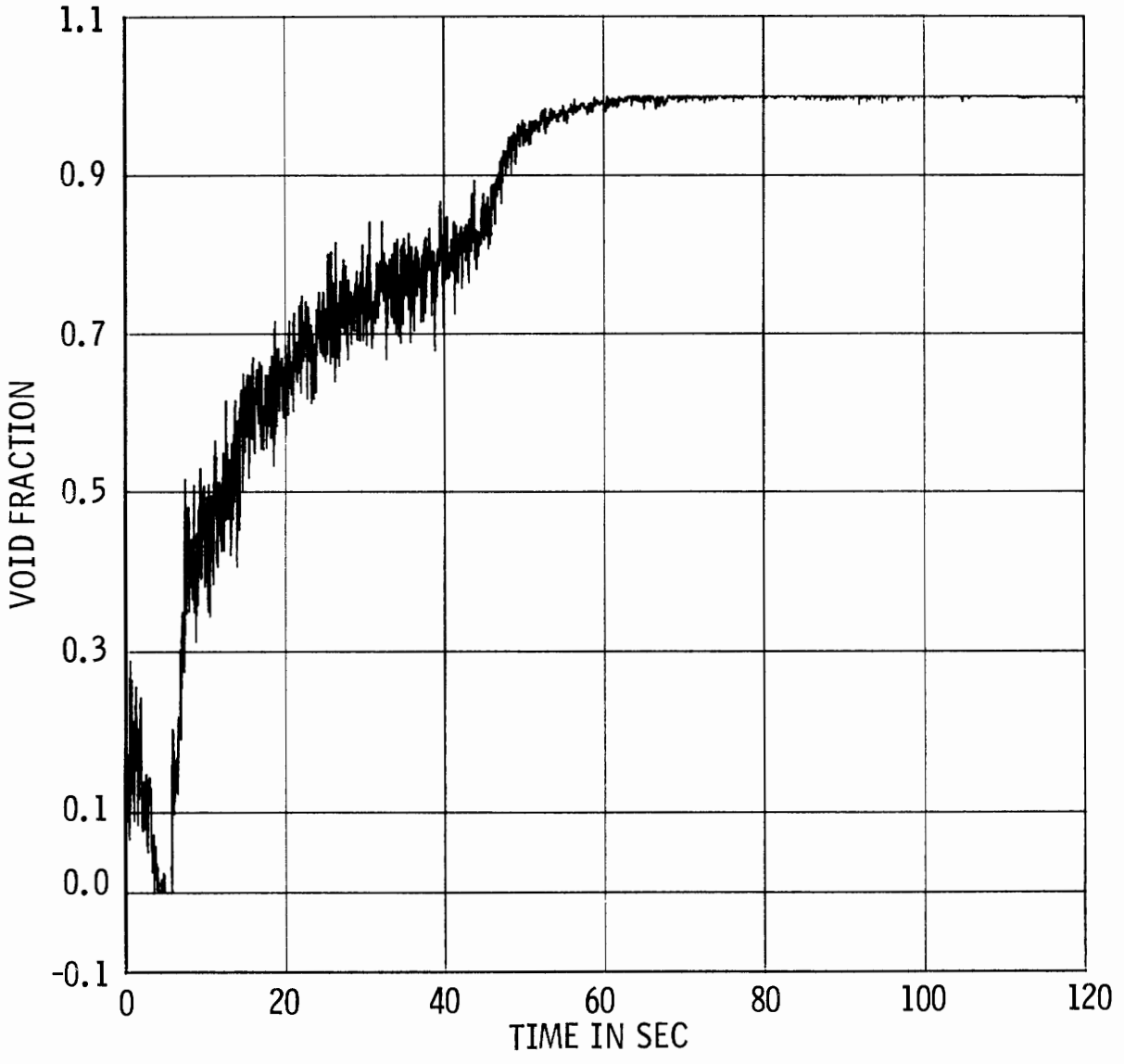

Figure 2-2. Test 1351, Machine-Plotted Curve of Upstream Void Fraction vs Time

TEST 1351/1000 PSIA PON FWD BD
PUMP SUCTION PRESSURE
PLOT No. 1

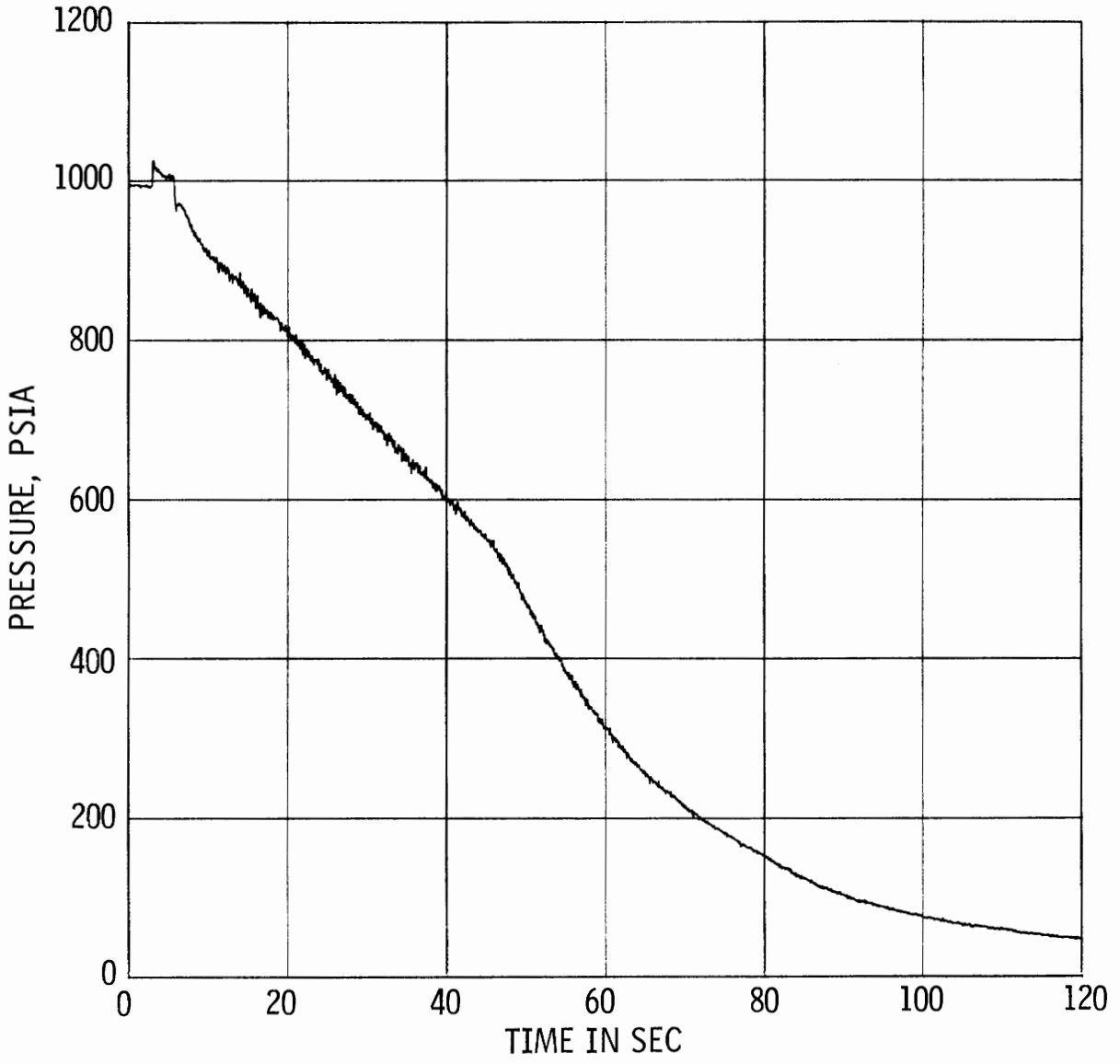

Figure 2-3. Test 1351, Pump Suction Pressure vs Time

TEST 1351/1000 PSIA PON FWD BD
PUMP SUCTION PRESSURE
PLOT No. 1

SMOOTH CURVE DRAWN MANUALLY THROUGH MACHINE PLOT OF
20 POINTS/SEC DATA (SEE SAME PLOT No., PRECEDING PAGE)

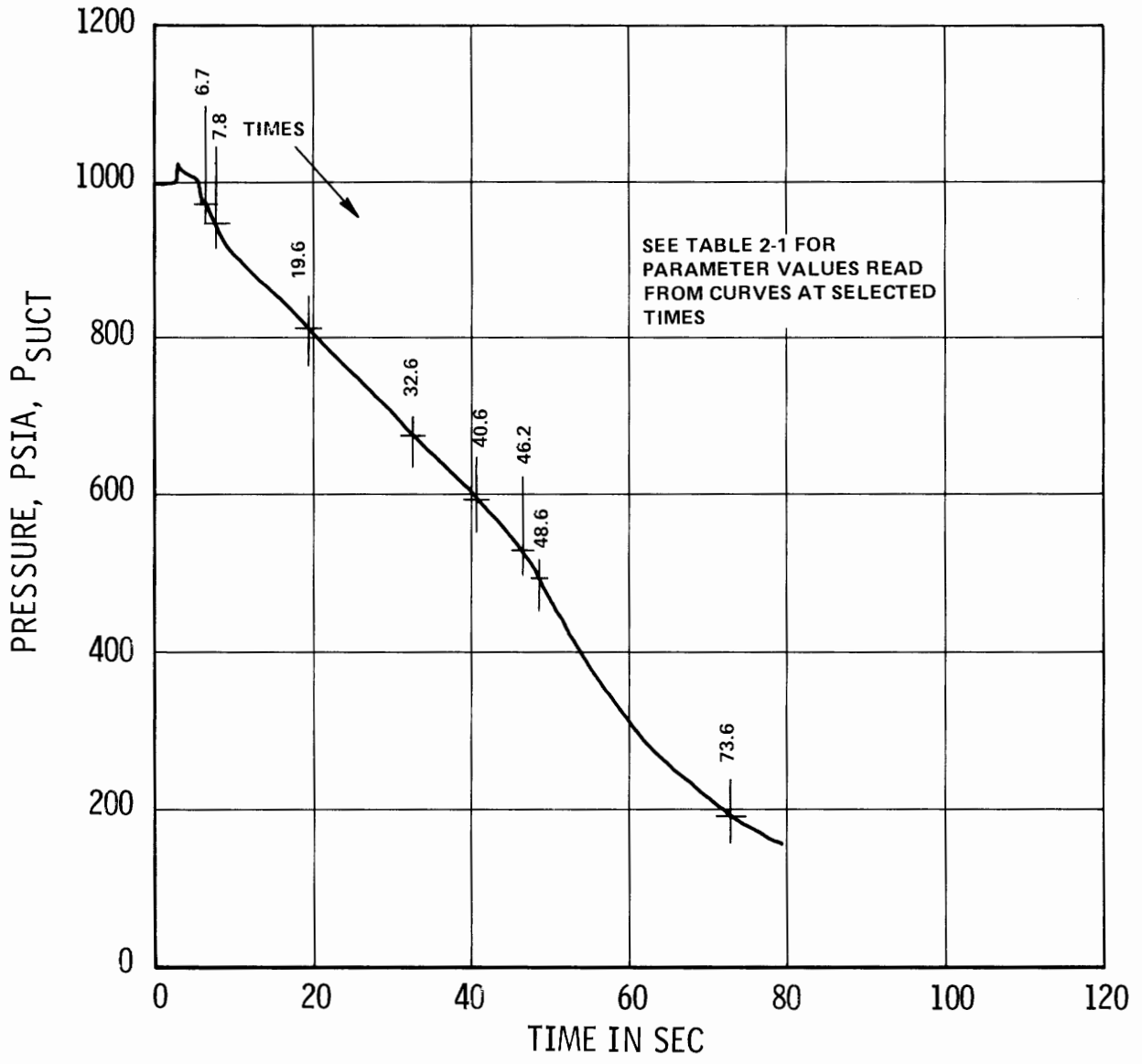

Figure 2-4. Smoothened Curve of Figure 2-3

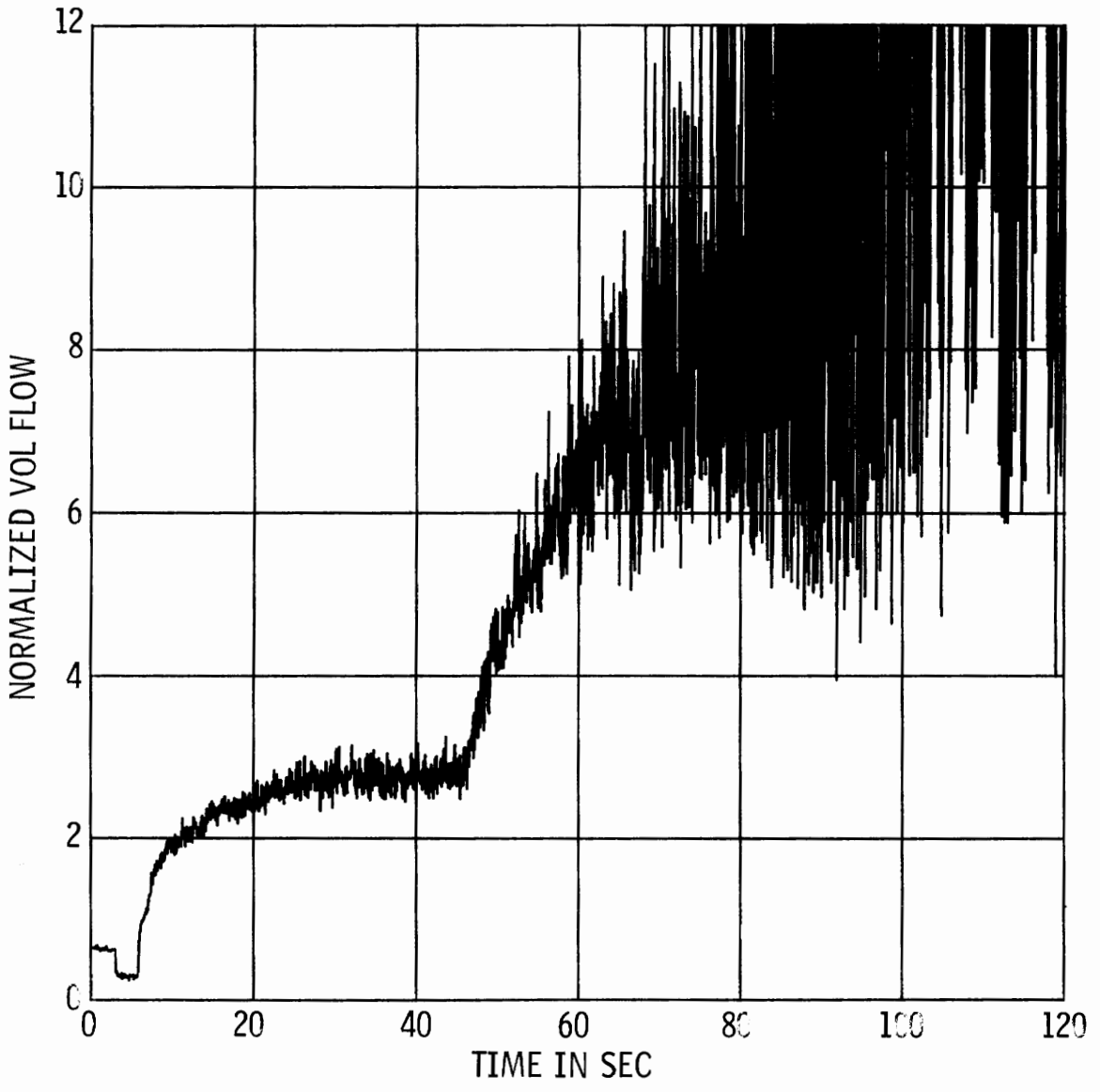

Figure 2-5. Test 1351, Normalized Suction Volumetric Flow Rate vs Time, Based on Gamma Densitometer Beam 2 and Averaged High and Low Drag Disc Data

TEST 1351/1000 PSI PON FWD BDN
N VOL FLOW GD/DD AVG S QR = 3500
PLOT No. 67

SMOOTH CURVE DRAWN MANUALLY THROUGH MACHINE PLOT OF
20 POINTS/SEC DATA (SEE SAME PLOT No., PRECEDING PAGE)

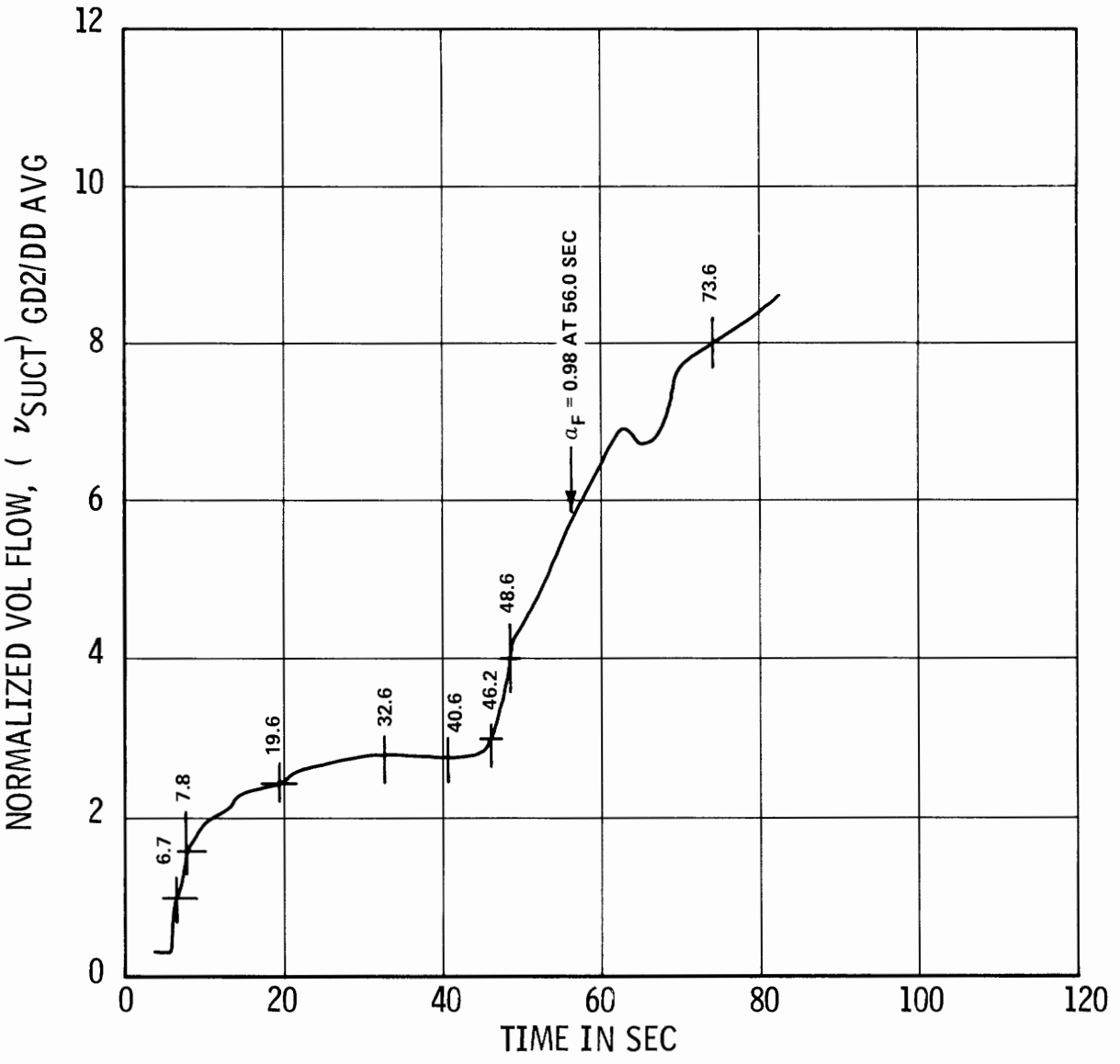

Figure 2-6. Smoothened Curve of Figure 2-5

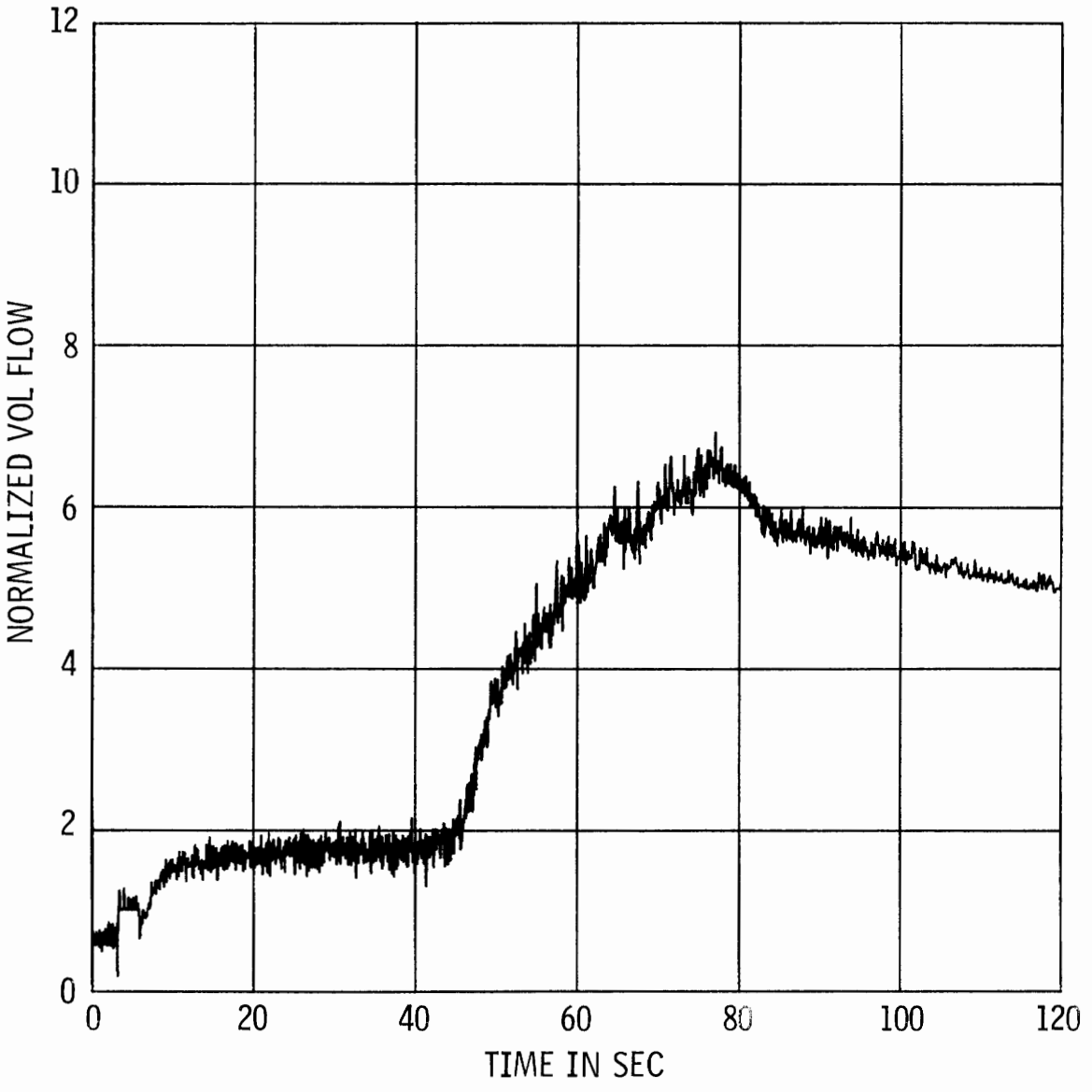

Figure 2-7. Test 1351, Normalized Suction Volumetric Flow Rate vs Time, Based on Averaged High and Low Turbine Meter Data

TEST 1351/1000 PSI PON FWD BDN
N VOL FLOW TM AVG SUC QR = 3500
PLOT No. 69

SMOOTH CURVE DRAWN MANUALLY THROUGH MACHINE PLOT OF
20 POINTS/SEC DATA (SEE SAME PLOT No., PRECEDING PAGE)

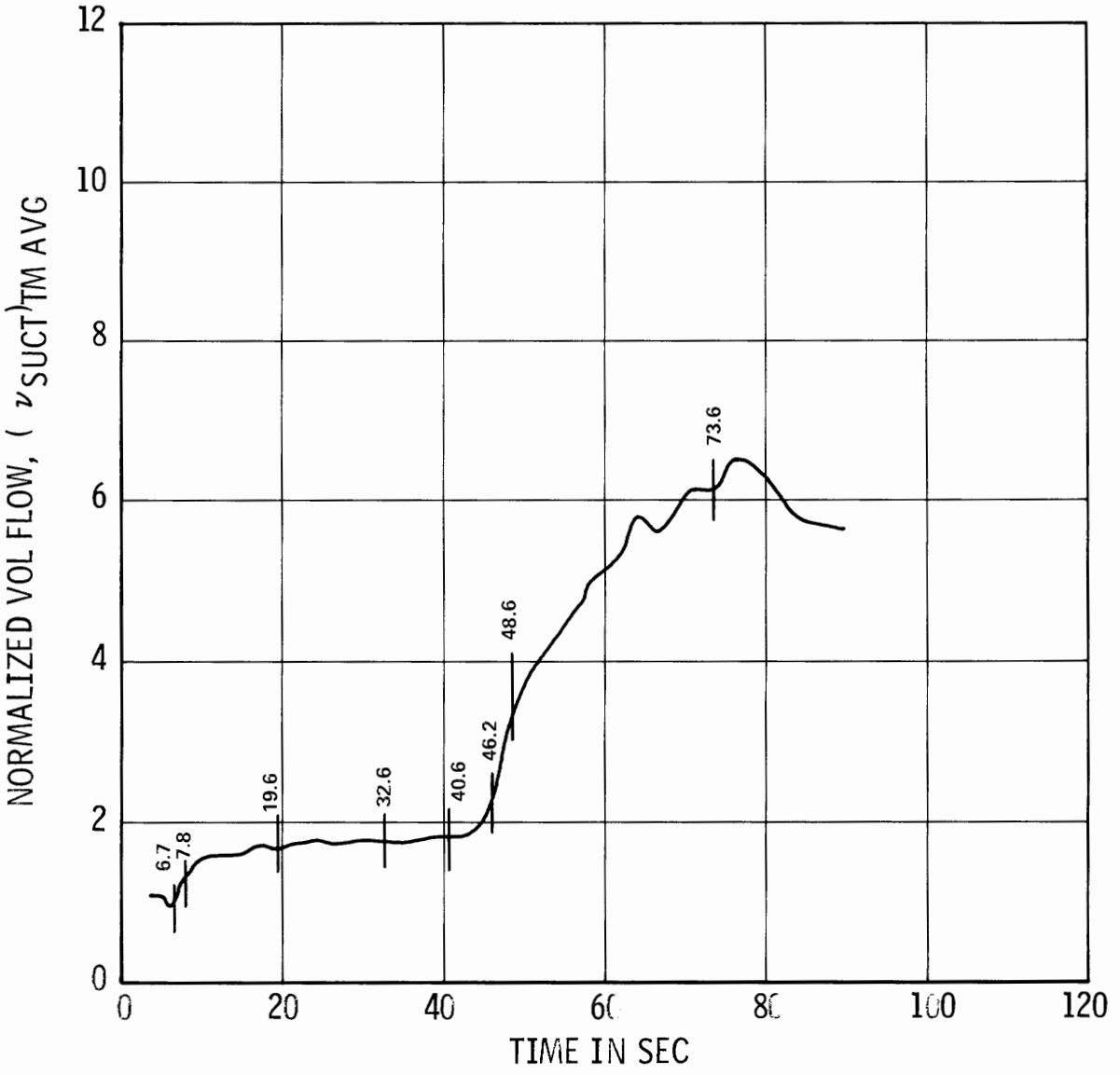

Figure 2-8. Smoothened Curve of Figure 2-7

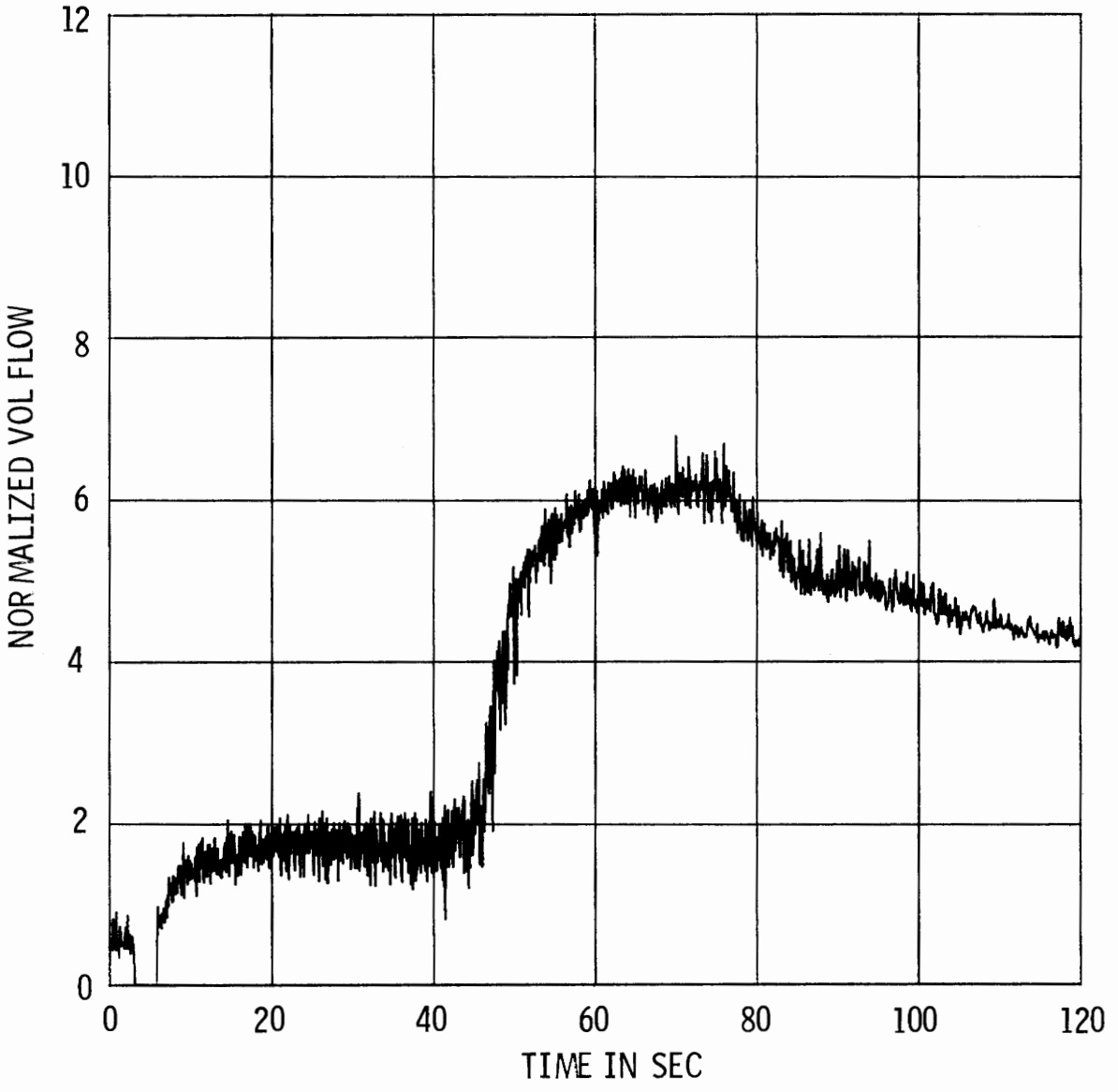

Figure 2-9. Test 1351, Normalized Suction Volumetric Flow Rate vs Time, Based on High Turbine Meter Data

TEST 1351/1000 PSIA PON FWD BD
N VOL FLOW HI-TM SUCT QR = 3500
PLOT No. 27

SMOOTH CURVE DRAWN MANUALLY THROUGH MACHINE PLOT OF
20 POINTS/SEC DATA (SEE SAME PLOT No., PRECEDING PAGE)

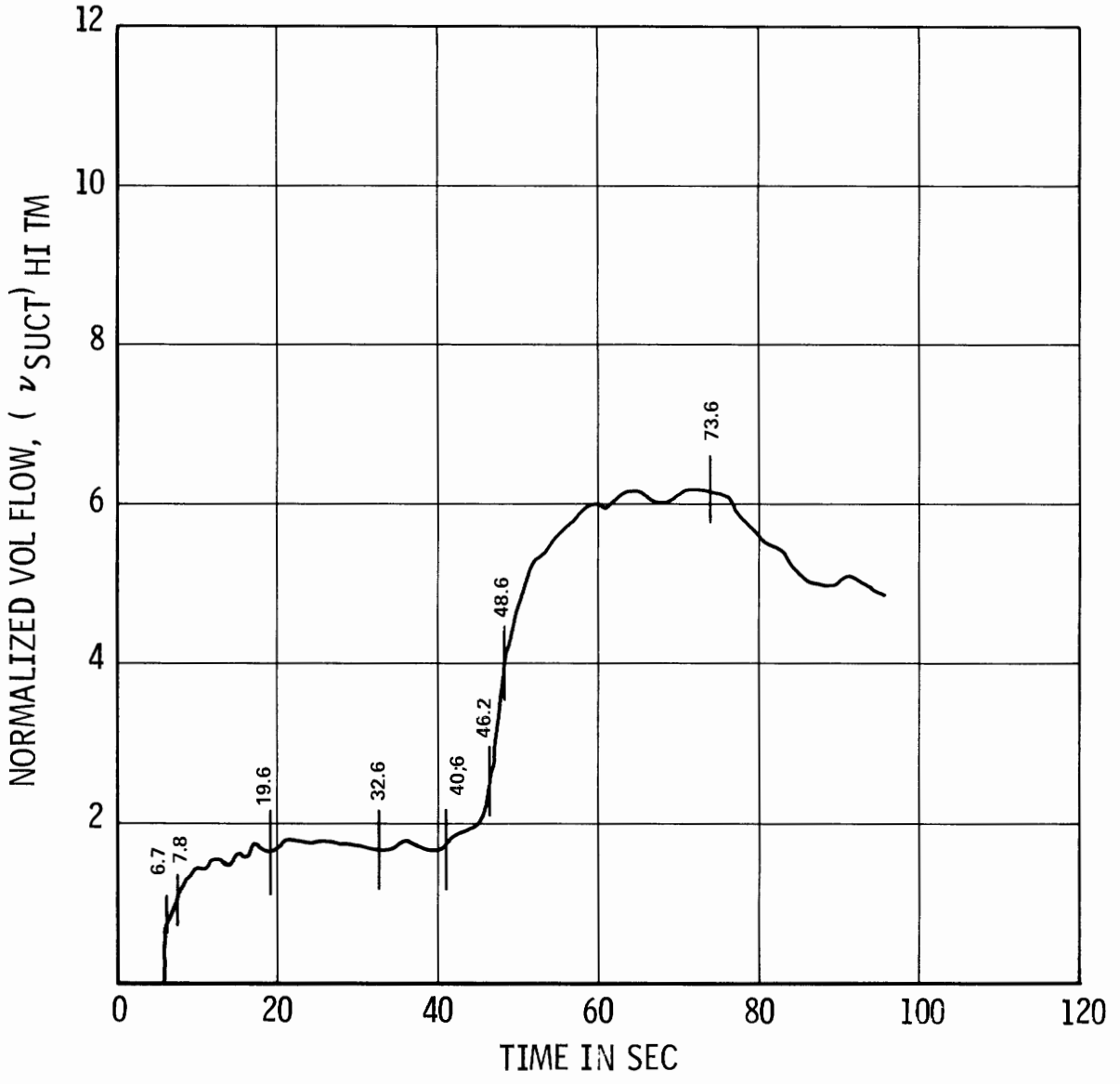

Figure 2-10. Smoothened Curve of Figure 2-9

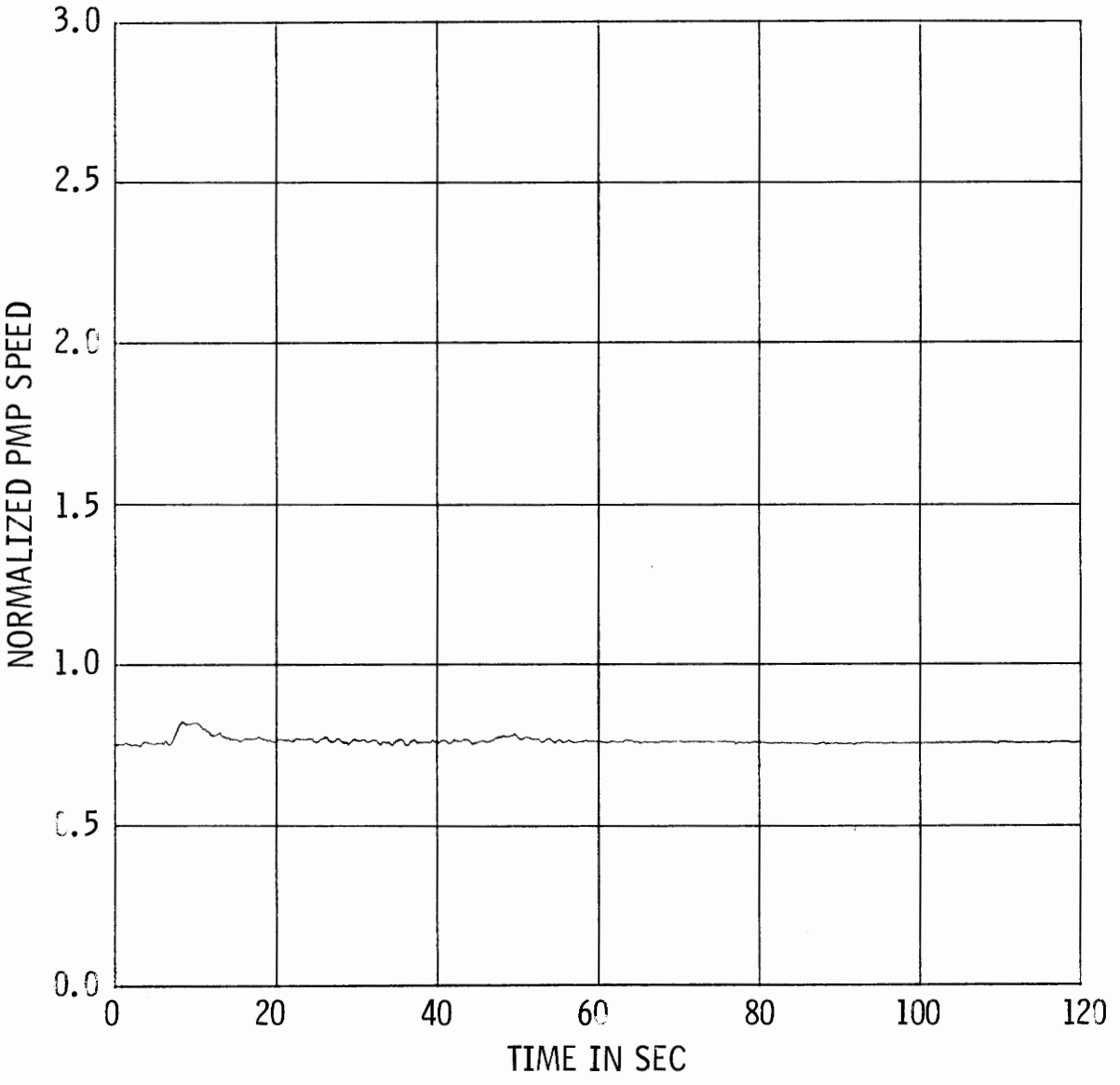

Figure 2-11. Test 1351, Normalized Pump Speed vs Time

TEST 1351/1000 PSIA PON FWD BD
N PUMP SPEED NR = 4500
PLOT No. 47

SMOOTH CURVE DRAWN MANUALLY THROUGH MACHINE PLOT OF
20 POINTS/SEC DATA (SEE SAME PLOT No., PRECEDING PAGE)

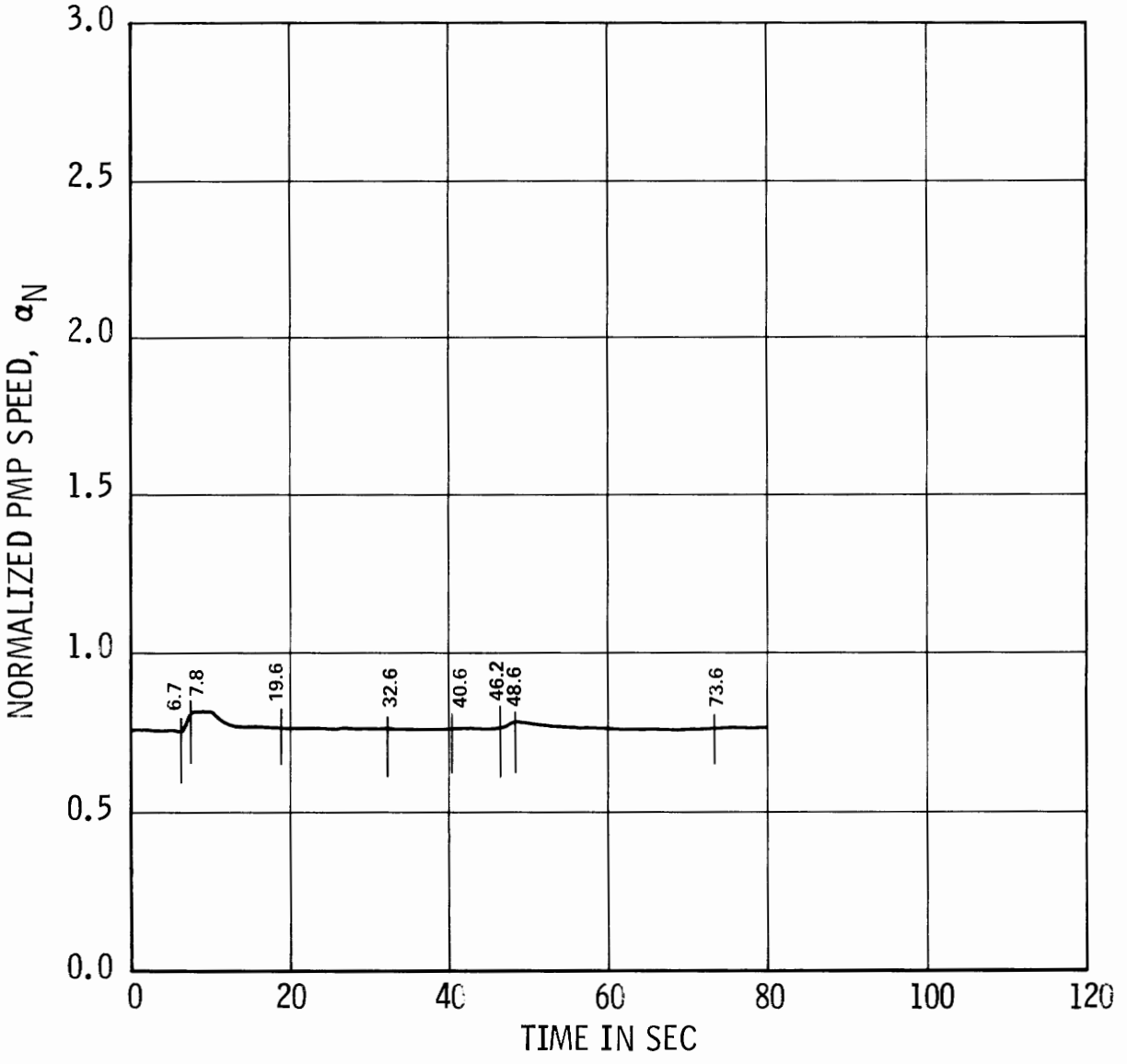

Figure 2-12. Smoothened Curve of Figure 2-11

TEST 1351/1000 PSIA PON FWD BD
DENSITY BEAM 2 GD SUCTION
PLOT No. 7

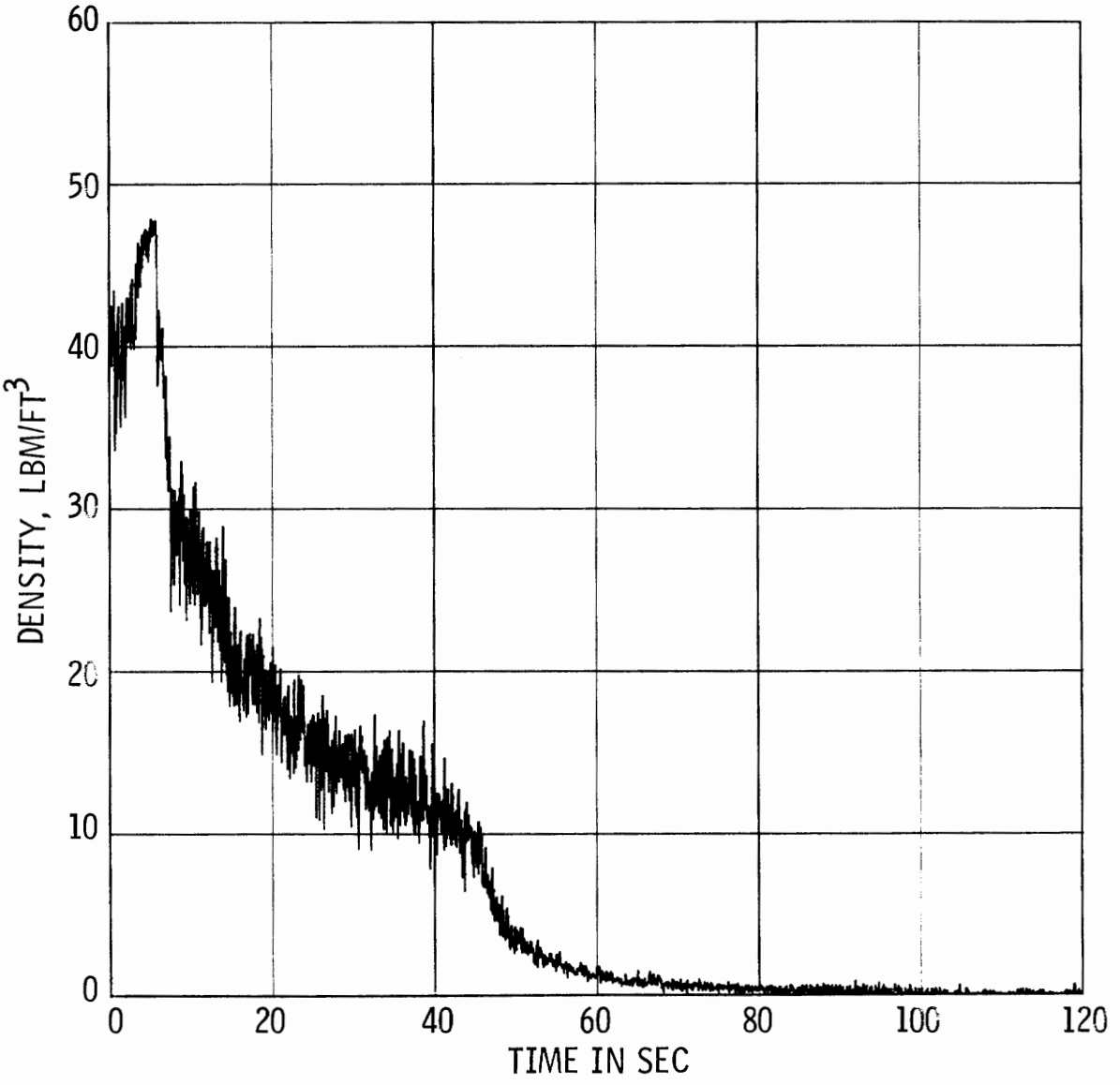

Figure 2-13. Test 1351, Suction Density vs Time, Based on Gamma Densitometer Data

TEST 1351/1000 PSIA PON FWD BD
DENSITY BEAM 2 GD SUCTION
PLOT No. 7

SMOOTH CURVE DRAWN MANUALLY THROUGH MACHINE PLOT OF
20 POINTS/SEC DATA (SEE SAME PLOT No., PRECEDING PAGE)

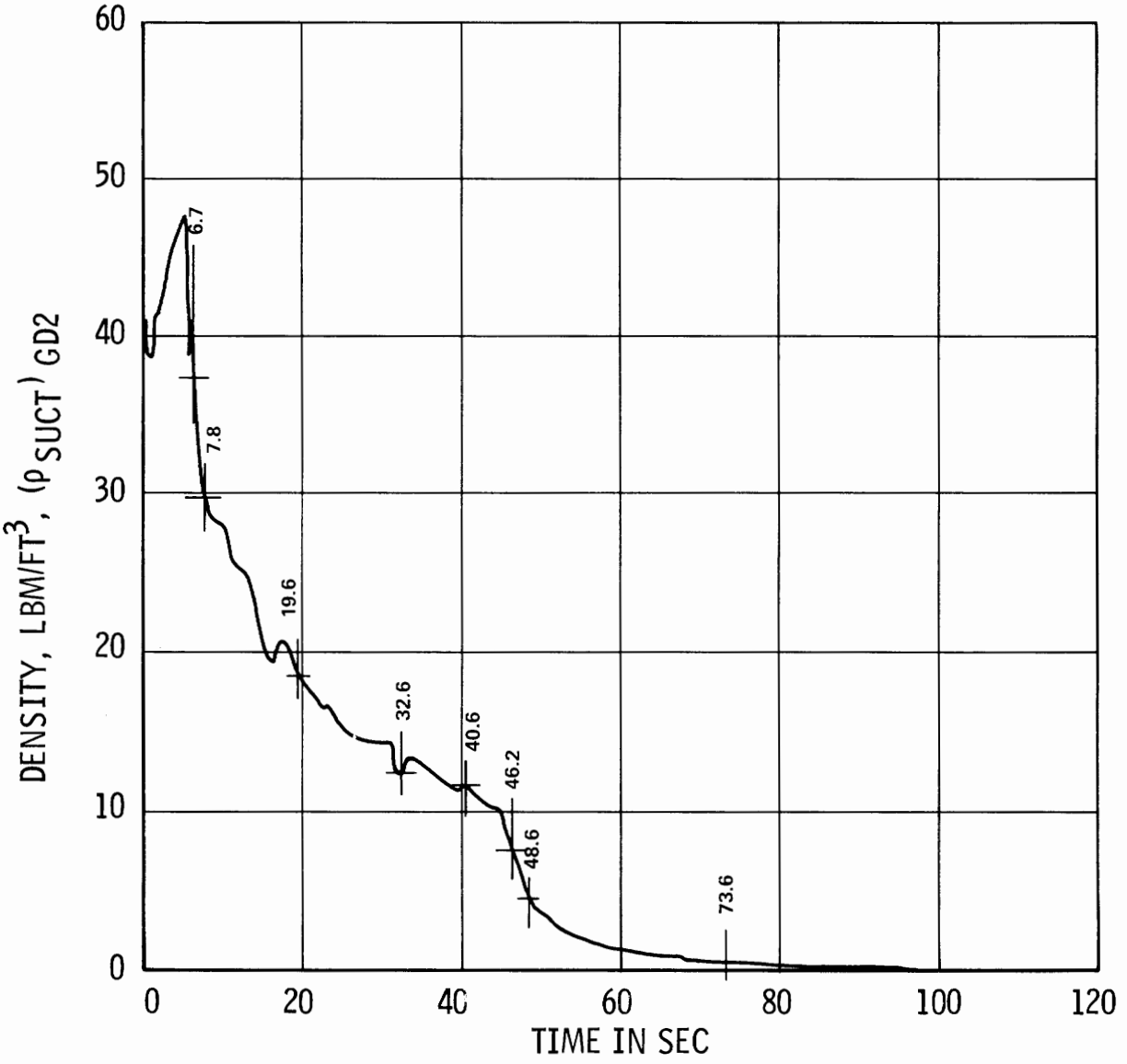

Figure 2-14. Smoothened Curve of Figure 2-13

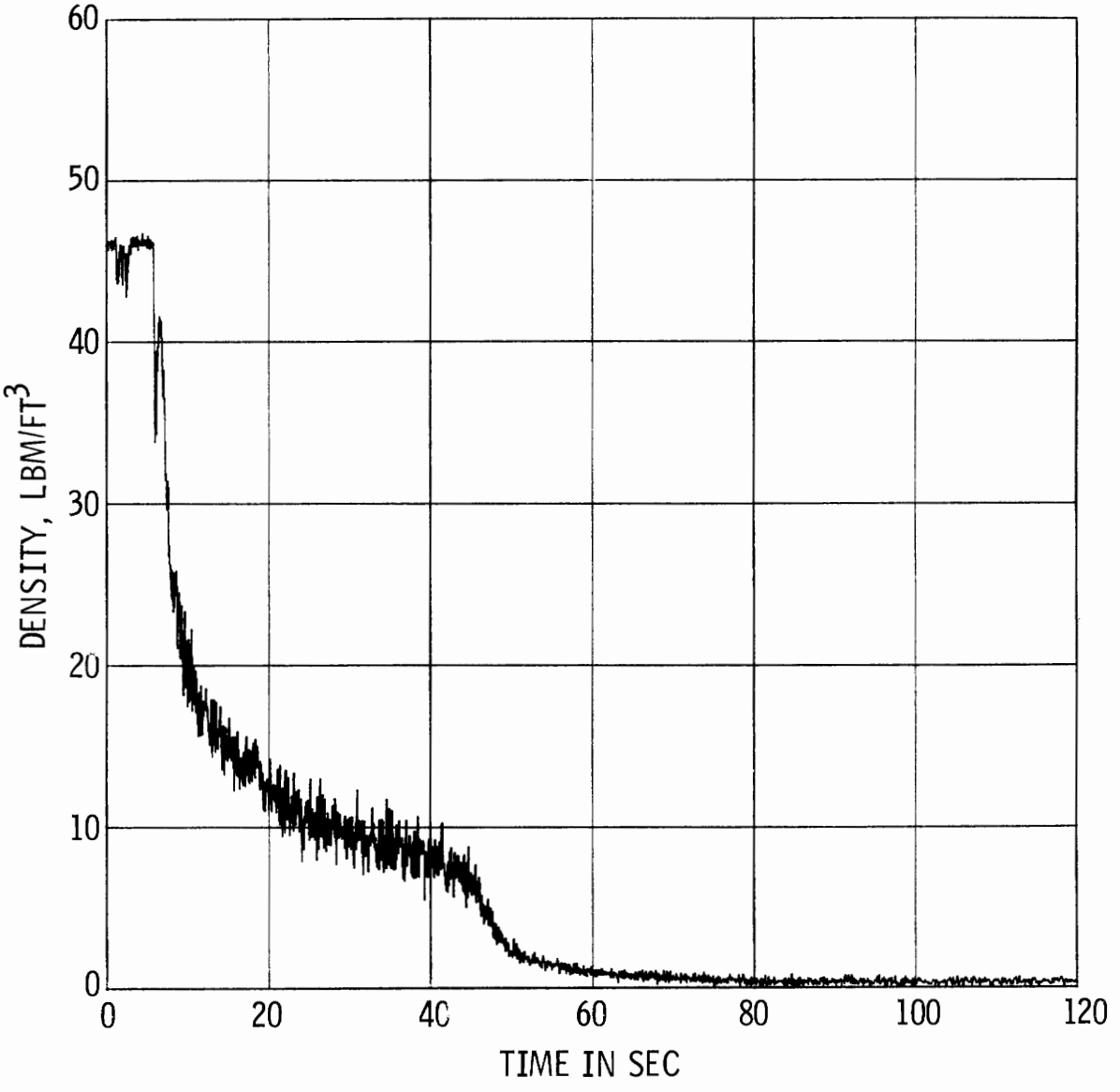

Figure 2-15. Test 1351, Discharge Density vs Time, Based on Gamma Densitometer Data

TEST 1351/1000 PSIA PON FWD BD
DENSITY BEAM 2 GD DISCHARGE
PLOT No. 10

SMOOTH CURVE DRAWN MANUALLY THROUGH MACHINE PLOT OF
20 POINTS/SEC DATA (SEE SAME PLOT No., PRECEDING PAGE)

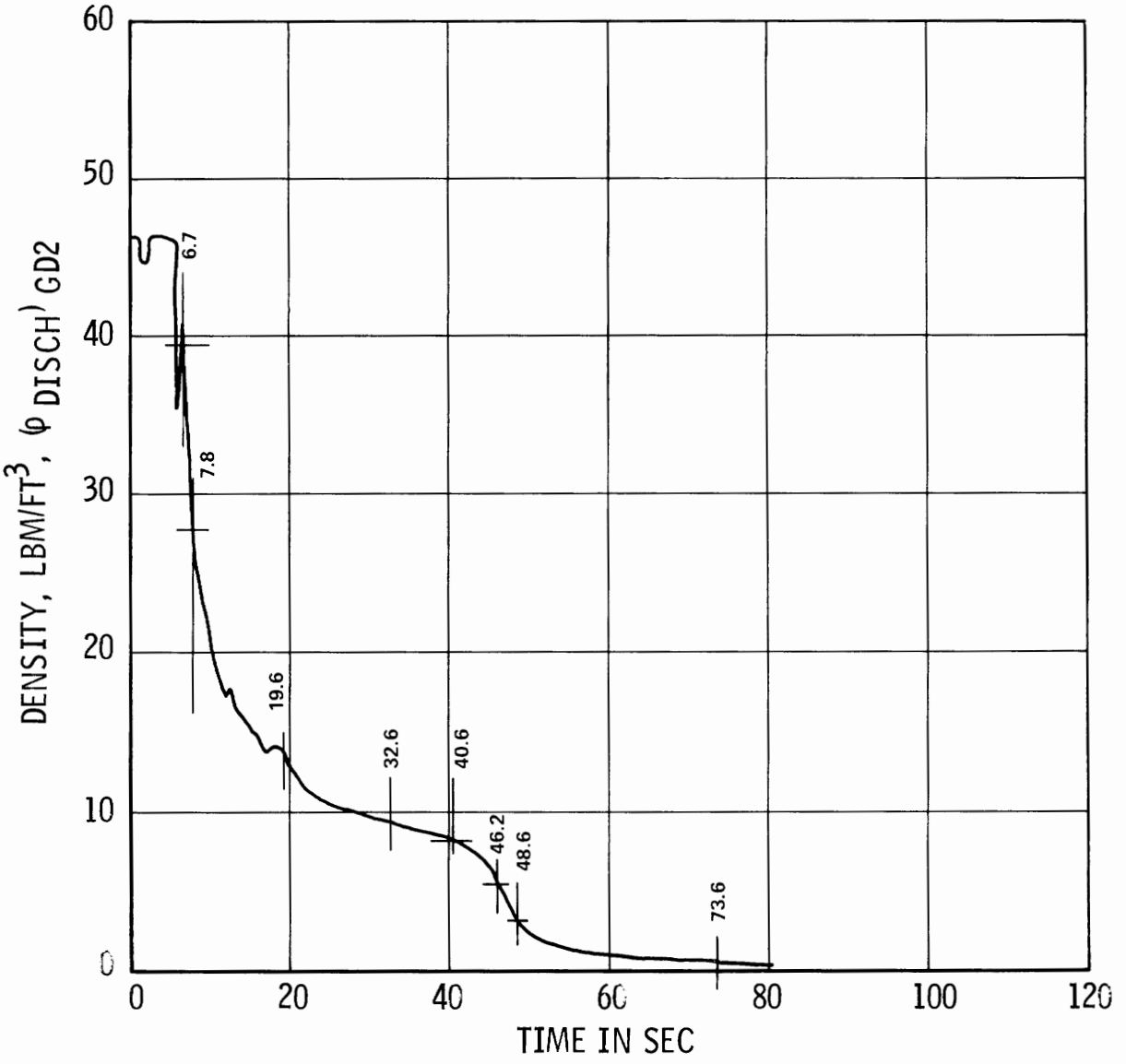

Figure 2-16. Smoothened Curve of Figure 2-15

Table 2-1

TRANSIENT PUMP CONDITIONS AND PERFORMANCE SNAPSHOTS FROM TRANSIENT TEST 1351

PARAMETER POINT:	A ORIGINAL	A REFINED	B	C	D	E	F	G	H
Quantities from smooth curves									
(α_F suct) GD2	.20	.20	.40	.65	.75$^+$	.80	.87	.934	.999
Time, sec	6.6	6.72$^+$	7.8	19.6	32.6	40.6	46.2$^+$	48.6	73.6
P suct, psia	972	Not Refined	948	812	674	594	528	492	190
(ν suct) GD2/DD AVG	1.044	1.065	1.62	2.44	2.80	2.78	3.03	4.00	
(ν suct) TM AVG									6.16
(ν suct) HI TM								4.00	6.16
α_N	.755	.752	.810	.765	.76	.76	.76	.78	.765
(ρ suct) GD2, lbm/ft^3	37.3	37.2	29.7	18.5	12.5	11.6	7.7	4.6	.485
(ρ disch) GD2, lbm/ft^3	39.4	41.2	27.8	13.4	9.3	8.1	5.3	3.0	.450
ΔP leg-leg, psi	-0.2	+2.0	-57.2	-141.8	-134.0	-120.8	-111.8	-123.8	-67.4
$T_h/308$	.30	.294	.06	-.540	-.504	-.42	-.428	-.536	-.409
Calculated quantities									
$\rho_{avg} = \frac{1}{\frac{1}{2}(\frac{1}{\rho_{suct}} + \frac{1}{\rho_{disch}})}$, $\frac{lbm}{ft^3}$	38.32	39.10	28.72	15.54	10.665	9.54	6.28	3.63	.467
ν/α_N	1.383	1.416	2.00	3.18	3.69	3.66	3.98	5.13	8.06
α_N/ν	.723	.706	.500	.314	.271	.273	.251	.195	.124
$h = \frac{144\ \Delta P}{\rho_{suct} \cdot 252}$	-.0031	.0307	-1.101	-4.380	-6.126	-5.951	-8.297	-15.38	-79.41
h/ν^2	-.003	.027	-.419	-.736	-.781	-.770	-.904	-.961	-2.09
$\beta_h = \frac{T_h}{308} \times \frac{62.3}{\rho_{avg}}$	.488	.468	.130	-2.165	-2.994	-2.743	-4.247	-9.145	-54.6
β_h/ν^2	.448	.413	.050	-.364	-.376	-.355	-.463	-.575	-1.44

TEST 1351/1000 PSIA PON FWD BD
PUMP HEAD IN PSI
PLOT No. 44

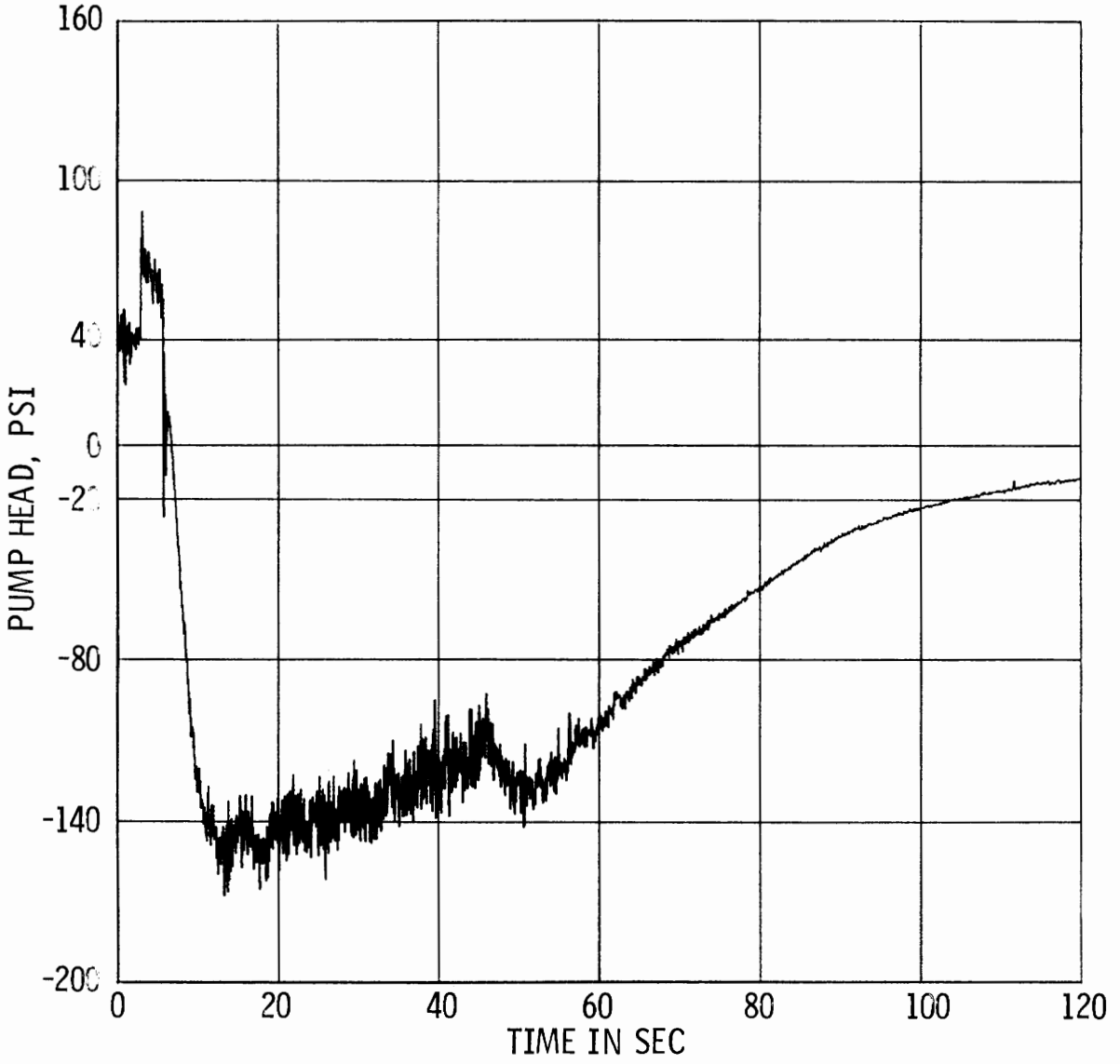

Figure 2-17. Test 1351, Pump Head in PSI vs Time

TEST 1351/1000 PSIA PON FWD BD
PUMP HEAD IN PSI
PLOT No. 44

SMOOTH CURVE DRAWN MANUALLY THROUGH MACHINE PLOT OF
20 POINTS/SEC DATA (SEE SAME PLOT No., PRECEDING PAGE)

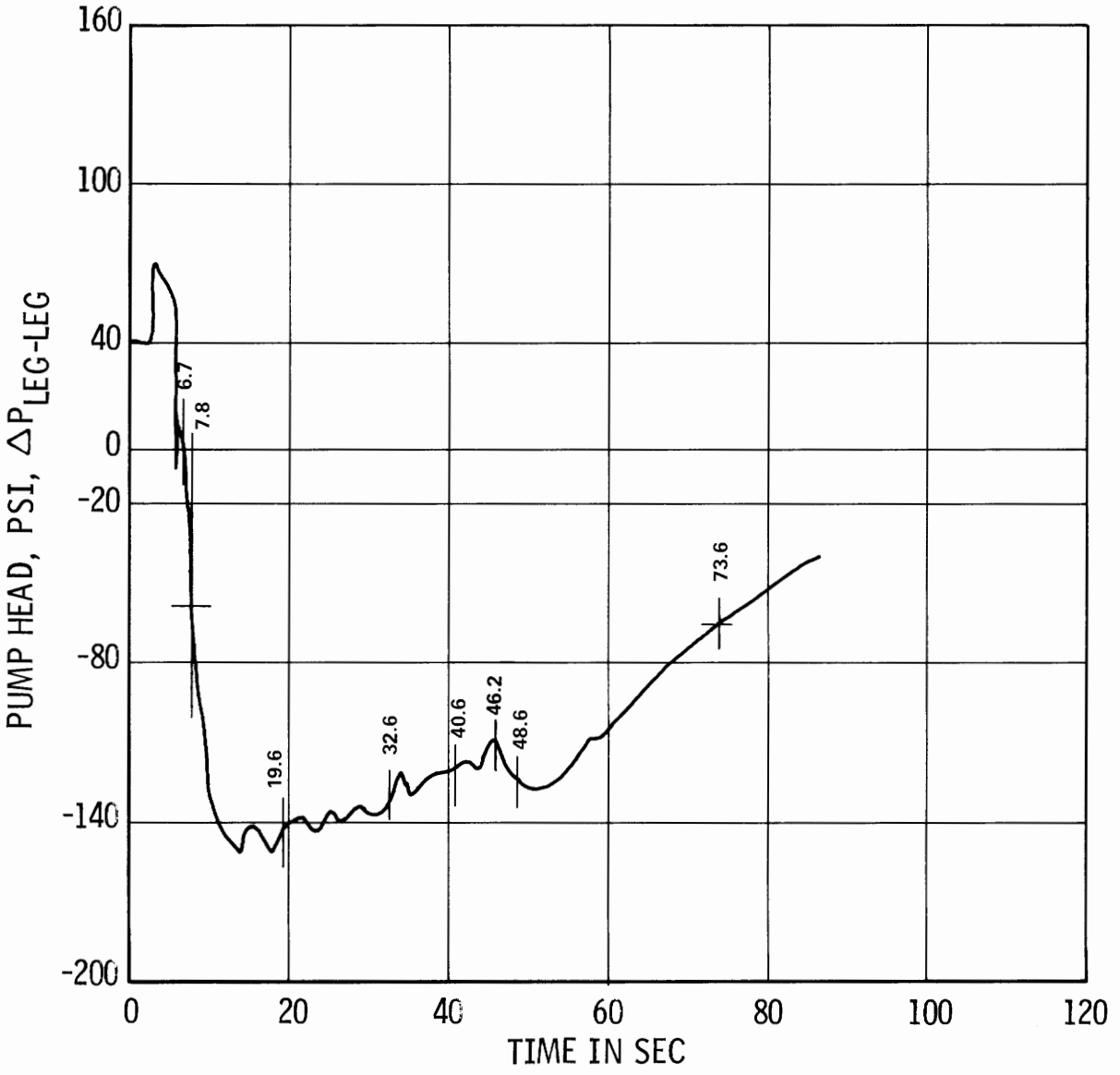

Figure 2-18. Smoothened Curve of Figure 2-17

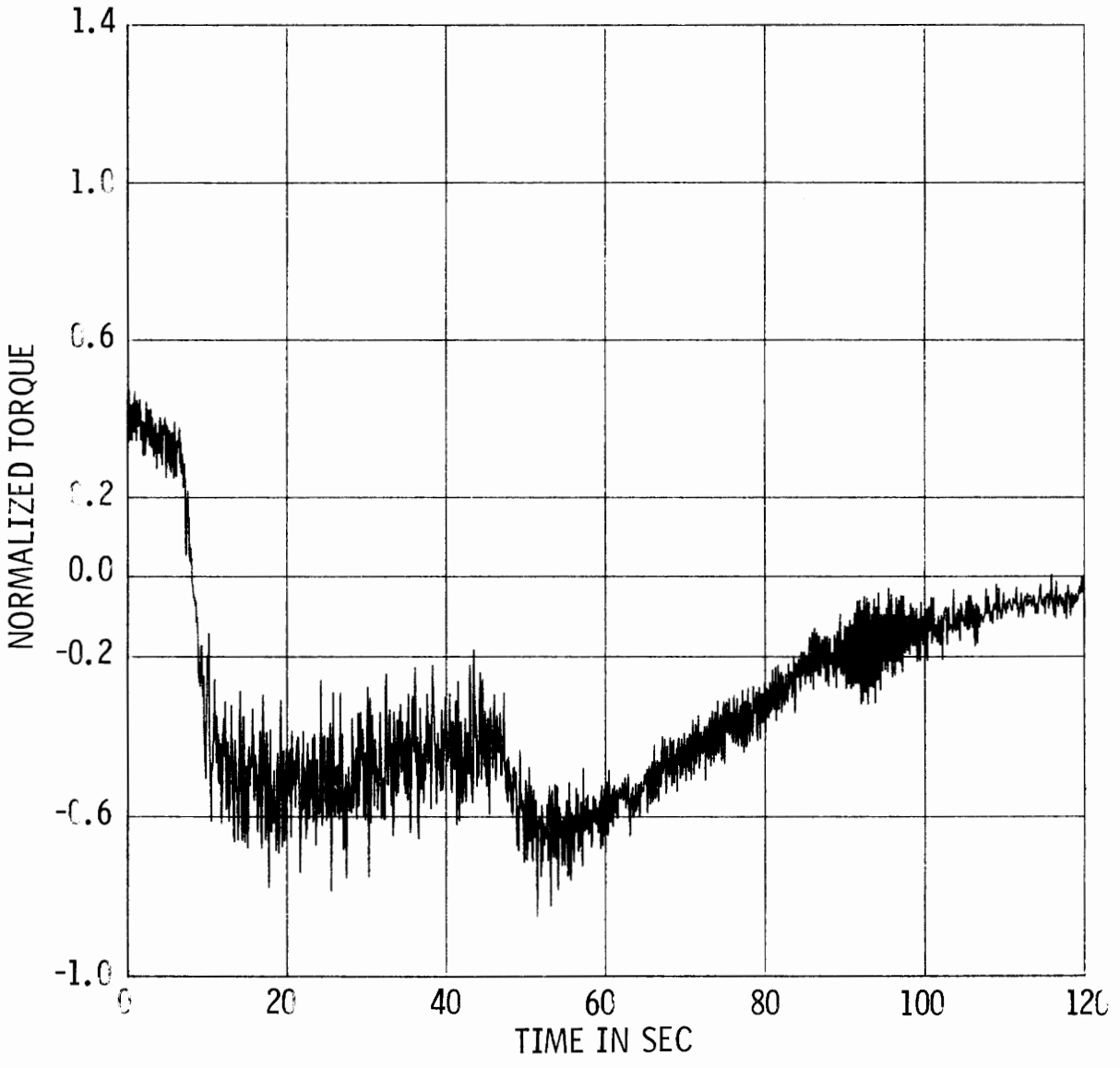

Figure 2-19. Test 1351, Normalized Hydraulic Torque vs Time

TEST 1351/1000 PSIA PON FWD BD
N PUMP HYDR TORQUE THR = 308
PLOT No. 49

SMOOTH CURVE DRAWN MANUALLY THROUGH MACHINE PLOT OF
20 POINTS/SEC DATA (SEE SAME PLOT No., PRECEDING PAGE)

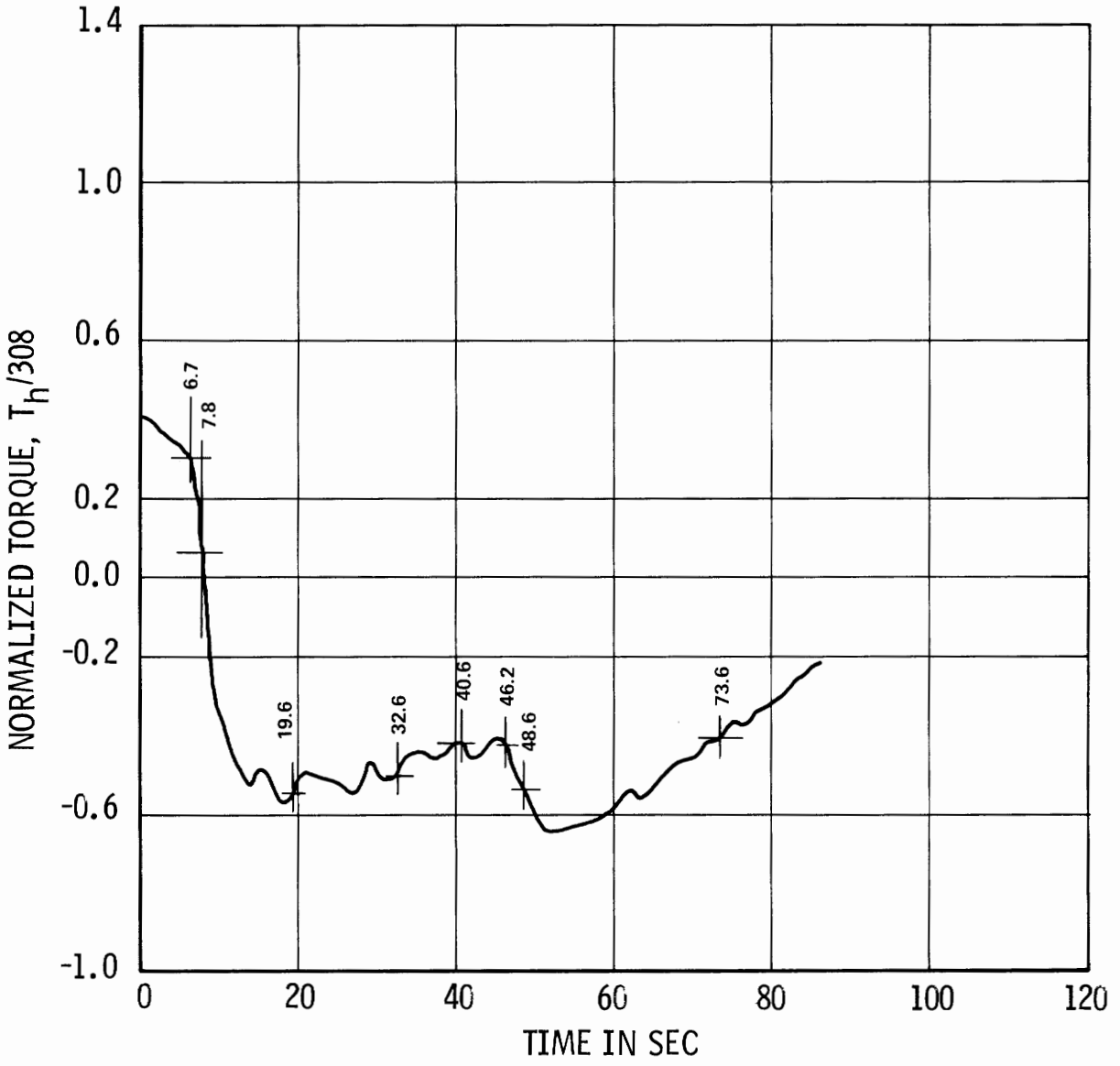

Figure 2-20. Smoothened Curve of Figure 2-19

repeated with the curves locally expanded to show the data points in detail (Figure 2-21). The refined curve readouts are also included in Table 2-1. These refinements involved only small changes in absolute magnitudes. Such expanded curves were also used for obtaining the values of void fraction and density for point H at 73.6 seconds, as shown in Figure 2-22.

Selecting the particular snapshot times and choosing which kinds of flow measurement data to use in developing Table 2-1 involved a blending of several factors. The void fractions of 0.20, 0.40, and 0.80 were selected because curves of steady-state performance at these foid fractions are available for comparison. Also, steady-state data are available at the void fraction of 0.65 for several values of v/α_N and pressure. The 0.20 and 0.40 void fractions occured at 6.7 and 7.8 seconds on the plots, which was during the initial rapid changes in void fraction, density, and flow rate. Thus, these points provide comparisons of steady-state data with measurements made during a rapid transient of several parameters, including the two-phase index $d\alpha_F/dt$. The snapshots of 0.65, 0.75, and 0.80 void fractions provide comparisons on the flow plateau where the volumetric flow rate changed very little, while void fraction continued to rise fairly rapidly (See Figures 2-6 and 2-1).

The point at 46.2 seconds with a void fraction of 0.87 was chosen to be where $v/\alpha_N = 4.0$ because a steady-state degradation curve is available at this v/α_N, although at a somewhat higher pressure. Also, this point was at the beginning of the second flow ramp. The remaining two snapshots at void fractions of 0.934 and approximately 1, at plot times of 48.6 and 73.6 seconds, were chosen to be along the second flow ramp or near maximum flow, respectively, plus being at times when there was favorable agreement of flow measurements as shown in Figure 2-23. These are discussed next.

The hand-smoothed curve for upstream flow rate based on the average of the two suction leg drag discs (DD AVG) and the suction leg gamma densitometer center beam (GD2) is shown in Figure 2-6. This was derived from the curve in Figure 2-5, which shows the computer calculated average of the individual GD2/DD curves in Figures 2-24 and 2-25. Similarly, average turbine meter (TM AVG) flow rate curves were derived from HI and LO turbine meter curves, as shown in Figure 2-9, 2-26, 2-7, and 2-8.

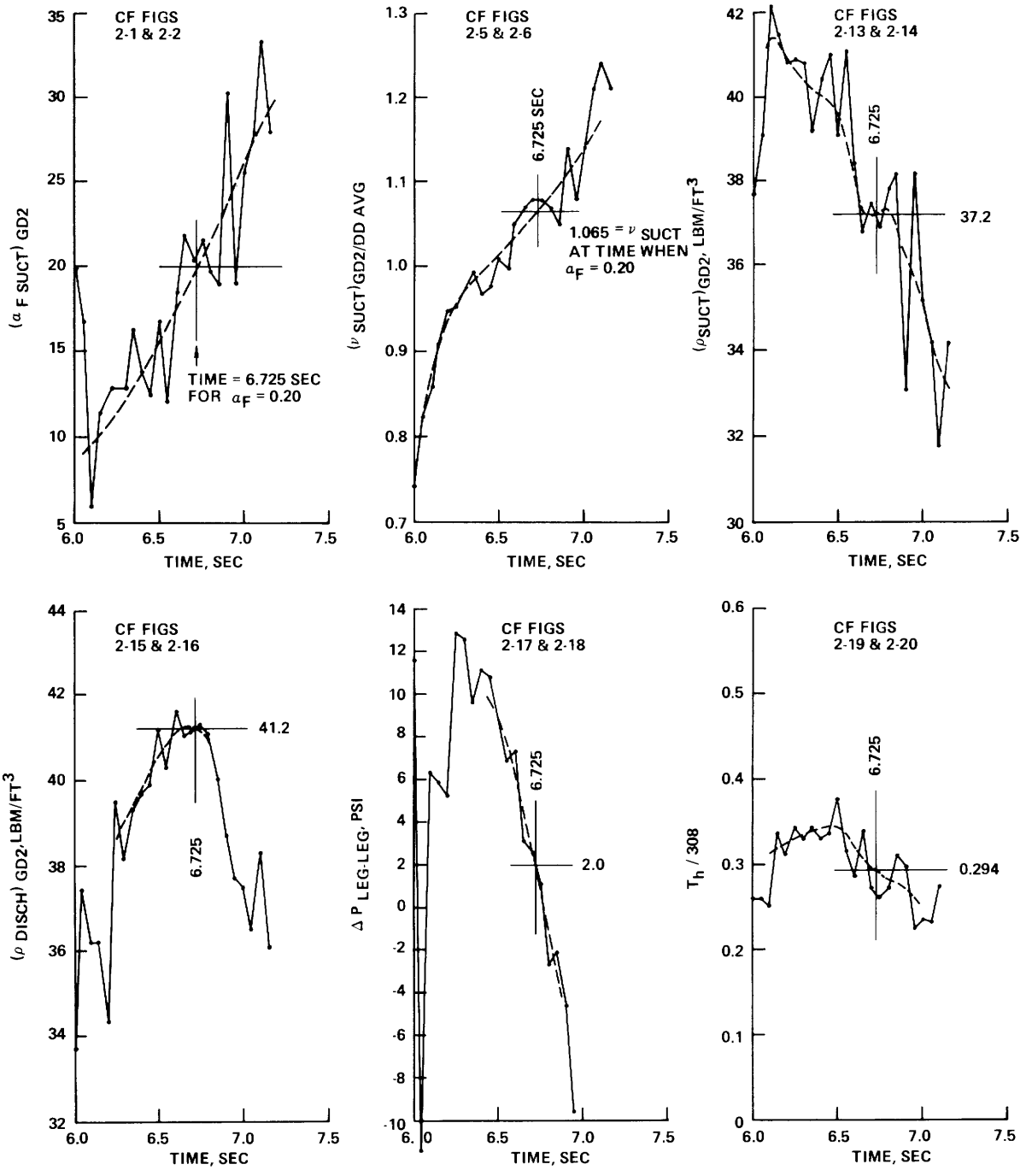

Figure 2-21. Test 1351, Expanded 20 Points/Second Curves and Smoothened Curves Near Time for α_F = 0.20

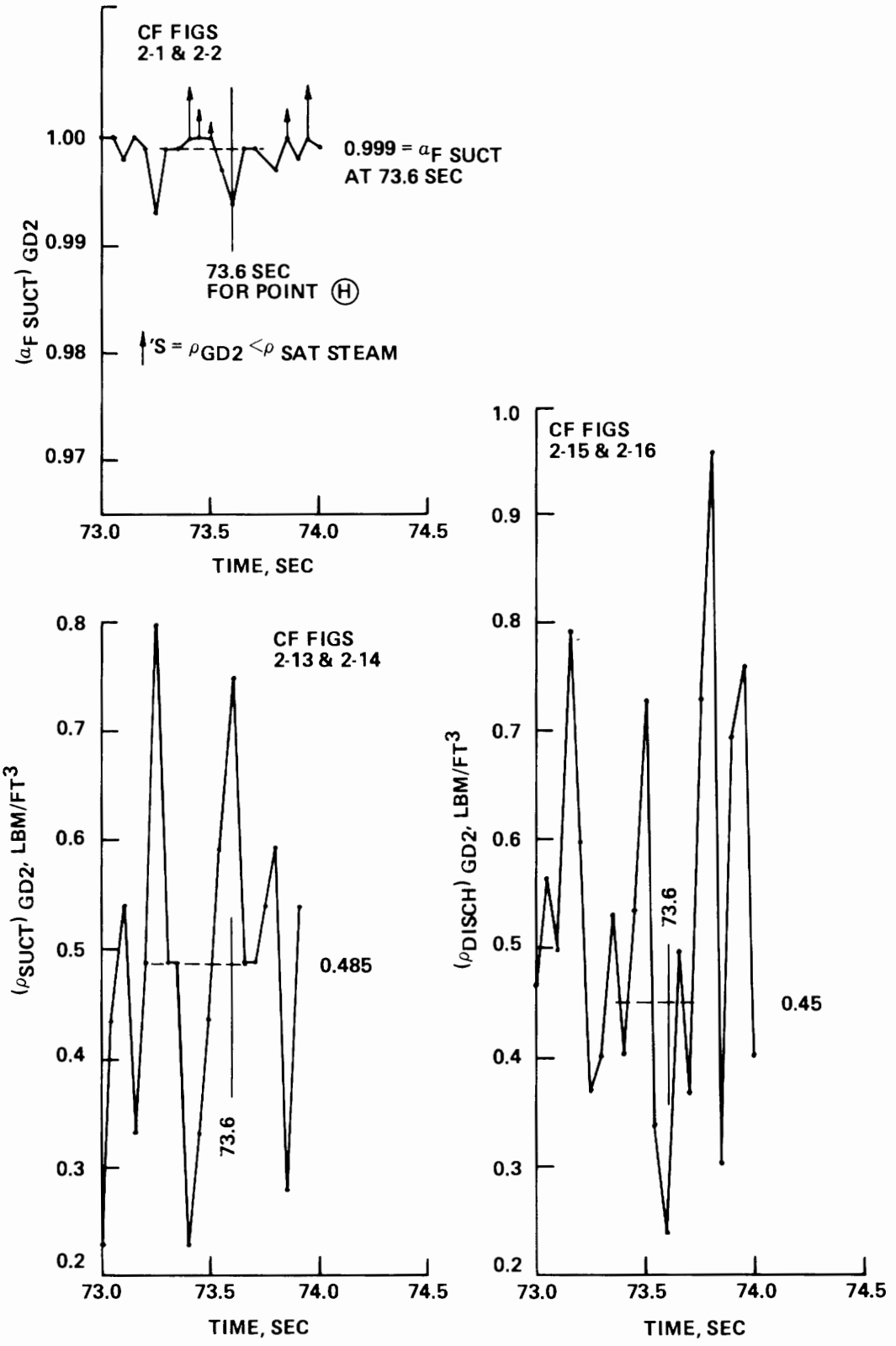

Figure 2-22. Test 1351, Expanded 20 Points/Second Curves and Smoothened Curves Near 76.3 Seconds

TEST 1351/1000 PSI PON FWD BDN
N VOL FLOW, SUCTION QR = 3500
PLOT No.'s 27, 67, 69

SMOOTH CURVES DRAWN MANUALLY THROUGH MACHINE PLOTS OF 20 POINTS/SEC DATA (SEE SAME PLOT No.'s ON PRECEDING PAGES)

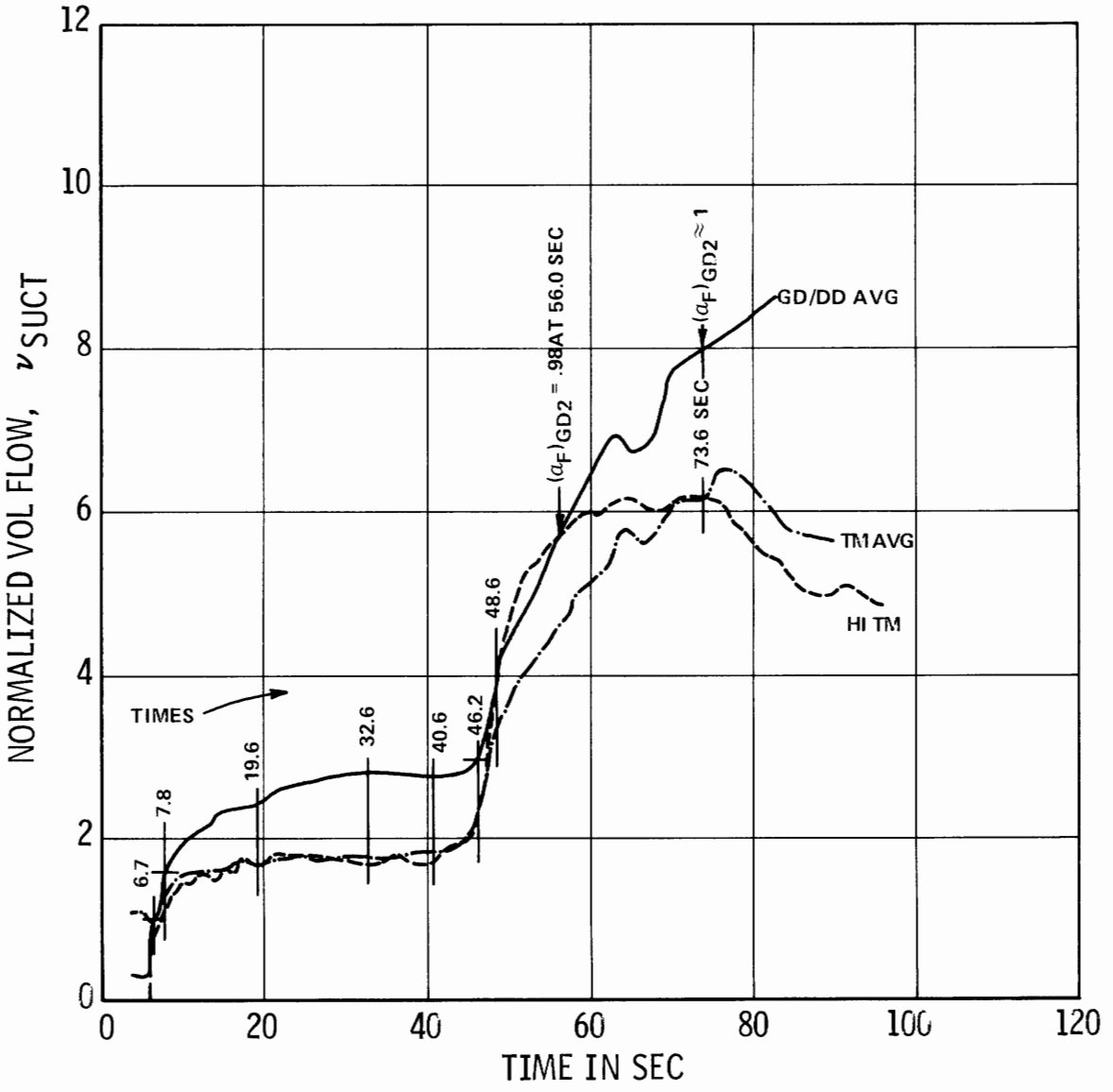

Figure 2-23. Composite of Normalized Volumetric Flow Rates from Figures 2-6, 2-8 and 2-10

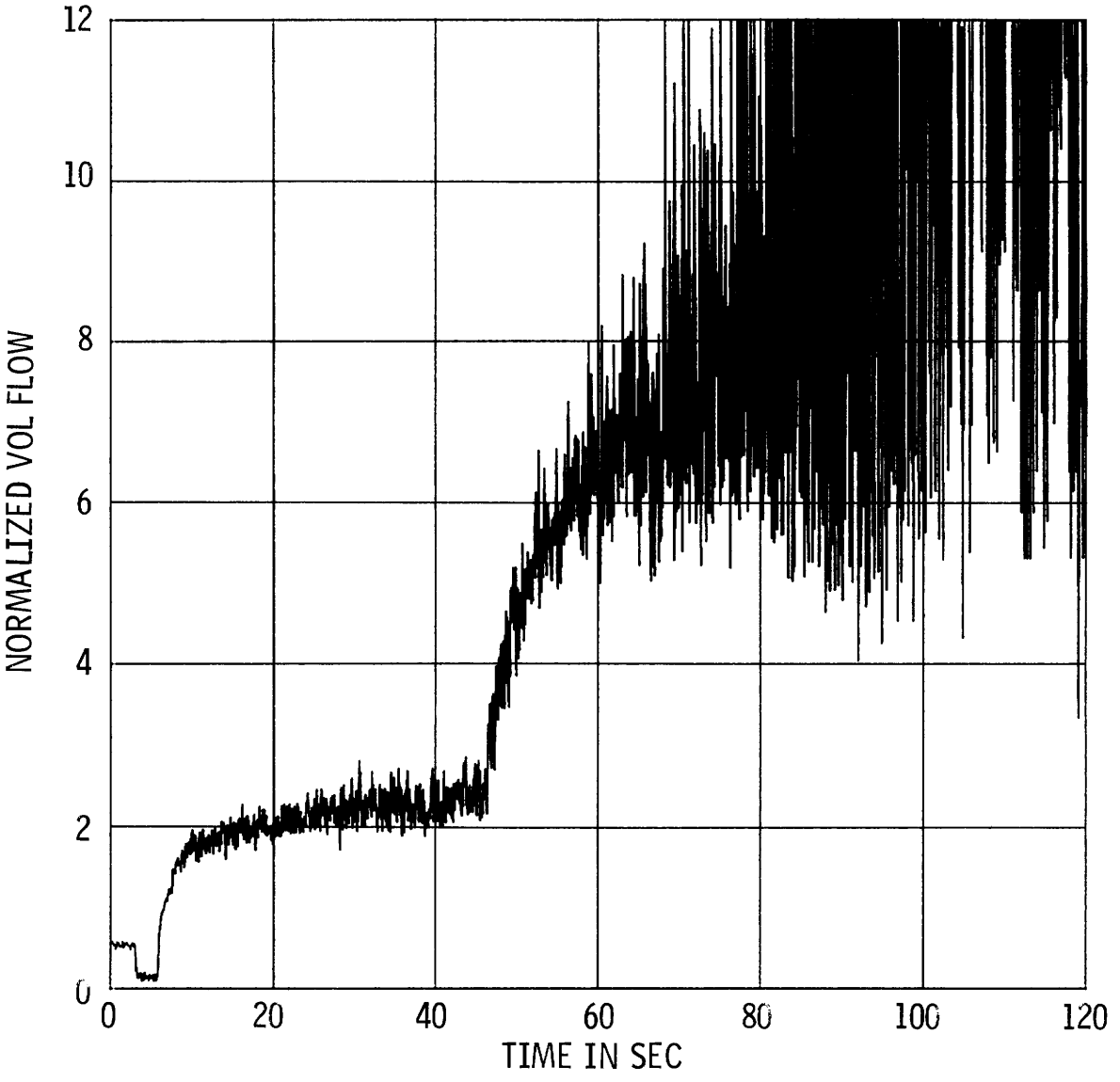

Figure 2-24. Test 1351, Normalized Suction Volumetric Flow Rate vs Time, Based on Gamma Densitometer and High Drag Disc Data

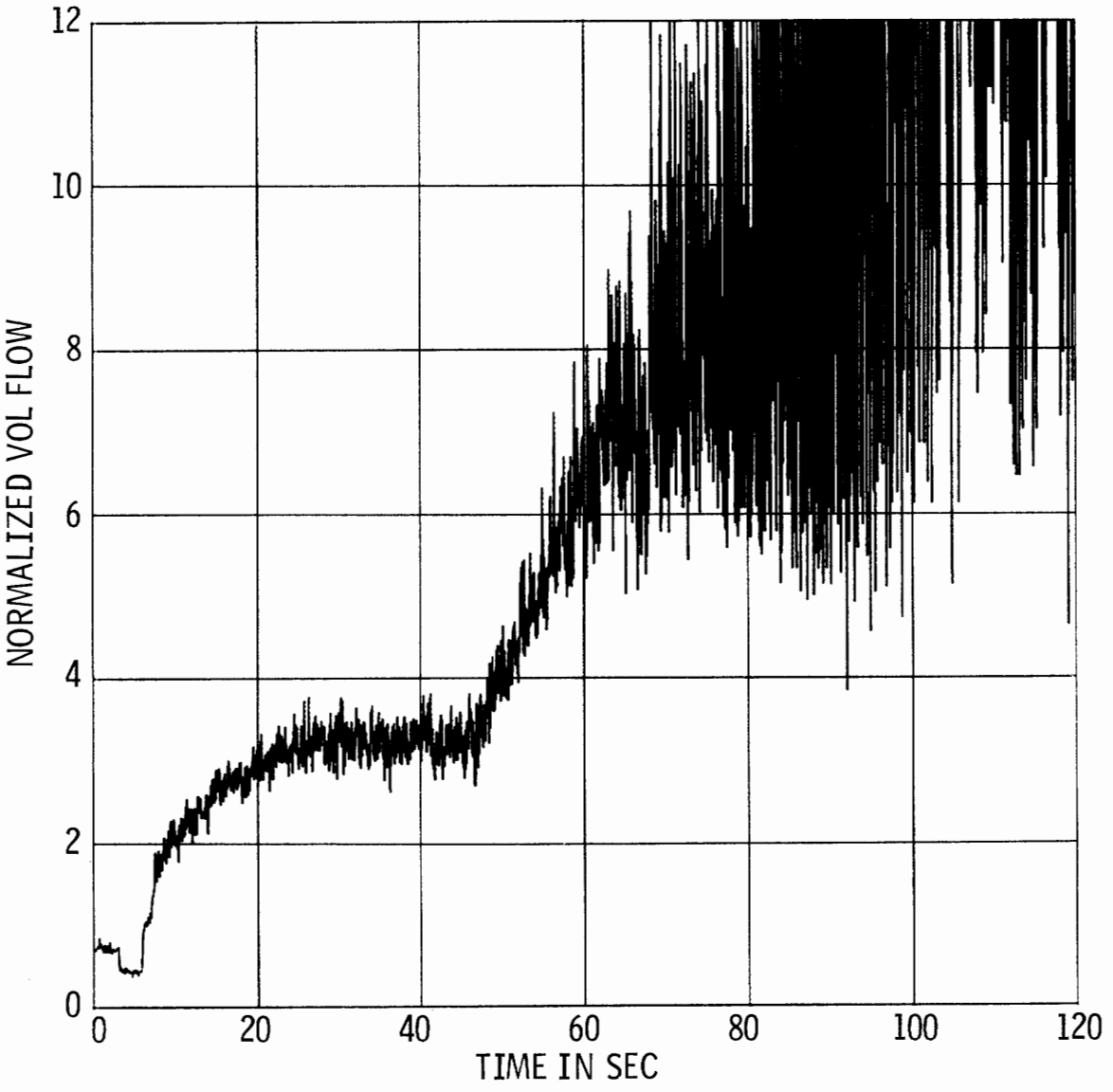

Figure 2-25. Test 1351, Normalized Suction Volumetric Flow Rate vs Time, Based on Gamma Densitometer and Low Drag Disc Data

TEST 1351/1000 PSIA PON FWD BD
N VOL FLOW LO-TM SUCT QR = 3500
PLOT No. 26

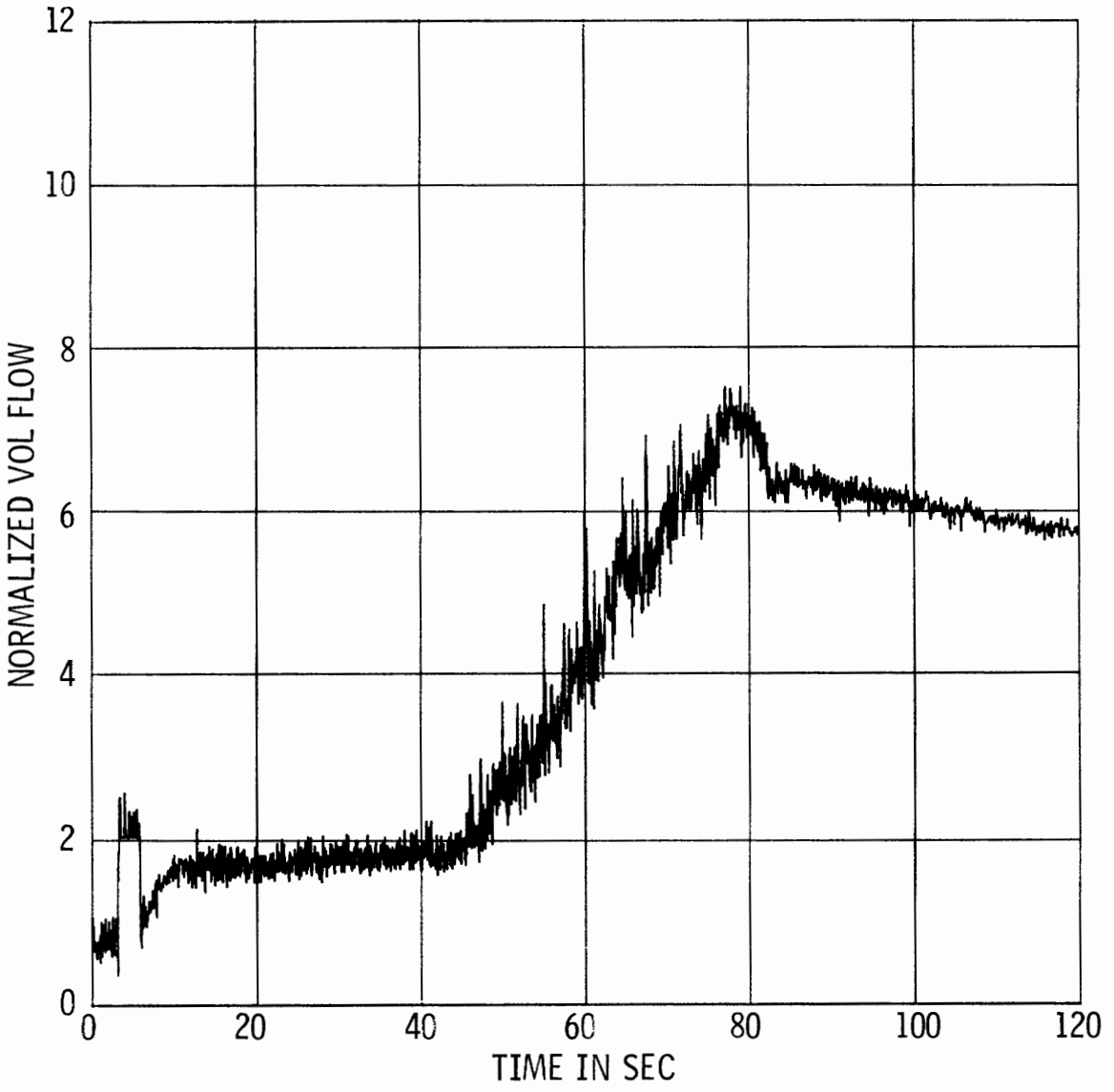

Figure 2-26. Test 1351, Normalized Suction Volumetric Flow Rate vs Time, Based on Low Turbine Meter Data

In accordance with the methods and discussion in Volume III, Sections 5.2.3 and 5.5, the transient snapshot flows for Test 1351 are based on the GD/DD AVG combination from the beginning of the blowdown but not beyond a void fraction of 0.98 where the division by fluctuating low density results in increased uncertainty in calculated flow. Beyond 0.98 void fraction the flow values derived from the TM AVG curve are preferred. However, for Test 1351, as shown in Figure 2-23, the TM AVG curve stays below the GD/DD AVG curve. A transition from the GD/DD AVG curve at a void fraction of 0.98 to the TM AVG curve can be made along the HI TM curve between approximately 56 and 70 seconds in Figure 2-23. This is possible because the HI TM curve is higher than the LO TM curve during most of the second flow ramp (see Figures 2-9, 2-26, 2-23 and discussion in Volume III, Section 5.2.3). To minimize the matter of interpreting the individual vs average turbine meter flowrates for initial comparison of transient and steady-state performance, the transient point at 73.6 seconds was selected where both individual and average turbine meter flowrates were the same (Figure 2-23). Also, for the intermediate flow point selected at 48.6 seconds there was agreement between the GD/DD AVG and HI TM curves.

Snapshots of the transient pump conditions were extracted from the Test 1319 data in a manner similar to that for Test 1351. Figure 2-27 shows the smooth curve of suction void fraction vs. time drawn manually through the machine-plotted gamma densitometer data shown in Figure 2-28. The void fractions selected for steady-state vs transient comparisons and corresponding plot times are indicated in Figure 2-27. Hand-smoothed curves of data for other operating conditions are also marked with the same plot times as shown in Figures 2-29 through 2-42. The values of the various operating parameters, as read from the smoothed curves at the designated times are presented in Table 2-2. Smoothed curves of data for the transient pump performance parameters, the pump head and pump hydraulic torque, were also generated in a similar fashion and are presented along with the machine-plotted curves in Figures 2-43 through 2-46. Using these curves as the basis, the homologous performance parameter values were derived for the designated plot times. These values are listed in Table 2-2 as the calculated quantities.

As seen from Figures 2-29 through 2-46, several of the parameter curves were very steep at the 0.20 void fraction point. For these curves, the snapshot

TEST 1319/1000 PSI FW FWD BDN
VOID FRACTION BEAM 2 GD SUCTION
PLOT No. 16

SMOOTH CURVE DRAWN MANUALLY THROUGH MACHINE PLOT OF 20 POINTS/SEC DATA (SEE SAME PLOT No., NEXT PAGE)

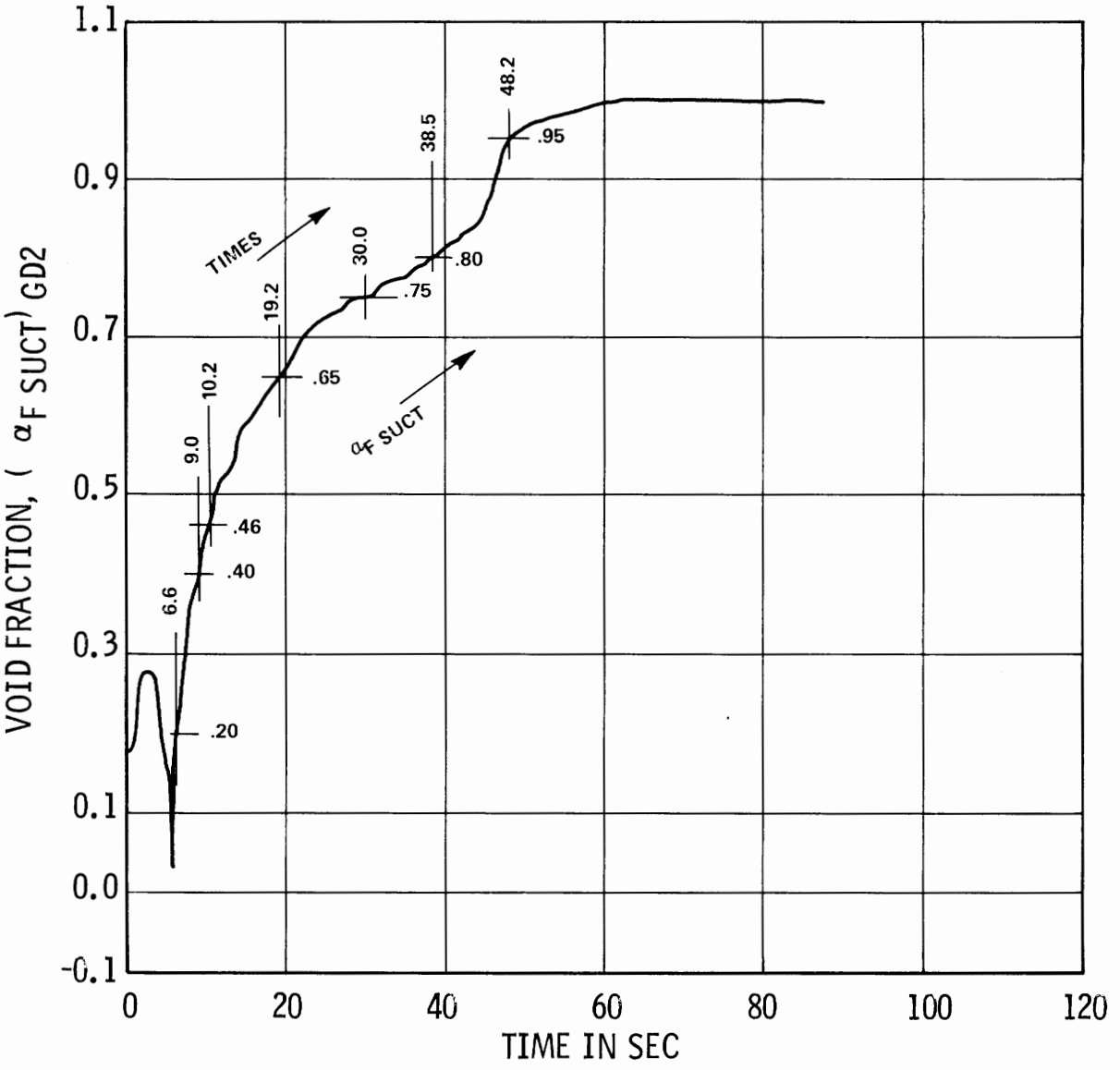

Figure 2-27. Test 1319, Smoothened Curve of Upstream Void Fraction vs Time

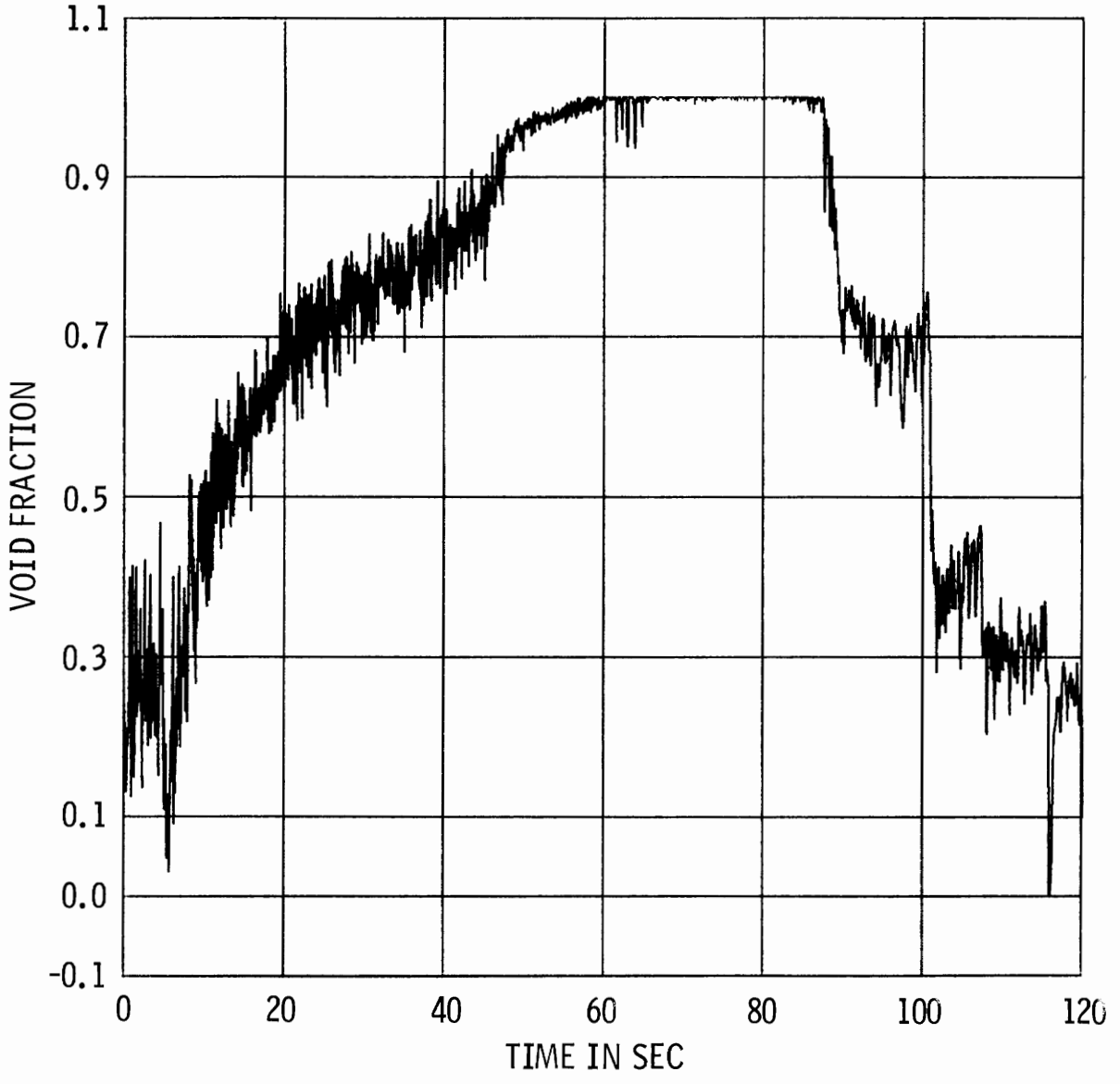

Figure 2-28. Test 1319, Machine-Plotted Curve of Upsteam Void Fraction vs Time

TEST 1319/1000 PSI FW FWD BDN
PUMP SUCTION PRESSURE
PLOT No. 1

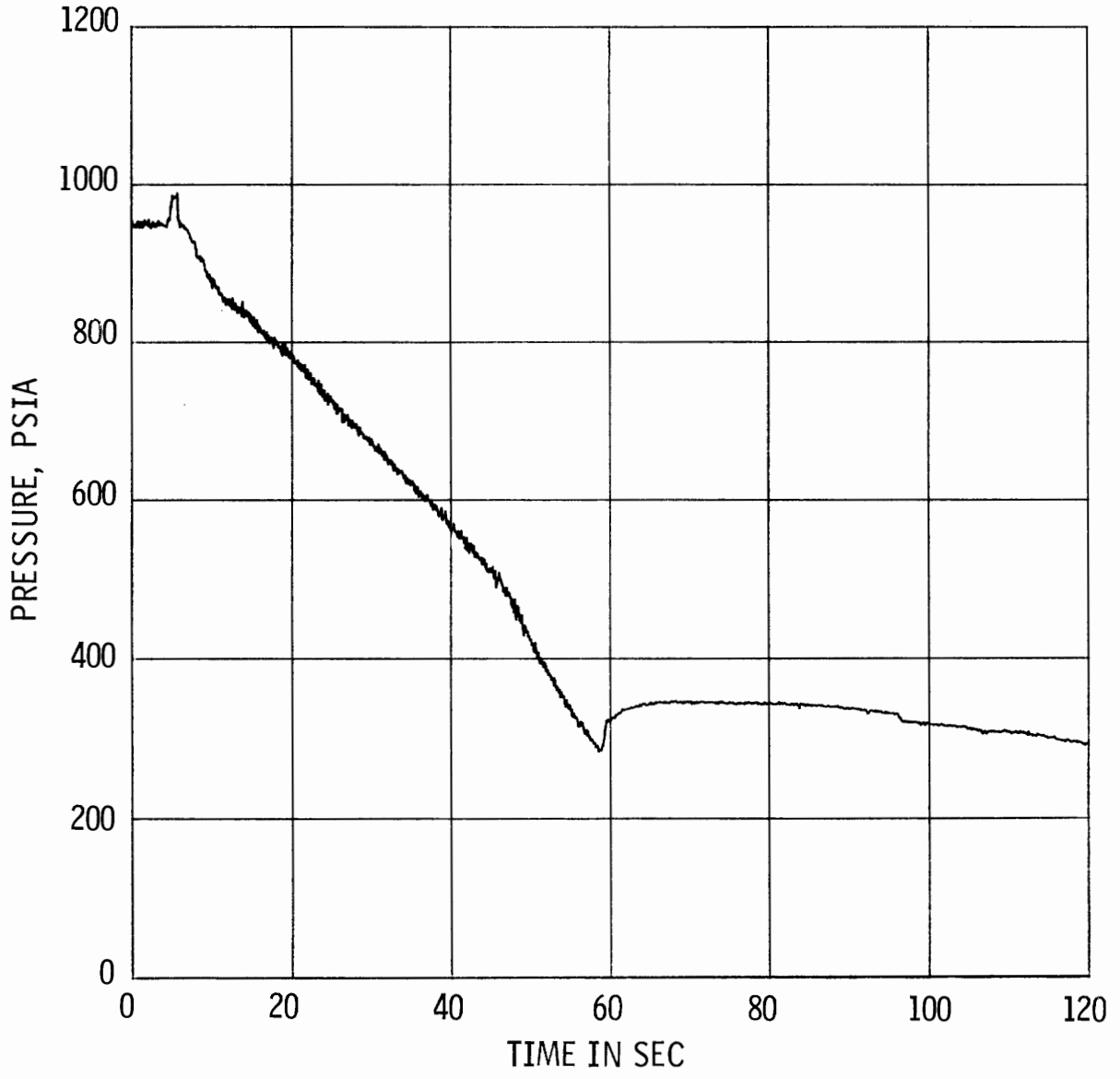

Figure 2-29. Test 1319, Pump Suction Pressure vs Time

TEST 1319/1000 PSI FW FWD BDN
PUMP SUCTION PRESSURE
PLOT No. 1

SMOOTH CURVE DRAWN MANUALLY THROUGH MACHINE PLOT OF
20 POINTS/SEC DATA (SEE SAME PLOT No., PRECEDING PAGE)

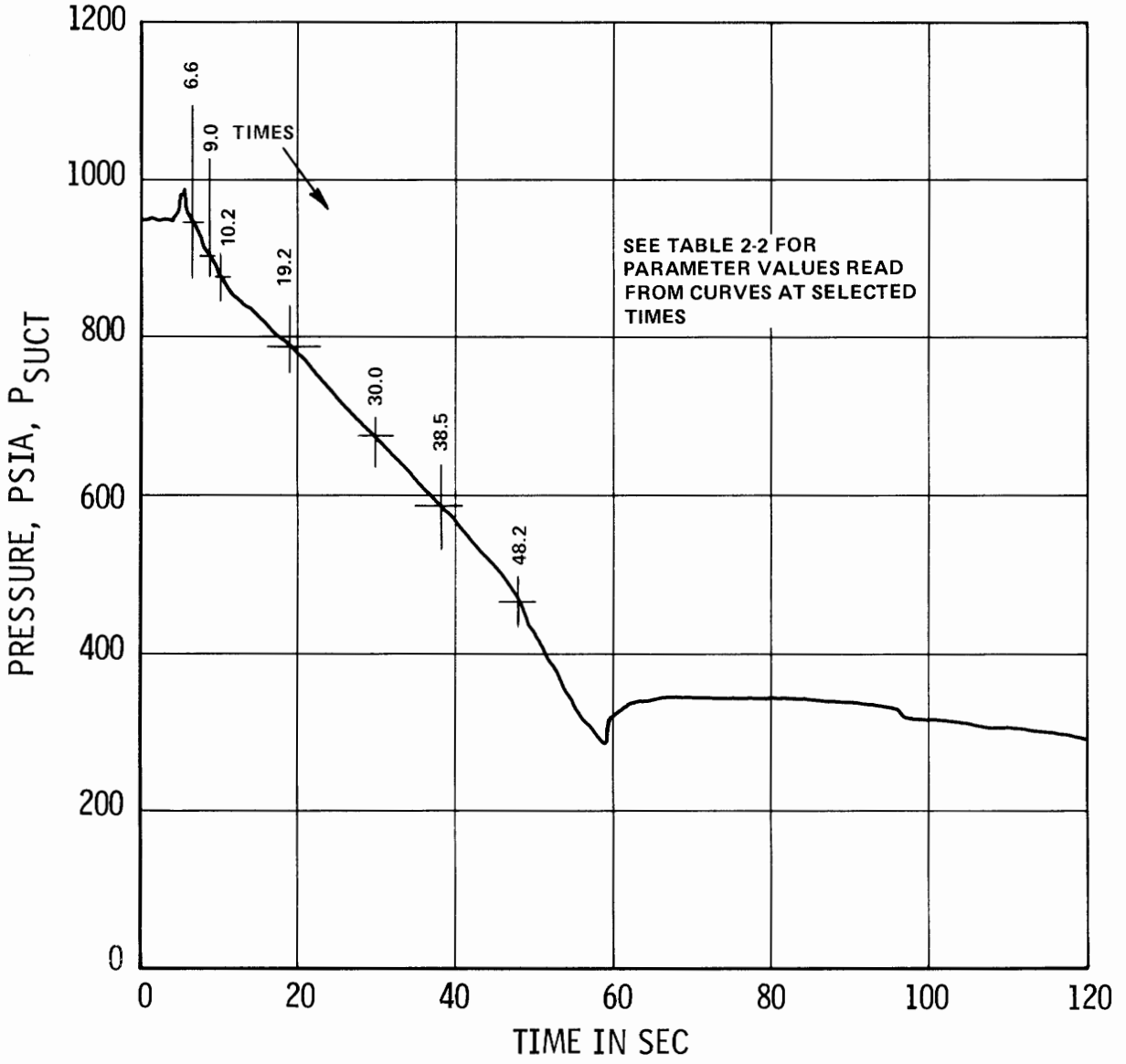

Figure 2-30. Smoothened Curve of Figure 2-29

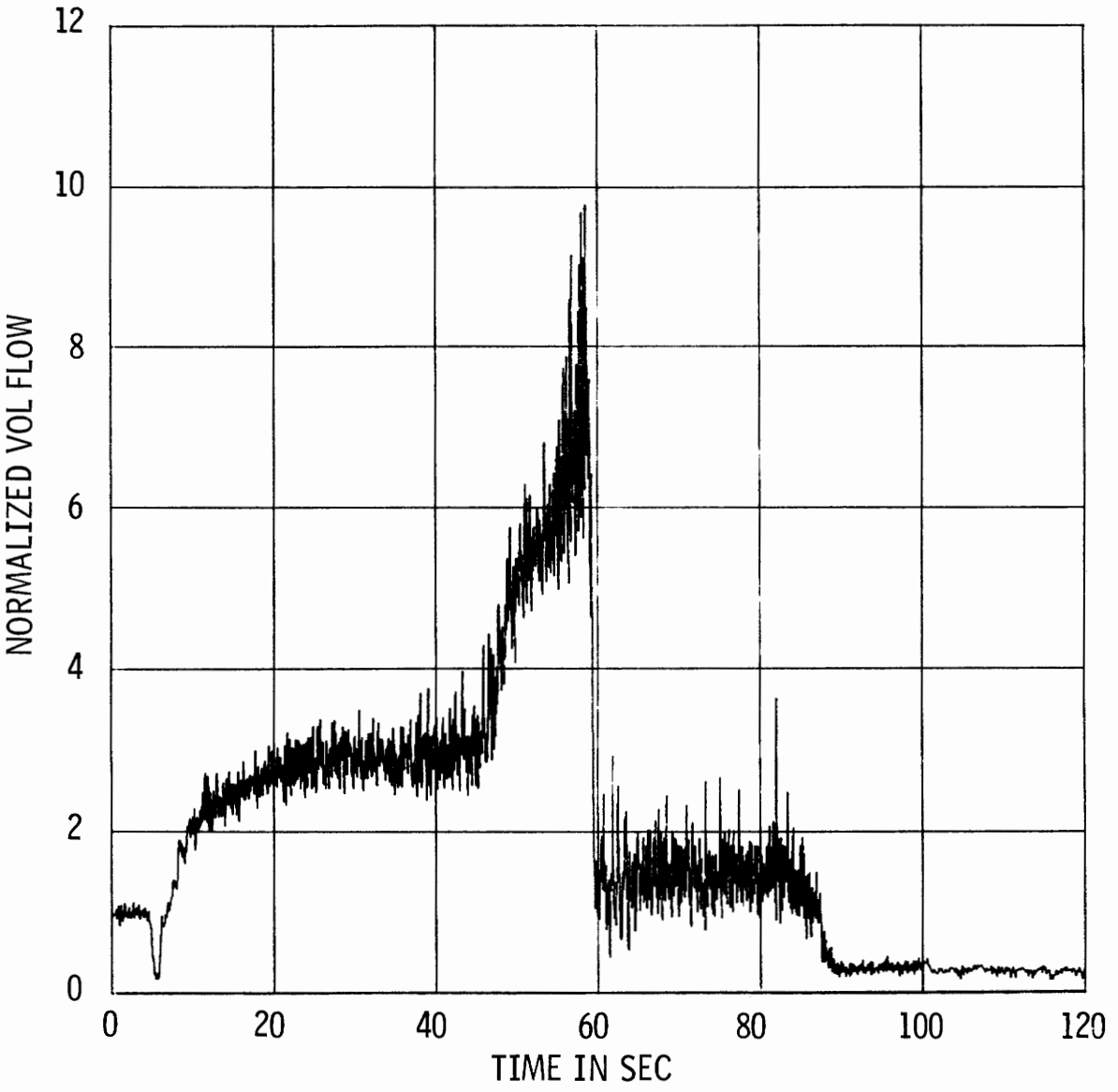

Figure 2-31. Test 1319, Normalized Suction Volumetric Flow Rate vs Time, Based on Gamma Densitometer Beam 2 and Averaged High and Low Drag Disc Data

TEST 1319/1000 PSIA FW FWD BDN
N VOL FLOW GD/DD AVG S QR = 3500
PLOT No. 67

SMOOTH CURVE DRAWN MANUALLY THROUGH MACHINE PLOT OF
20 POINTS/SEC DATA (SEE SAME PLOT No., PRECEDING PAGE)

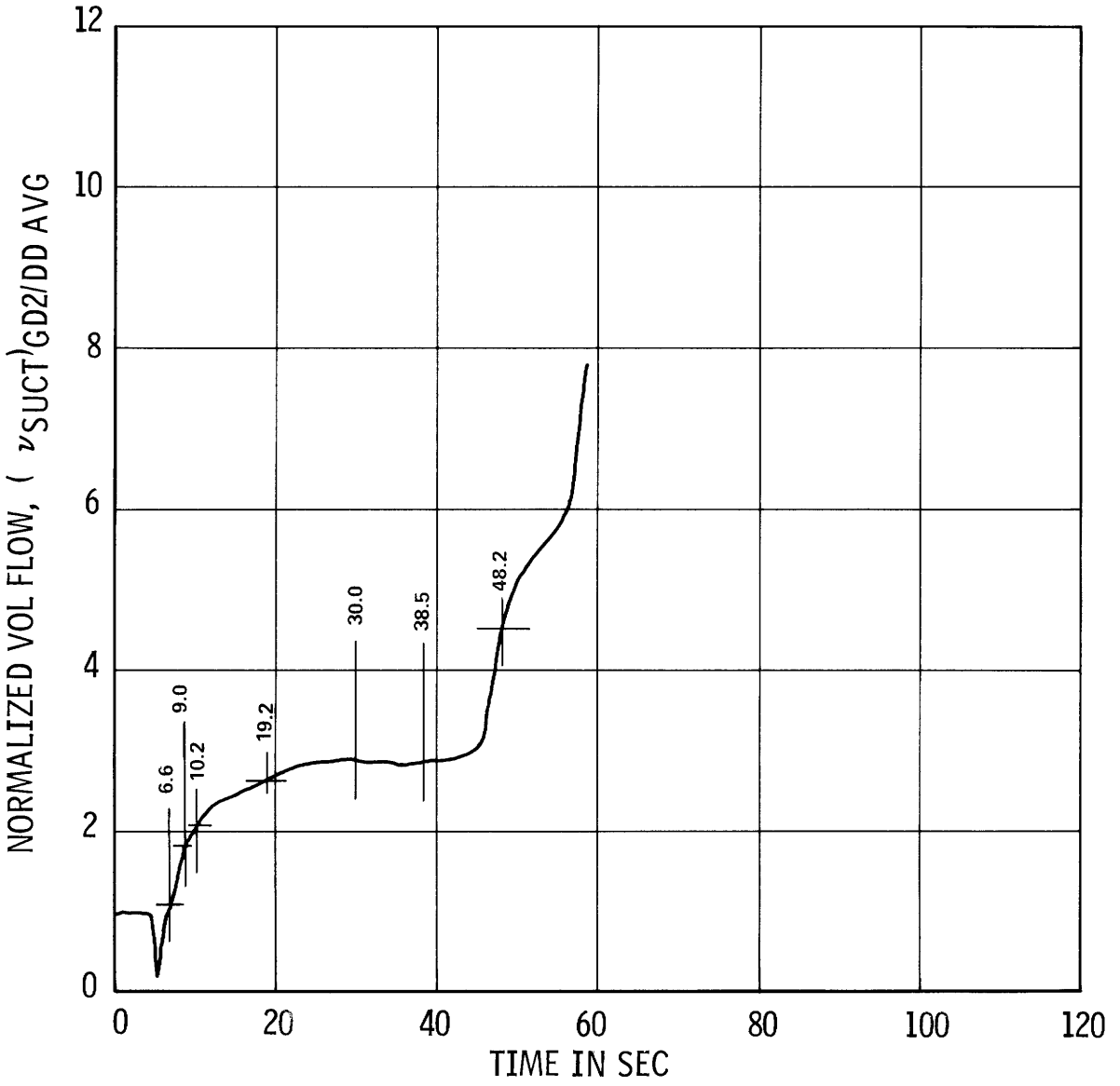

Figure 2-32. Smoothened Curve of Figure 2-31

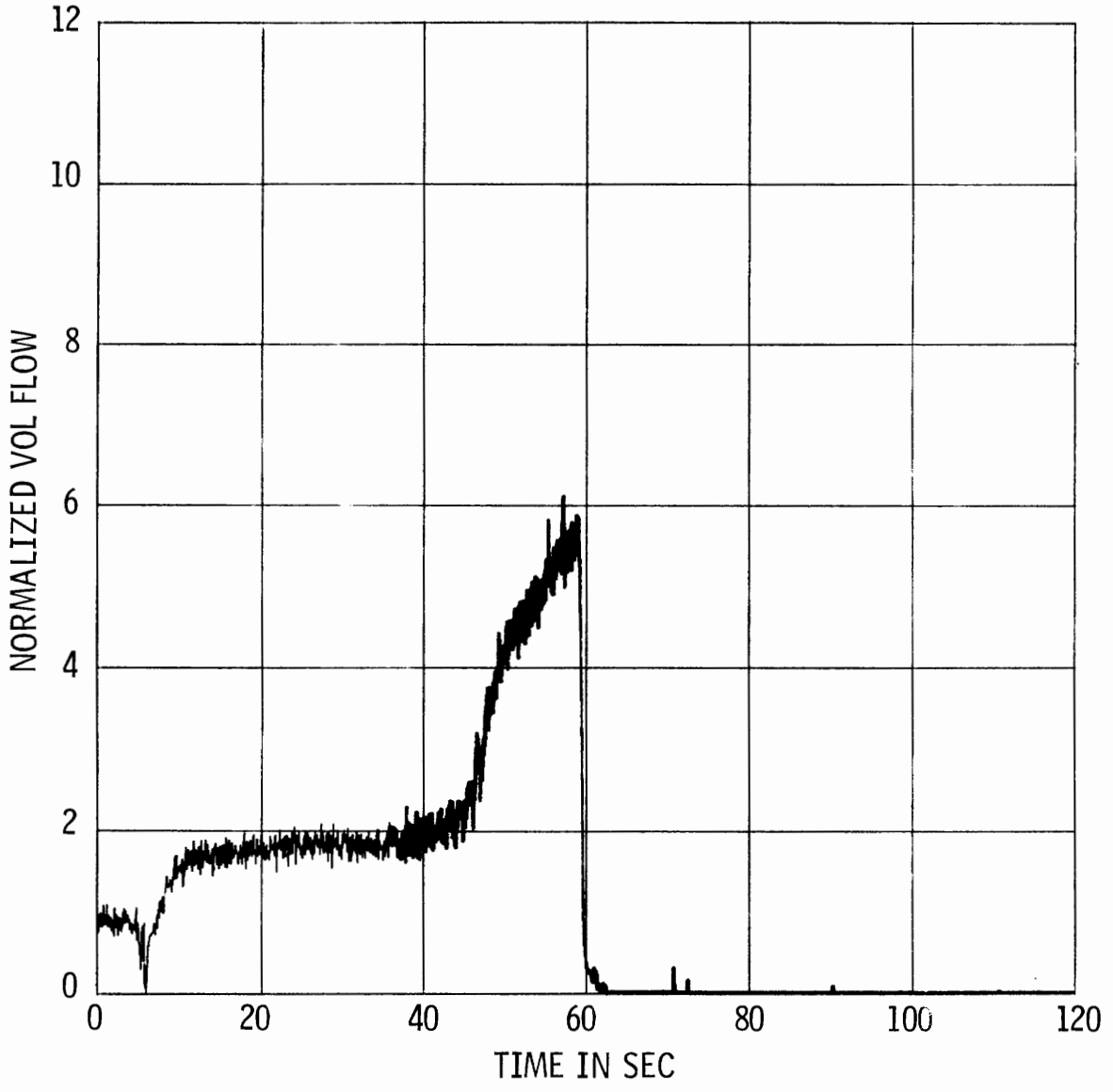

Figure 2-33. Test 1319, Noramlized Suction Volumetric Flow Rate vs Time, Based on Averaged High and Low Turbine Meter Data

TEST 1319/1000 PSIA FW FWD BDN
N VOL FLOW TM AVG SUC QR = 3500
PLOT No. 69

SMOOTH CURVE DRAWN MANUALLY THROUGH MACHINE PLOT OF
20 POINTS/SEC DATA (SEE SAME PLOT No., PRECEDING PAGE)

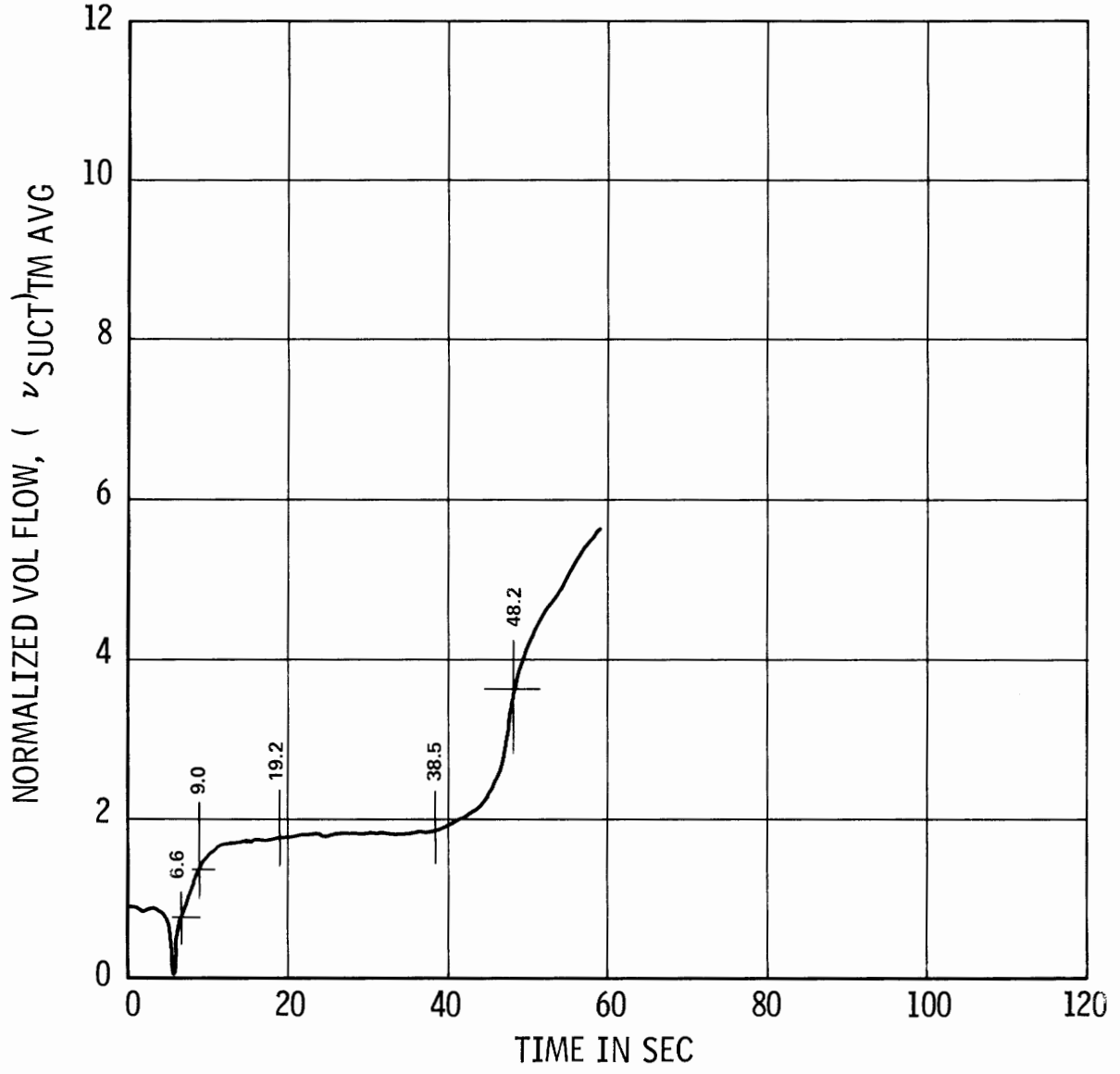

Figure 2-34. Smoothened Curve of Figure 2-33

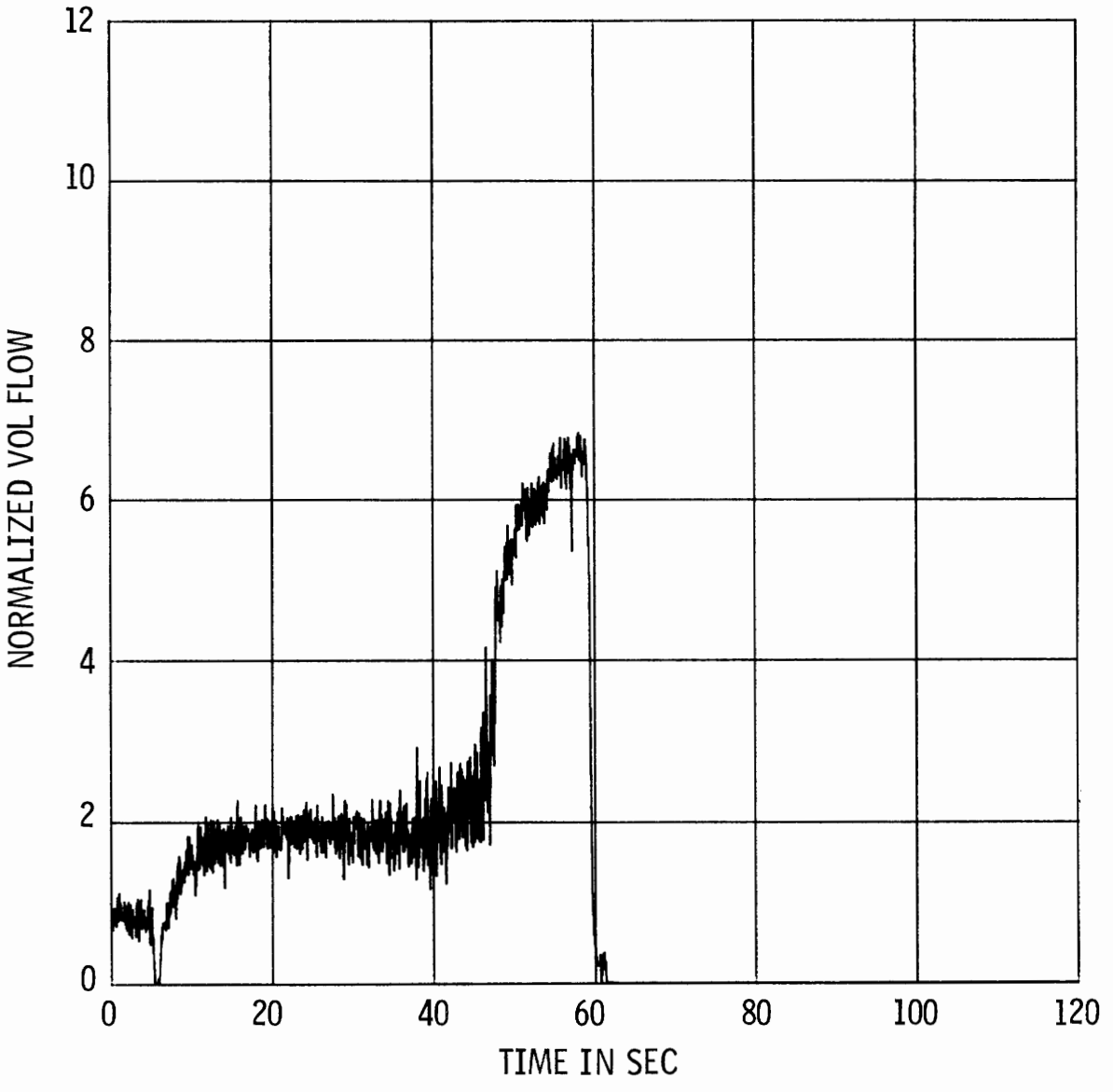

Figure 2-35. Test 1319, Normalized Suction Volumetric Flow Rate vs Time, Based on High Turbine Meter Data

TEST 1319/1000 PSI FW FWD BDN
N VOL FLOW HI-TM SUCT QR = 3500
PLOT No. 27

SMOOTH CURVE DRAWN MANUALLY THROUGH MACHINE PLOT OF 20 POINTS/SEC DATA (SEE SAME PLOT No., PRECEDING PAGE)

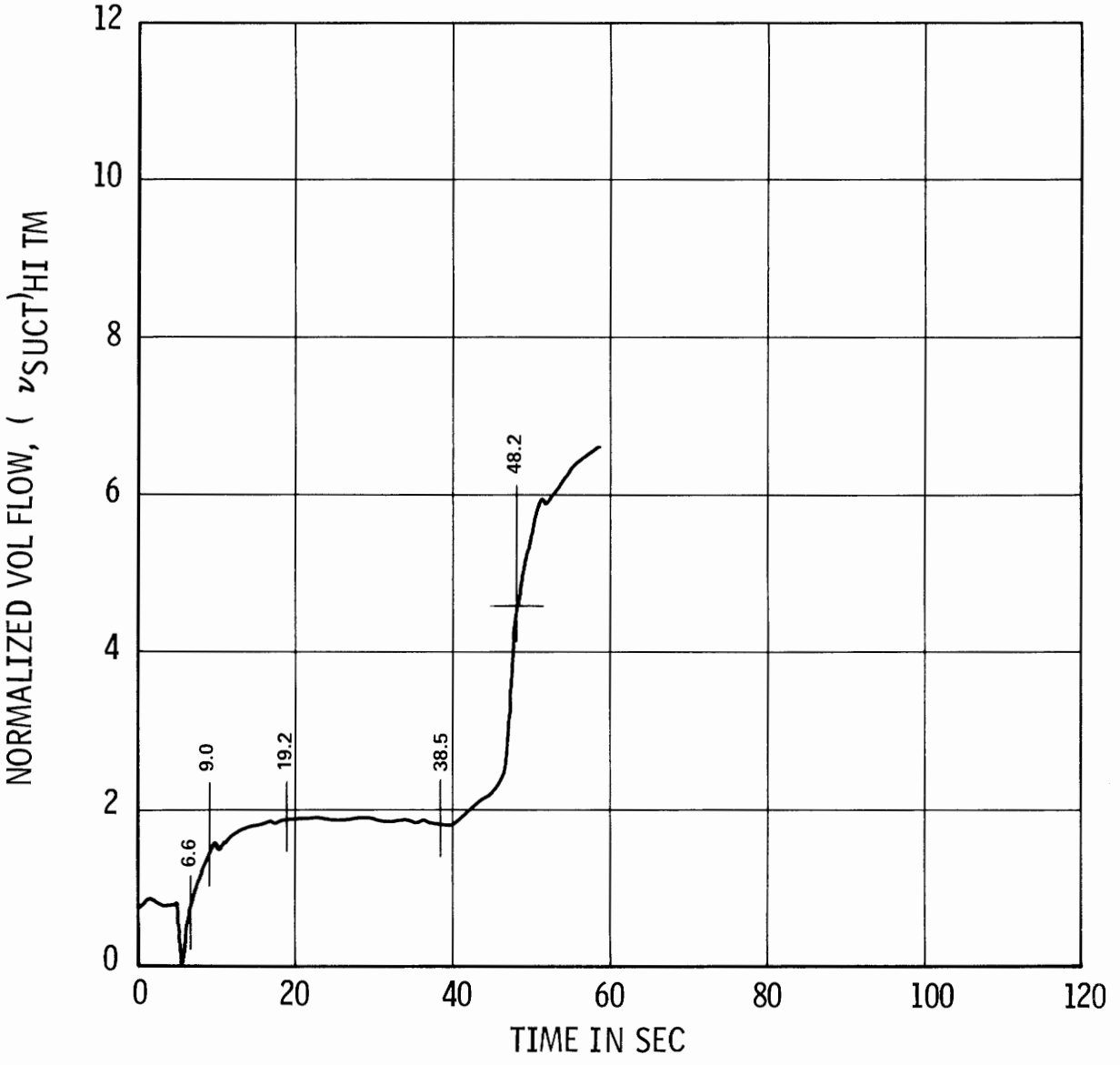

Figure 2-36. Smoothened Curve of Figure 2-35

TEST 1319/1000 PSI FW FWD BDN
N PUMP SPEED NR = 4500
PLOT No. 47

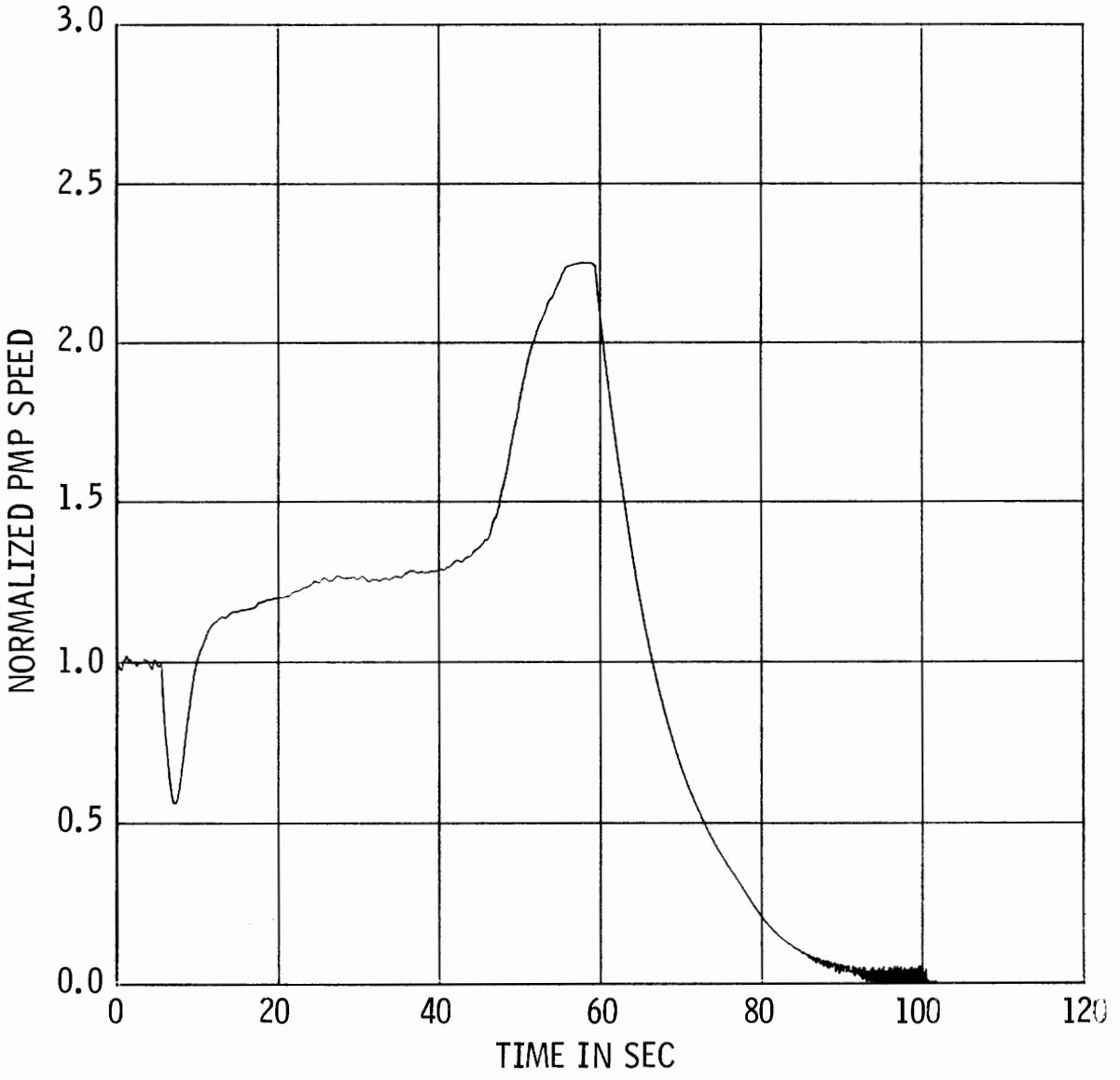

Figure 2-37. Test 1319, Normalized Pump Speed vs Time

TEST 1319/1000 PSI FW FWD BDN
N PUMP SPEED NR = 4500
PLOT No. 47

SMOOTH CURVE DRAWN MANUALLY THROUGH MACHINE PLOT OF
20 POINTS/SEC DATA (SEE SAME PLOT No., PRECEDING PAGE)

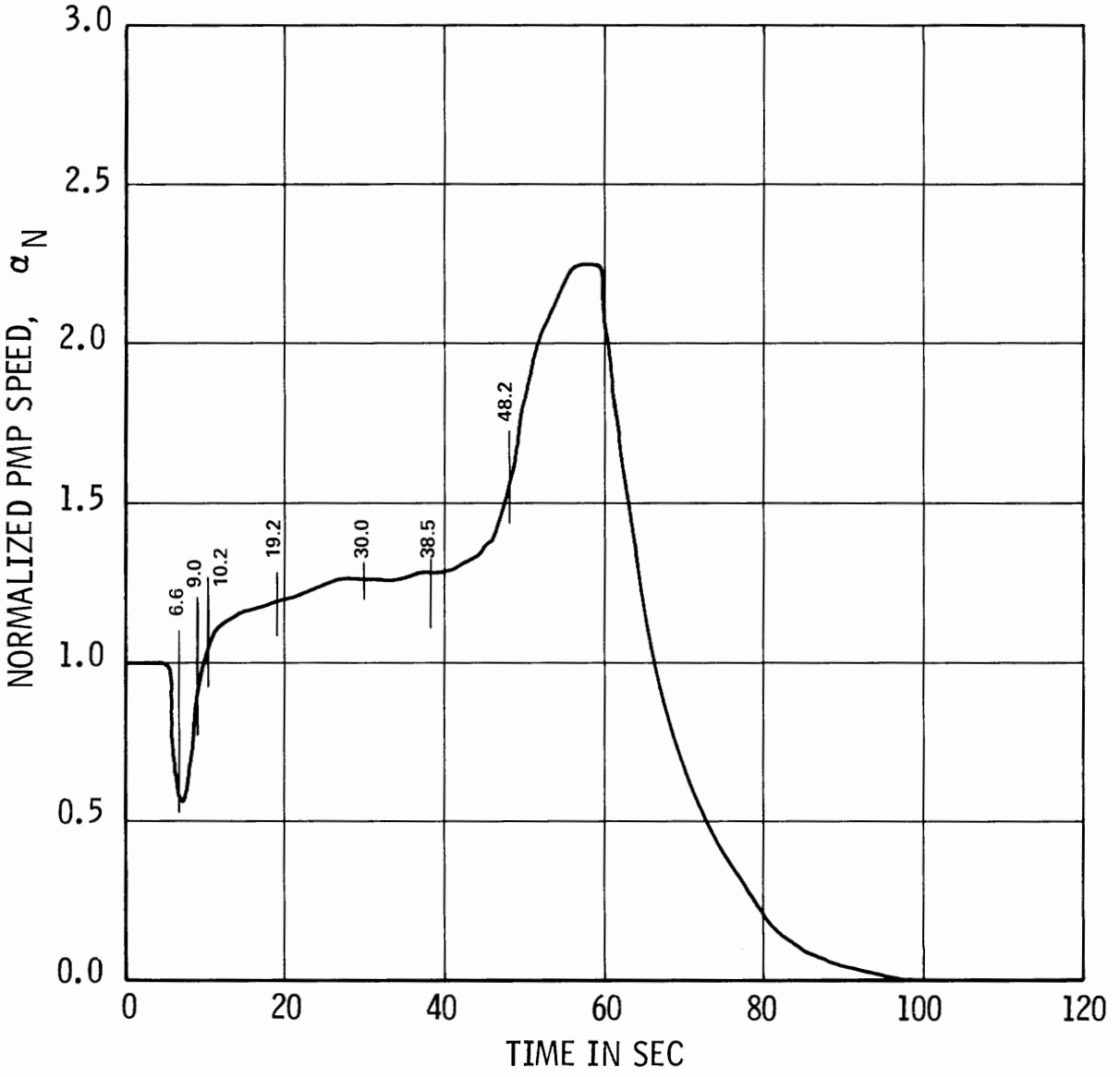

Figure 2-38. Smoothened Curve of Figure 2-37

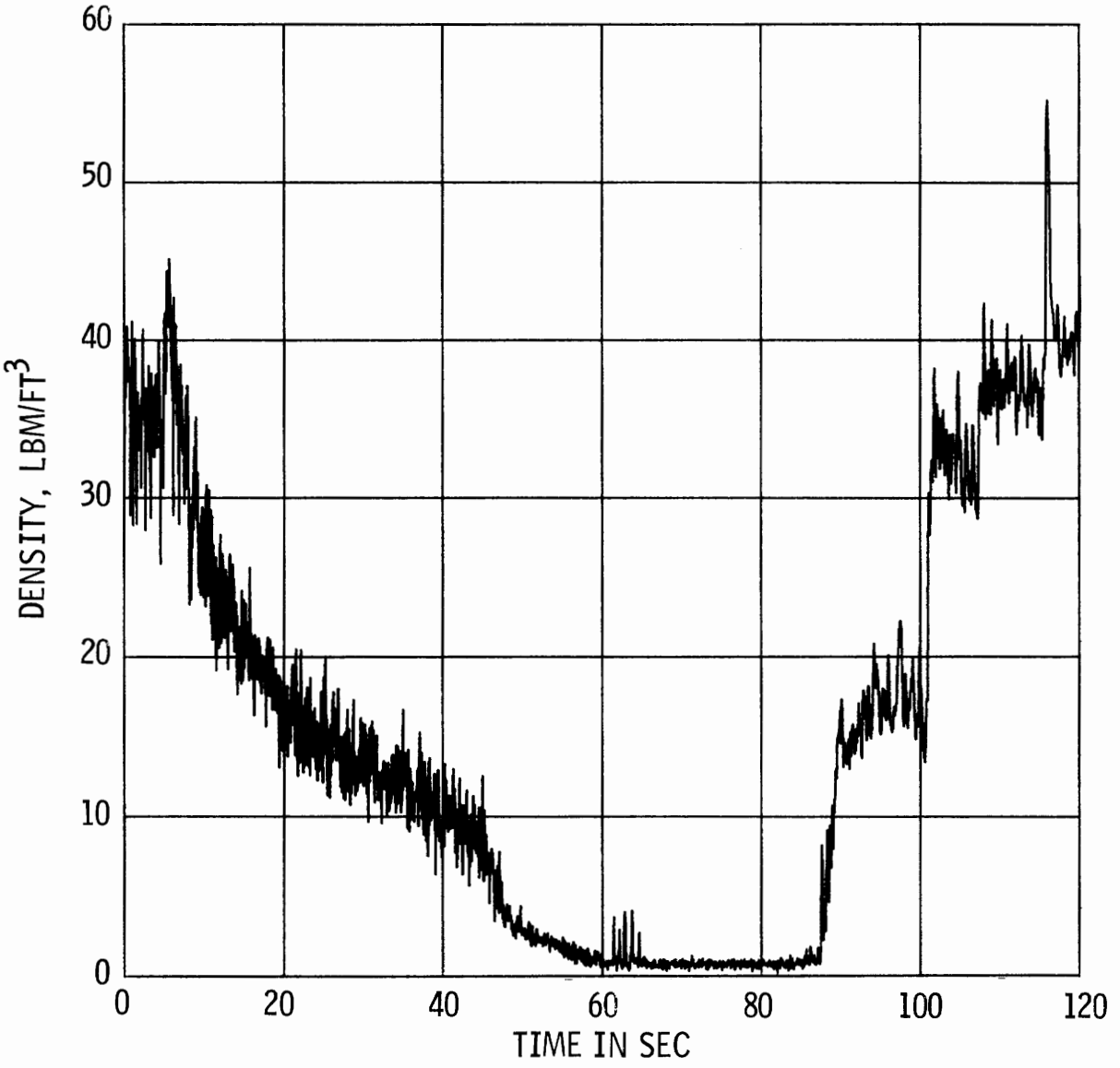

Figure 2-39. Test 1319, Suction Density vs Time, Based on Gamma Densitometer Data

TEST 1319/1000 PSI FW FWD BDN
DENSITY BEAM 2 GD SUCTION
PLOT No. 7

SMOOTH CURVE DRAWN MANUALLY THROUGH MACHINE PLOT OF
20 POINTS/SEC DATA (SEE SAME PLOT No., PRECEDING PAGE)

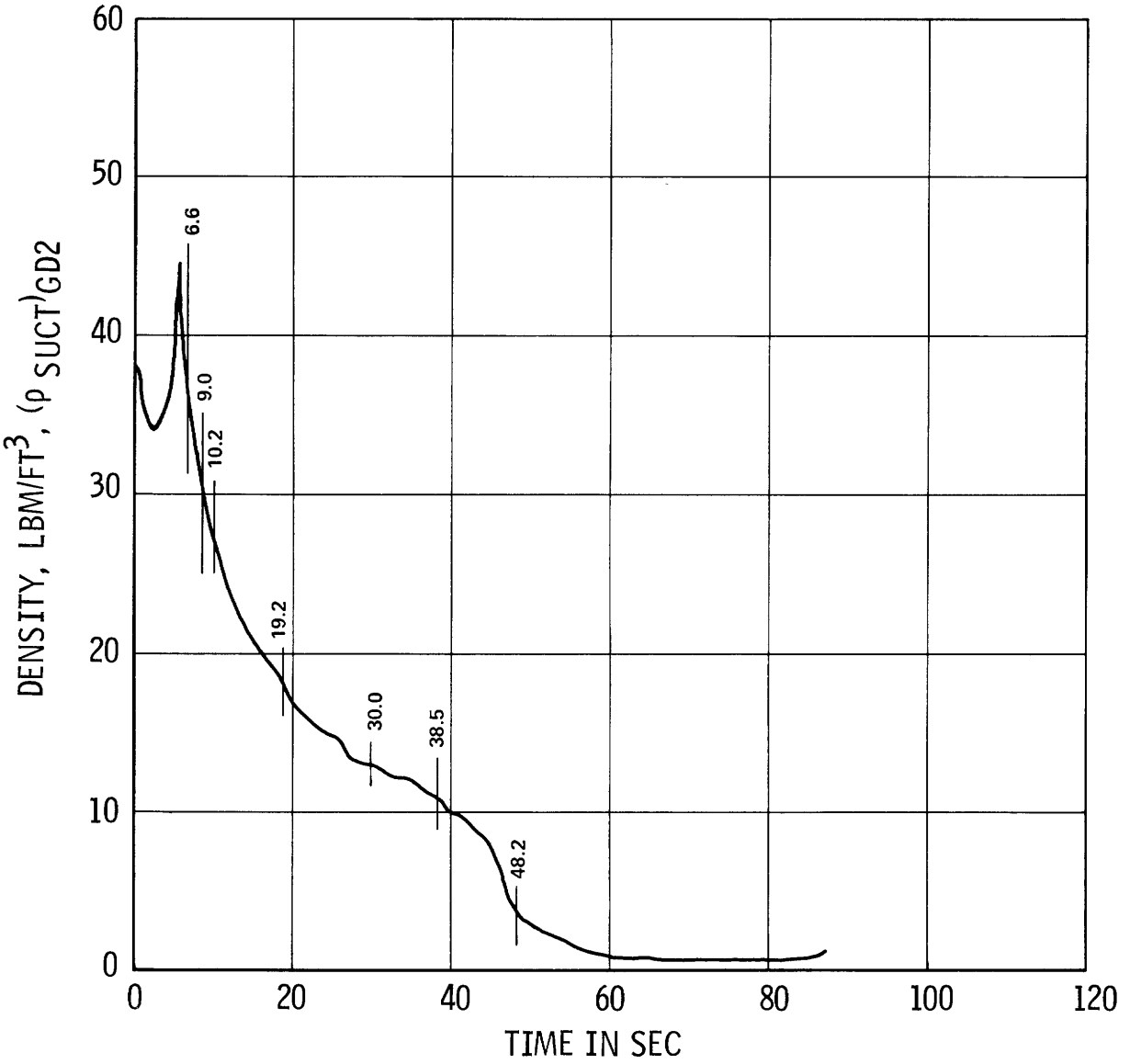

Figure 2-40. Smoothened Curve of Figure 2-39

TEST 1319/1000 PSI FW FWD BDN
DENSITY BEAM 2 GD DISCHARGE
PLOT No. 10

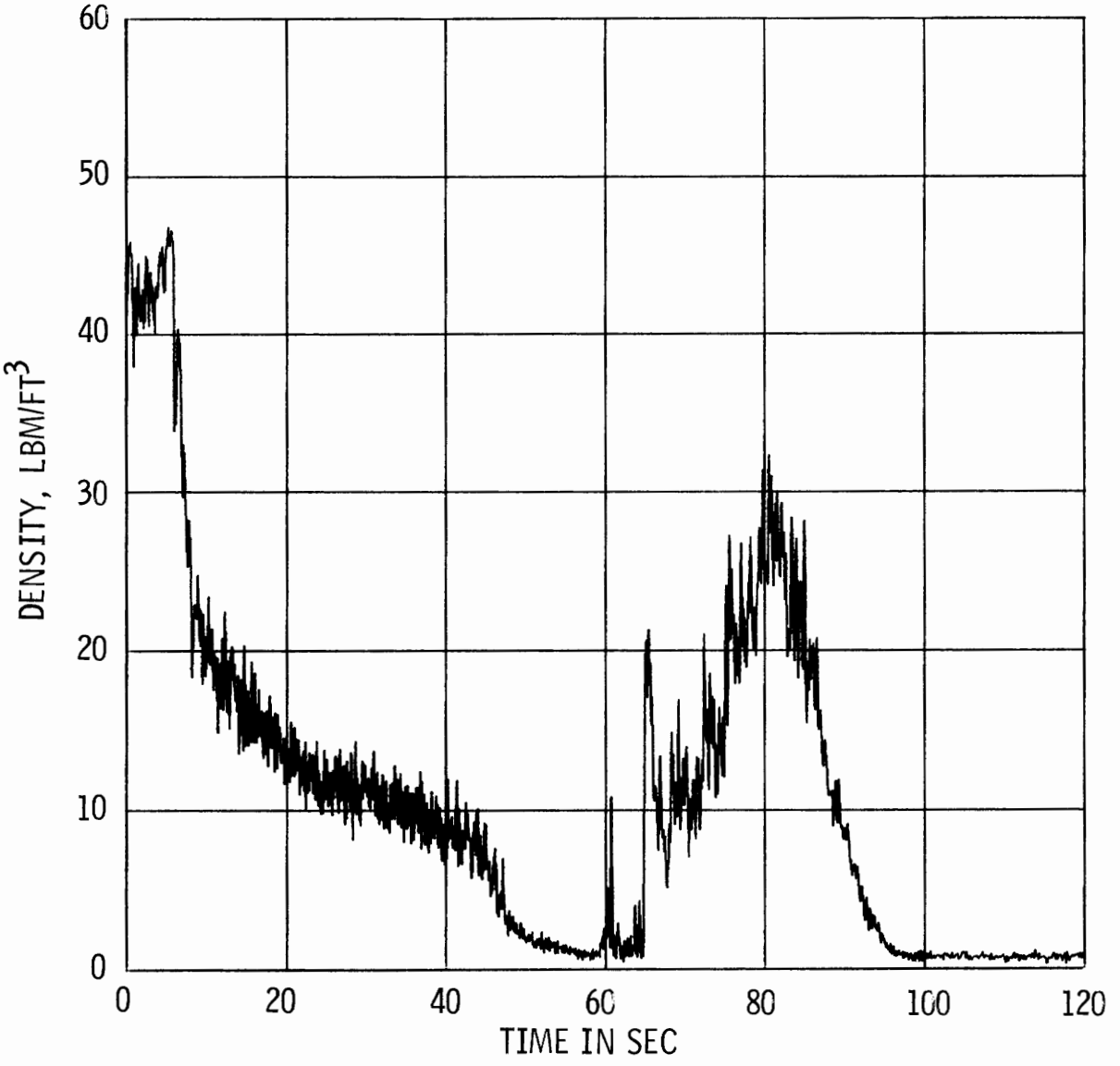

Figure 2-41. Test 1319, Discharge Density vs Time, Based on Gamma Densitometer Data

TEST 1319/1000 PSI FW FWD BDN
DENSITY BEAM 2 GD DISCHARGE
PLOT No. 10

SMOOTH CURVE DRAWN MANUALLY THROUGH MACHINE PLOT OF
20 POINTS/SEC DATA (SEE SAME PLOT No., PRECEDING PAGE)

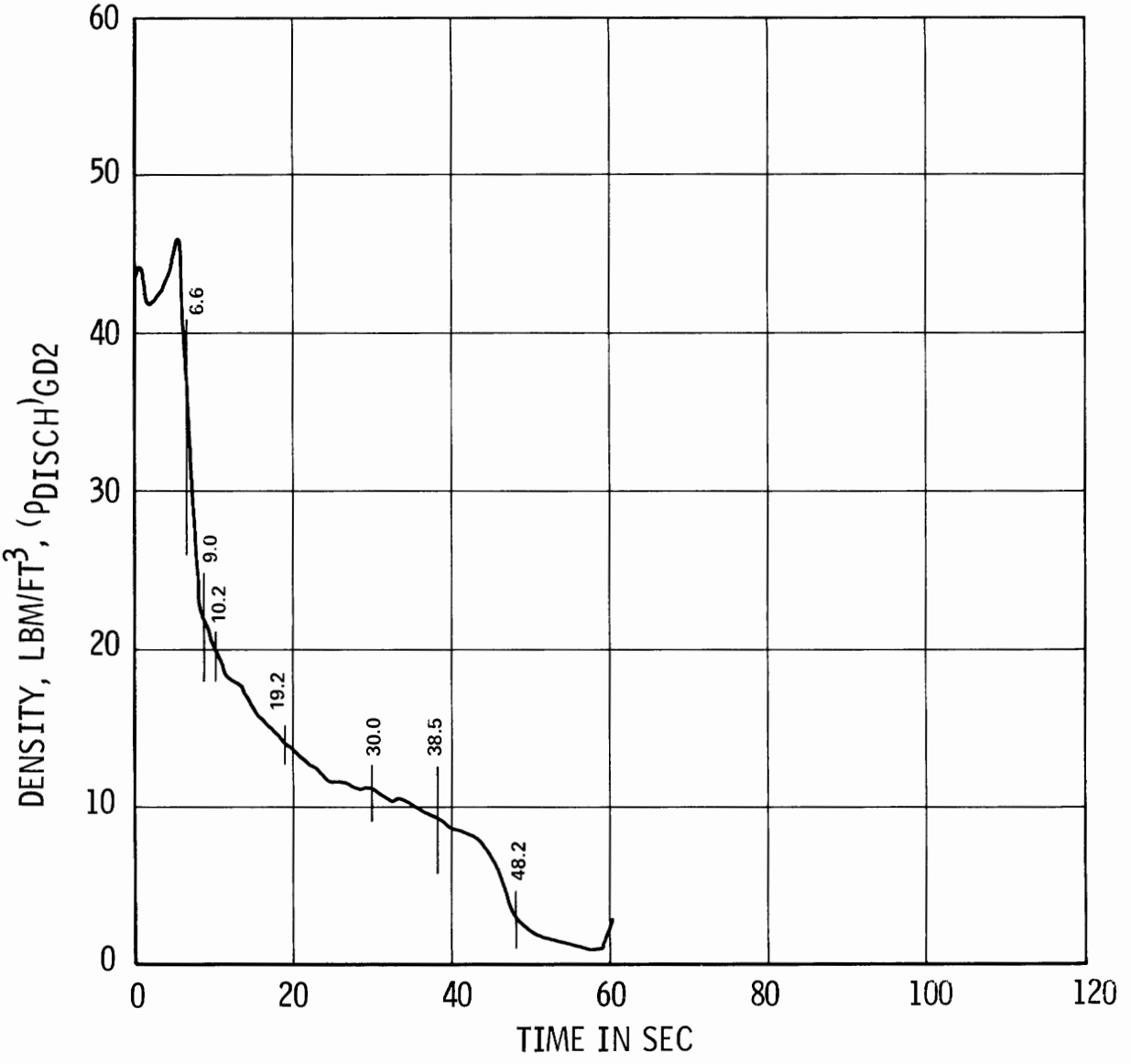

Figure 2-42. Smoothened Curve of Figure 2-41

Table 2-2

TRANSIENT PUMP CONDITIONS AND PERFORMANCE SNAPSHOTS FROM TRANSIENT TEST 1319

PARAMETER	POINT:	T	U	V	W	X	Y	Z
Quantities from smooth curves								
(α_F suct) GD2		0.20	0.40	0.46	0.65	0.75	0.80	0.95
Time, sec		6.6	9.0	10.2	19.2	30.0	38.5	48.2
P suct, psia		947	900	876	786	674	587	466
(ν suct) GD2/DD AVG		0.915	1.824	2.060	2.640	2.900	2.875	4.532
(ν suct) TM AVG								3.636
(ν suct) HI TM								4.576
α_N		0.598	0.853	1.030	1.195	1.26	1.279	1.558
(ρ suct) GD2, lbm/ft^3		36.8	30.32	26.9	18.0	13.0	10.94	3.66
(ρ disch) GD2, lbm/ft^3		39.7	22.0	20.0	14.1	11.1	9.28	3.00
ΔP leg-leg, psi		-3.5	-102.44	-113.6	-107.0	-96.8	-86.96	-95.48
$T_h/308$		0.155	-0.22	-0.144	-0.08	-0.088	-0.094	-0.213
Calculated quantities								
$\rho_{avg} = \frac{1}{\frac{1}{2}(\frac{1}{\rho_{suct}} + \frac{1}{\rho_{disch}})}$, $\frac{lbm}{ft^3}$		38.2	25.5	22.94	15.81	11.975	10.04	3.297
ν/α_N		1.53	2.138	2.00	2.209	2.302	2.248	2.909
α_N/ν		0.654	0.468	0.50	0.453	0.434	0.445	0.344
$h = \frac{144\ \Delta P}{\rho_{suct} \cdot 252}$		-0.054	-1.931	-2.413	-3.397	4.225	4.542	-14.907
h/ν^2		-0.065	-0.58	-0.569	-0.487	-0.506	-0.55	-0.712
$\beta_h = \frac{T_h}{308} \times \frac{62.3}{\rho_{avg}}$		0.253	-0.538	-0.391	-0.315	-0.458	-0.583	-4.025
β_h/ν^2		0.302	-0.162	-0.092	-0.045	-0.054	-0.071	-0.192

TEST 1319/1000 PSI FW FWD BDN
PUMP HEAD IN PSI
PLOT No. 44

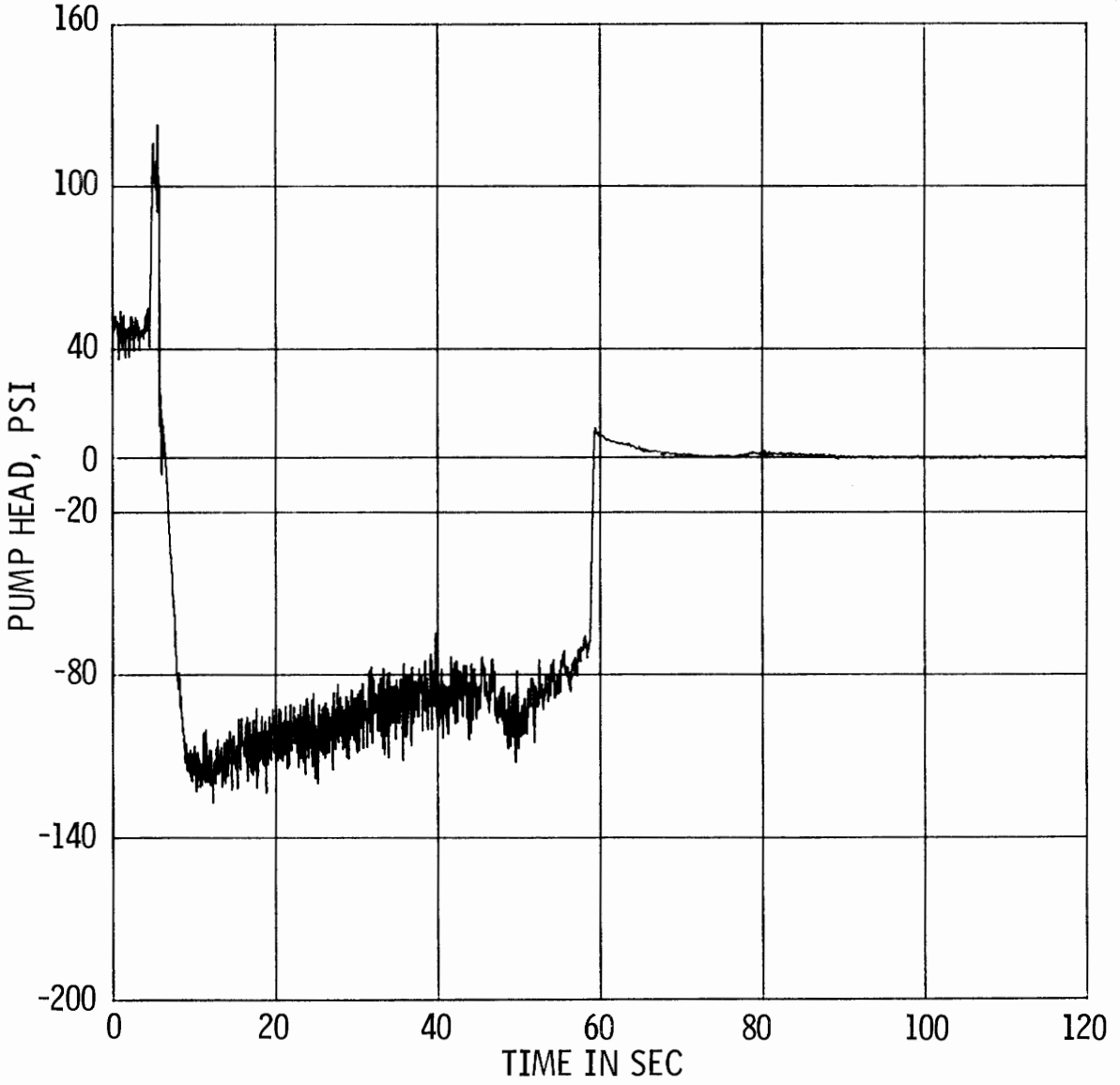

Figure 2-43. Test 1319, Pump Head vs Time

TEST 1319/1000 PSI FW FWD BDN
PUMP HEAD IN PSI
PLOT No. 44

SMOOTH CURVE DRAWN MANUALLY THROUGH MACHINE PLOT OF
20 POINTS/SEC DATA (SEE SAME PLOT No., PRECEDING PAGE)

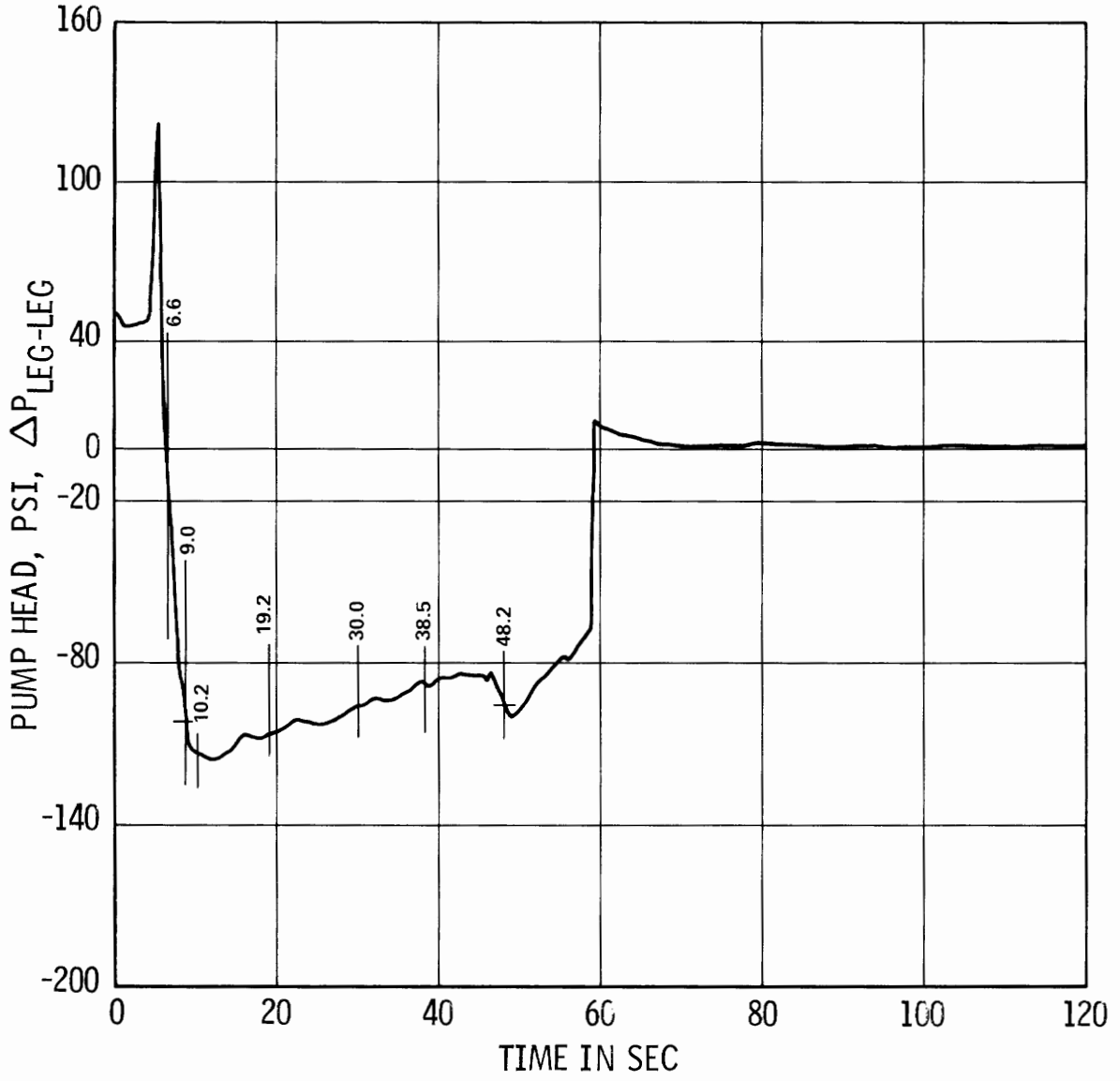

Figure 2-44. Smoothened Curve of Figure 2-43

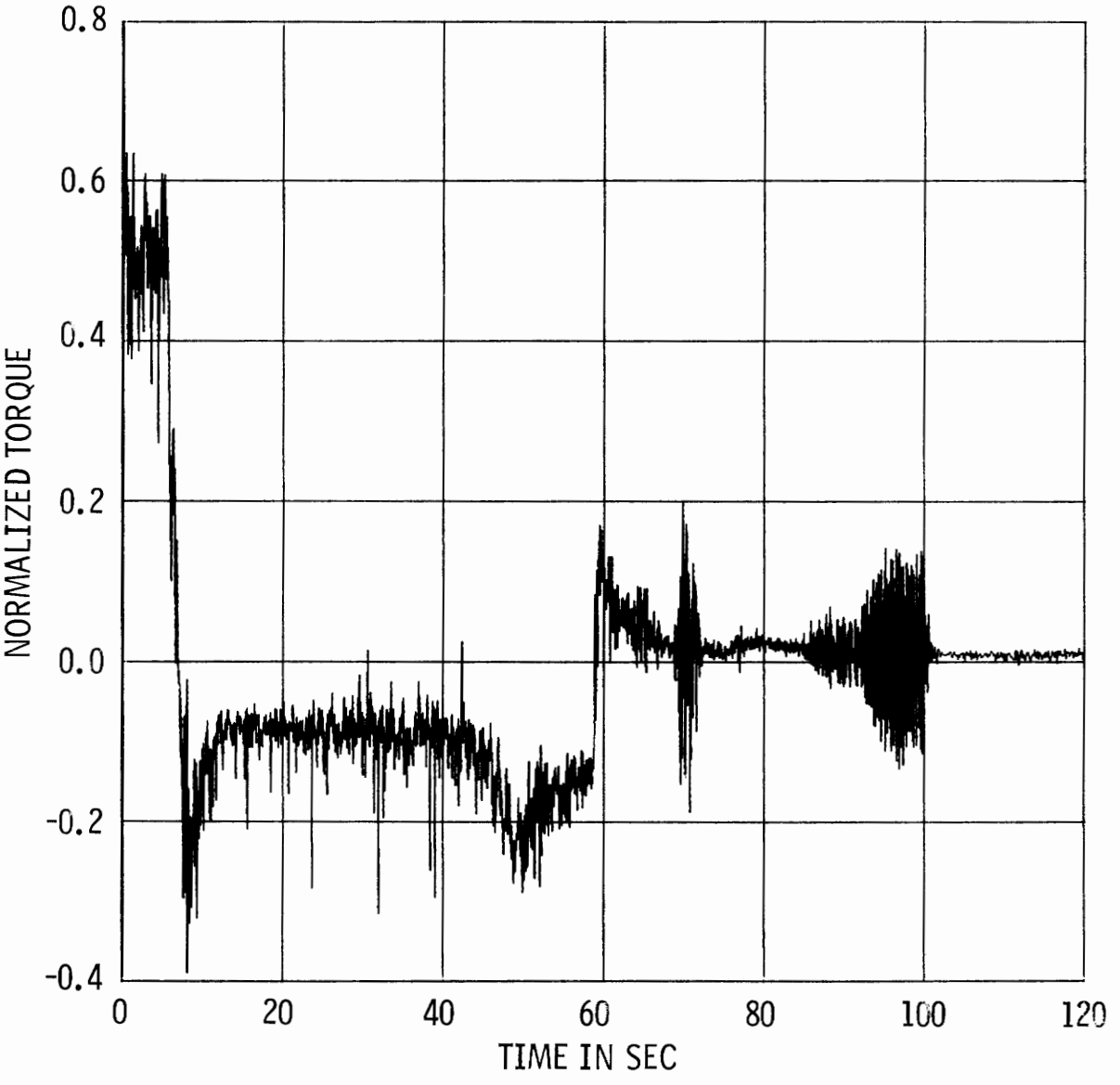

Figure 2-45. Test 1319, Normalized Hydraulic Torque vs Time

TEST 1319/1000 PSI FW FWD BDN
N PUMP HYDR TORQUE THR = 308
PLOT No. 49

SMOOTH CURVE DRAWN MANUALLY THROUGH MACHINE PLOT OF
20 POINTS/SEC DATA (SEE SAME PLOT No., PRECEDING PAGE)

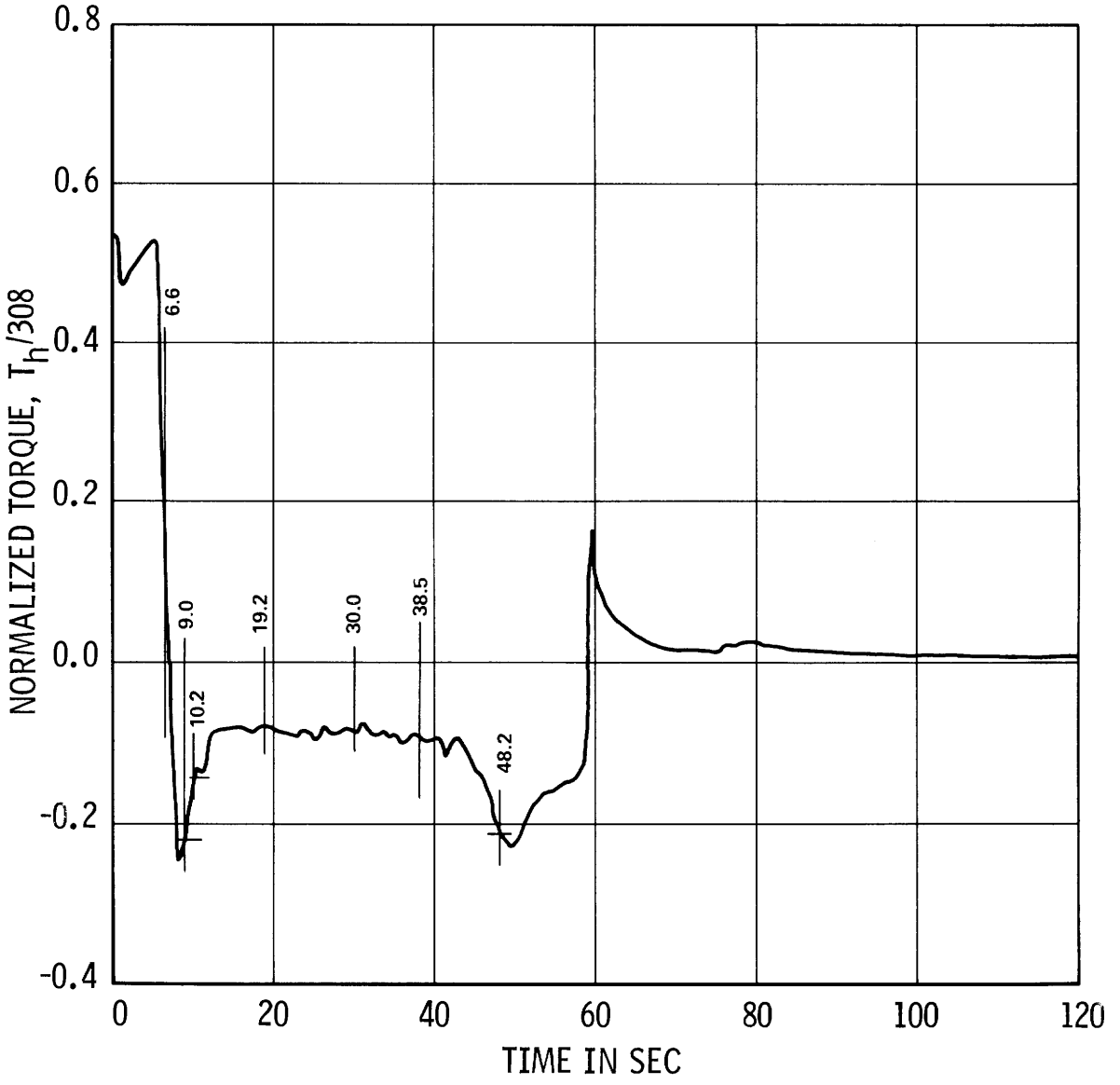

Figure 2-46. Smoothened Curve of Figure 2-45

extraction process was repeated as before, with the curves locally expanded to show the data points in detail (Figure 2-47).

For Test 1319, a total of seven snapshot point were selected similar to those for Test 1351. The 0.20 (point T), 0.40 (point U) and 0.80 (point Y) void fraction points were chosen because performance curves generated from steady-state test data are available for comparison. Points T and U occurred during the initial surge time period (6.6 and 9.0 seconds, respectively on the plots) which is characterized by rapid changes in almost all the operating parameters (α_F, ν, α_N and ρ).

The snapshots at 0.65 (point W), 0.75 (point X) and 0.80 (point Y) void fractions provide comparisons at the intermediate (quasi-steady) time periods during which flow and speed, as well as the performance parameters, changed very little, while the void fraction continued to rise fairly rapidly (see Figures 2-32, 2-38, 2-44, 2-46 and 2-27). The point at 10.2 seconds (point V) with a void fraction of 0.46 was extracted at a ν/α_N ratio of 2.0, because a degradation curve generated from steady-state test data is available at this ν/α_N ratio. This point is located towards the end of the initial surge time period. The remaining snapshot at a void fraction of 0.95 and at a plot time of 48.2 seconds was selected to be during the second surge time period, again to provide comparison at a rapid transient of several conditions, including $d\alpha_F/dt$ (see Figure 2-27). Since the blowdown was terminated before the void fraction reached the value of 1.0, steady-state vs. transient comparison cannot be made at single phase steam condition for Test 1319.

The hand-smoothed curve for the suction side (SIS) volumetric flow rate is based on the average of the two SIS drag discs (DD AVG) and the SIS gamma densitometer center beam (GD2). This curve was developed from the machine-plotted average curve which in turn was generated from the individual SIS GD2/DD curves of Volume III, Figures 5-120 and 5-121. Similarly, the average turbine meter (TM AVG) SIS volumetric flow rate curve (Figure 2-33) was derived from the HI and LO turbine meter SIS volumetric flow rate curves of Figure 2-35 and Volume III Figure 5-123. The volumetric flow rates for the Test 1319 snapshots are also based on the SIS GD2/DD AVG combination. This extended from the beginning of the blowdown until exceeded by values derived from the turbine meter. This is consistent with the criterion employed in the determination of the volumetric

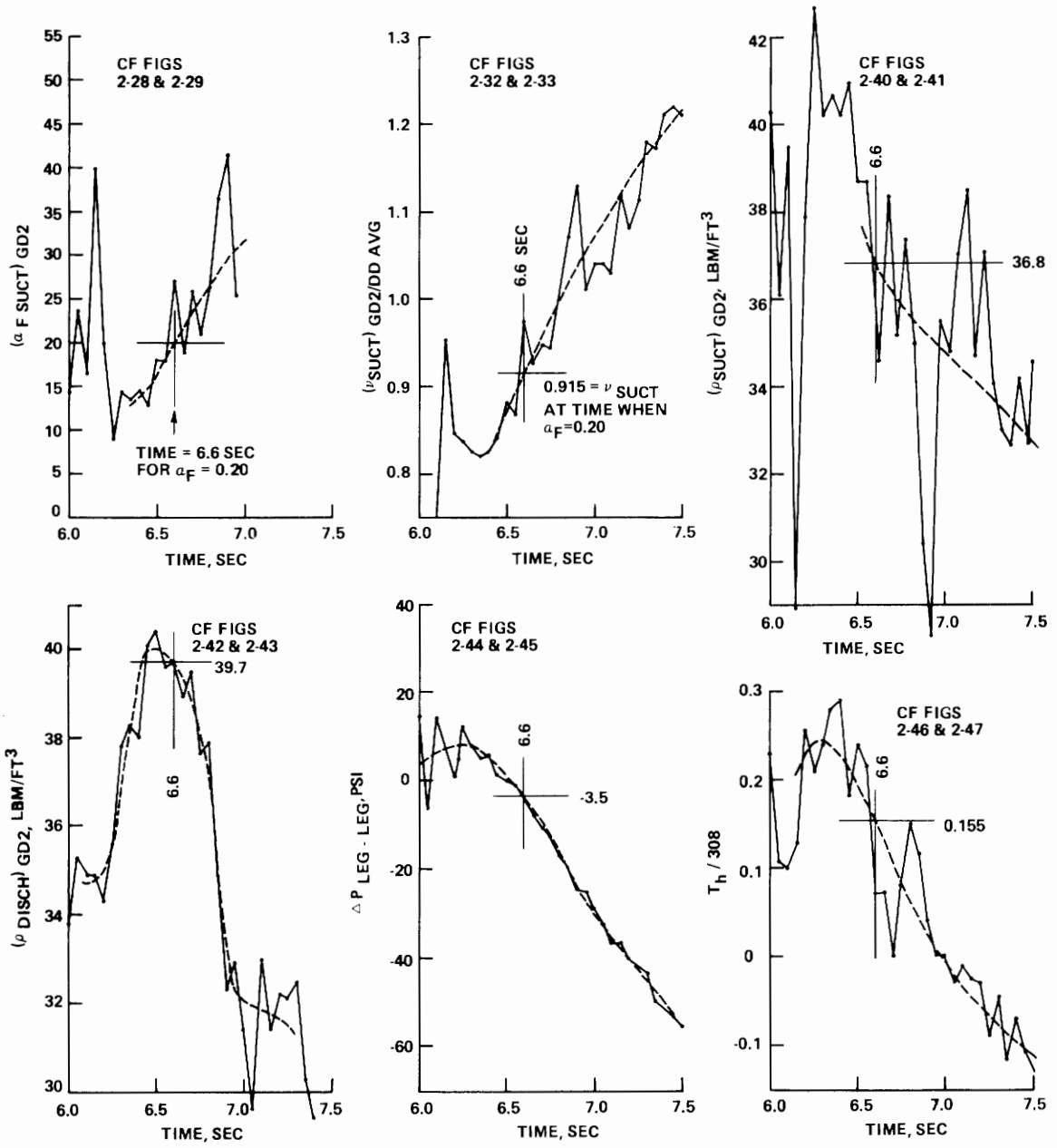

Figure 2-47. Test 1319, Expanded 20 Points/Second Curves and Smoothened Curves Near Time for α_F = 0.20

flow rates for Test 1351 snapshots. As described in Volume III, Section 5.5, the LO turbine meter at the SIS exhibited an atypical behavior after about 45 seconds (see Volume III, Figure 5-123). Consequently, the HI-TM volumetric flow rates at the SIS were employed for blowdown times beyond which the GD2/DD AVG combination volumetric flow rate values remained below those indicated by this turbine meter. There was only one such snapshot point (point Z) for which the HI turbine meter provided the volumetric flow rate. This volumetric flow rate is only slightly larger than that extracted from the GD2/DD AVG volumetric flow rate curve (see Table 2-2).

To show how the transient performance values in Tables 2-1 and 2-2 compare with steady-state data, the transient points are plotted on copies of the pertinent steady-state performance curves in Figures 2-48 to 2-61. Thus, the transient points at void fractions of 0.20, 0.40, 0.80, and approximately 1 are displayed on the steady state performance plots for these same void fractions (Figures 2-48 to 2-55). The transient points at other void fractions are shown on the composite steady-state plots (Figures 2-56 and 2-57), where the comparisons can be made by interpolation. The transient point F at ν/α_N = 4.0 is shown also on the steady-state degradation plots for this ν/α_N in Figures 2-58 and 2-59. Finally, the snapshot at α_F = 0.46 (point V) is shown on the steady-state degradation plots of Figures 2-60 and 2-61 for the ν/α_N ratio of 2.0. Comments on these comparisons are given in Section 4 below.

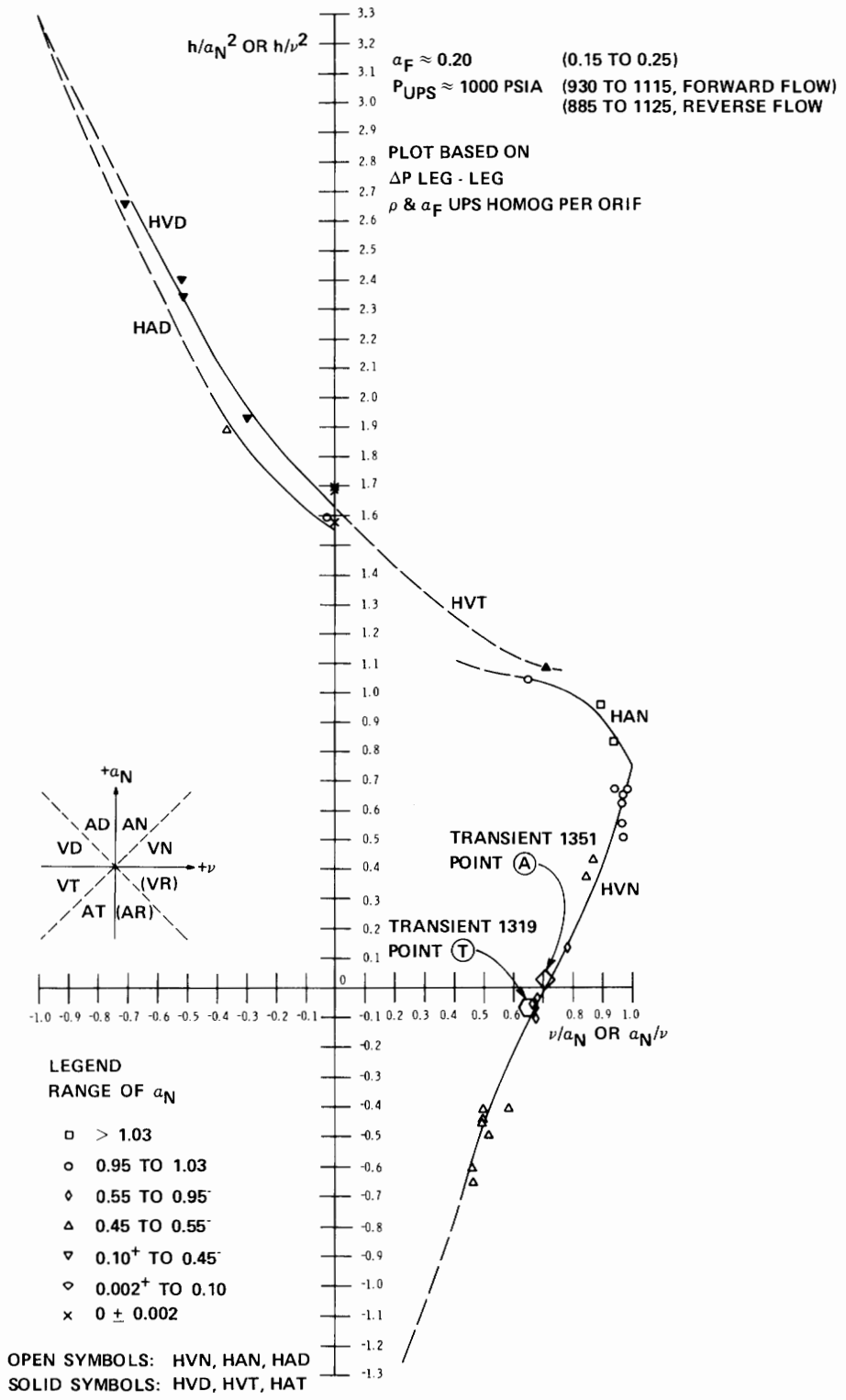

Figure 2-48. Comparison of Transient and Steady-State Performance Data, Homologous Head for Two-Phase, α_F = 0.20

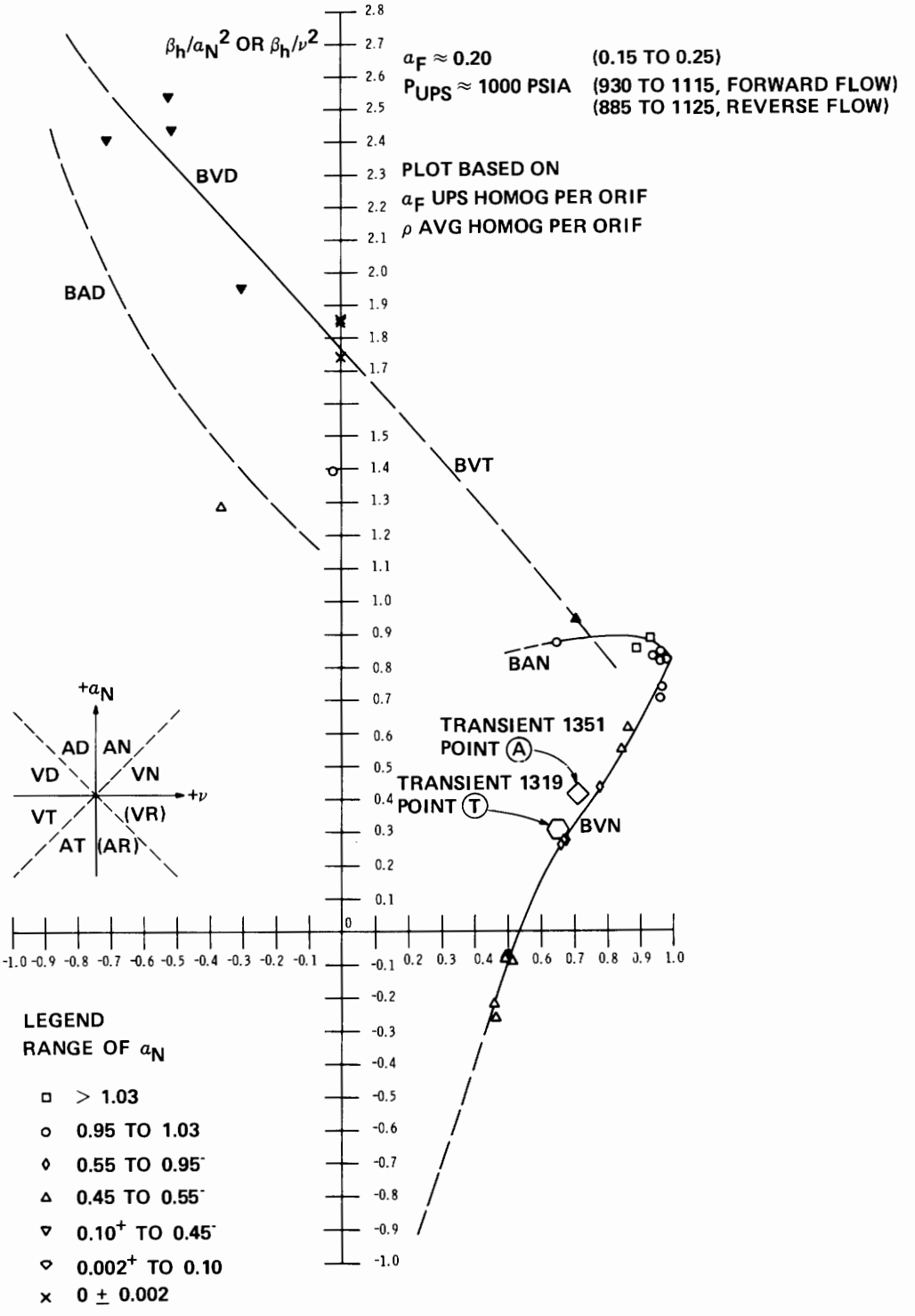

Figure 2-49. Comparison of Transient and Steady-State Performance Data, Homologous Torque for Two-Phase, α_F = 0.20

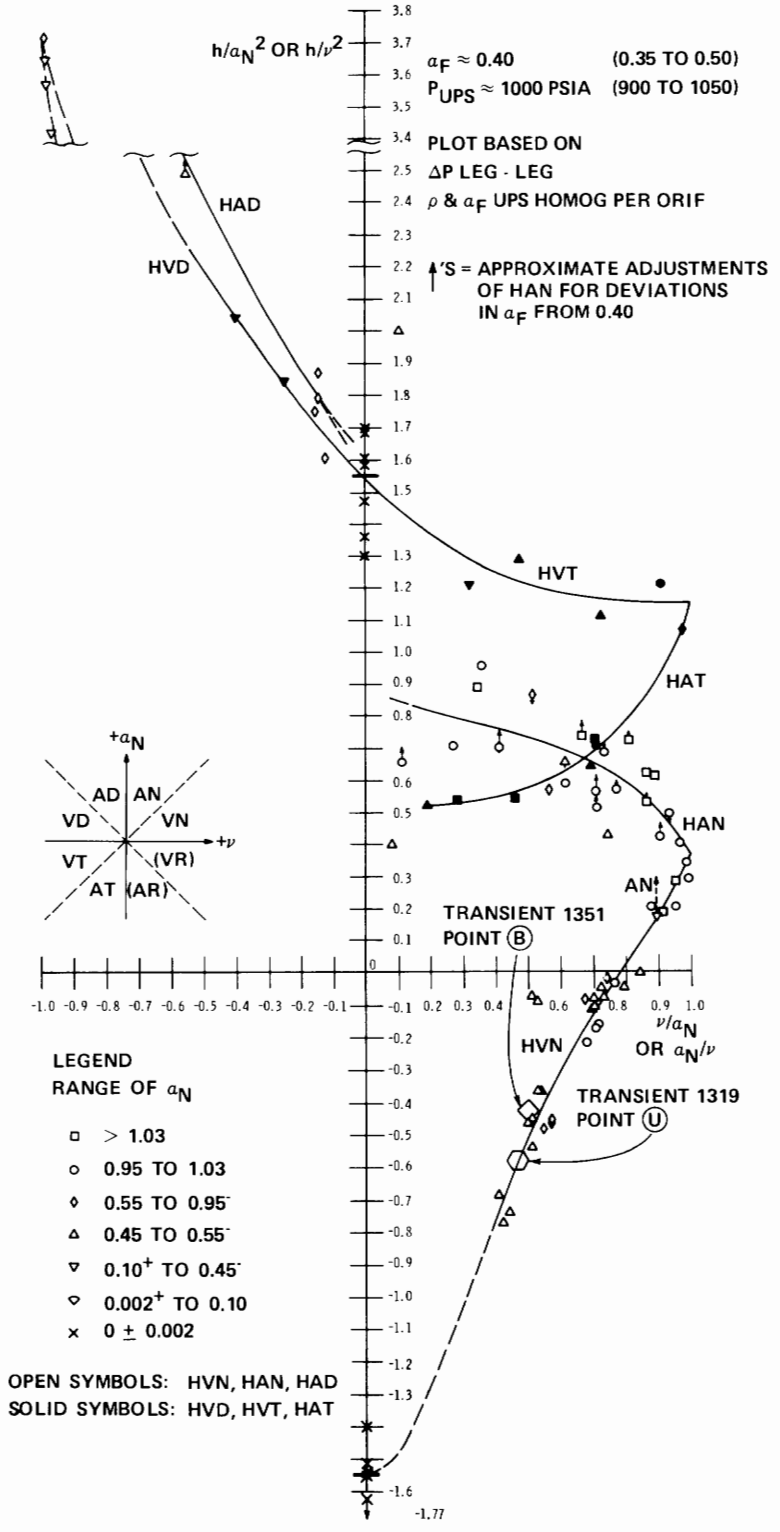

Figure 2-50. Comparison of Transient and Steady-State Performance Data, Homologous Head for Two-Phase, α_F = 0.40

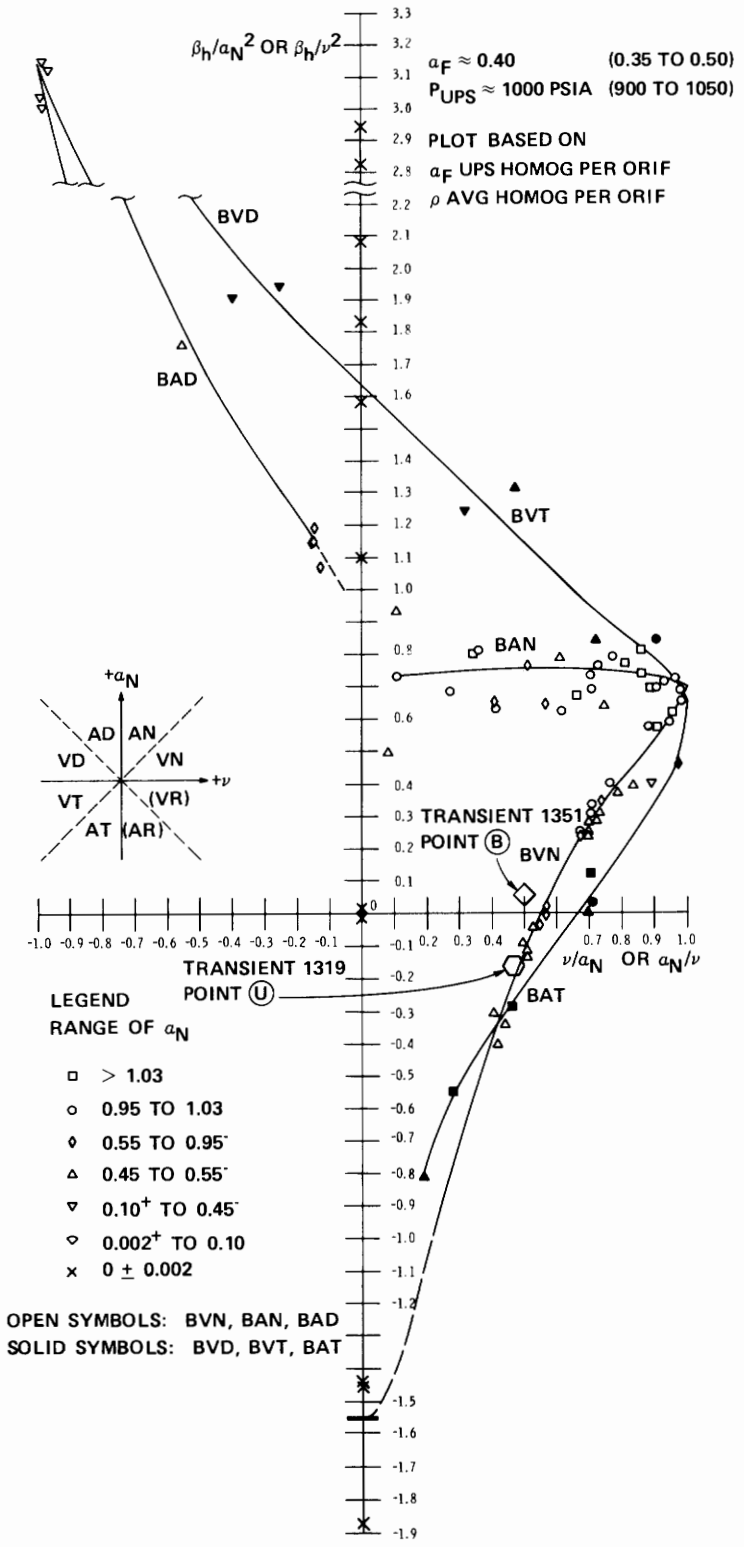

Figure 2-51. Comparison of Transient and Steady-State Performance Data, Homologous Torque for Two-Phase, α_F = 0.40

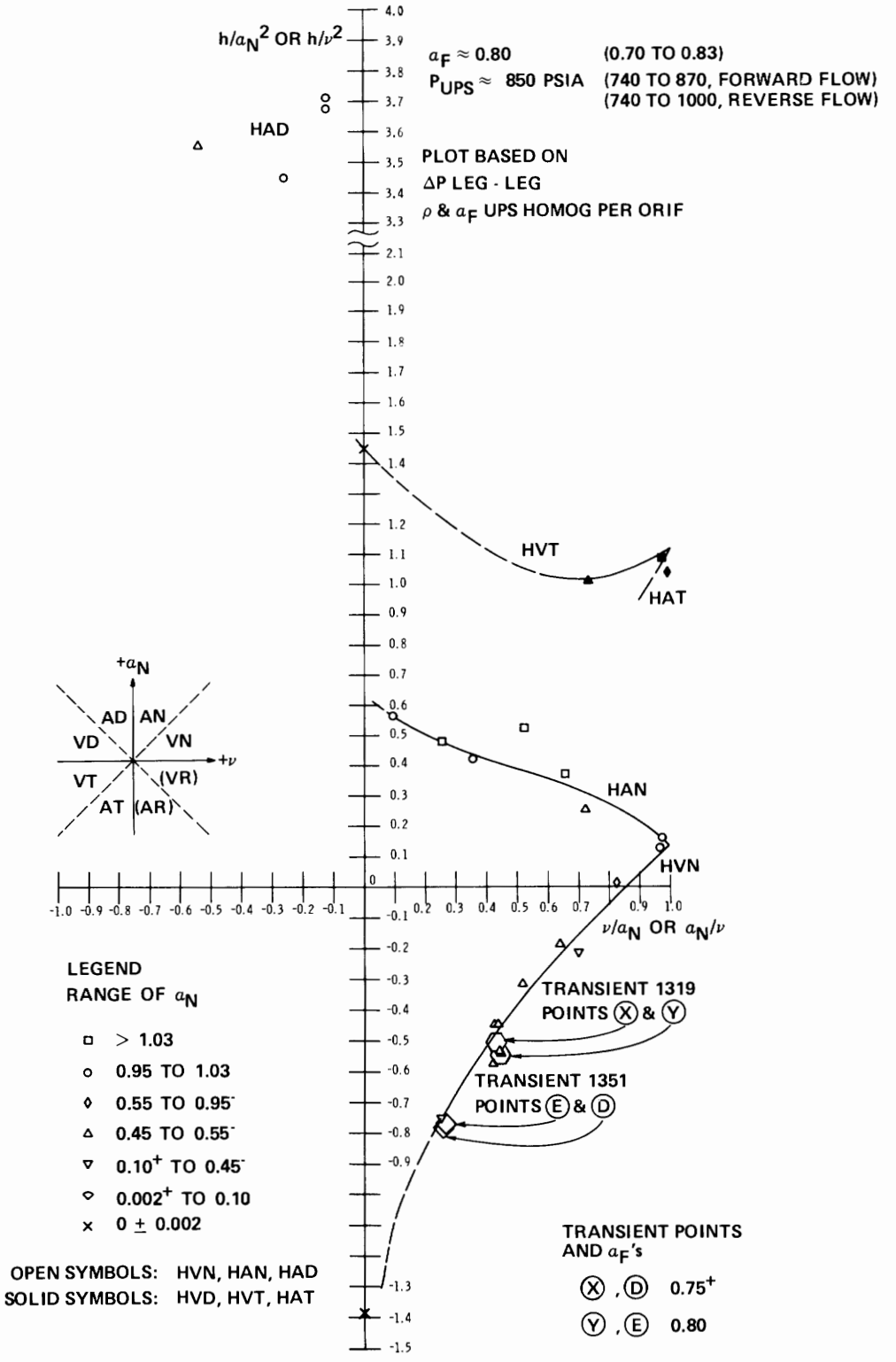

Figure 2-52. Comparison of Transient and Steady-State Performance Data, Homologous Head for Two-Phase, α_F = 0.80

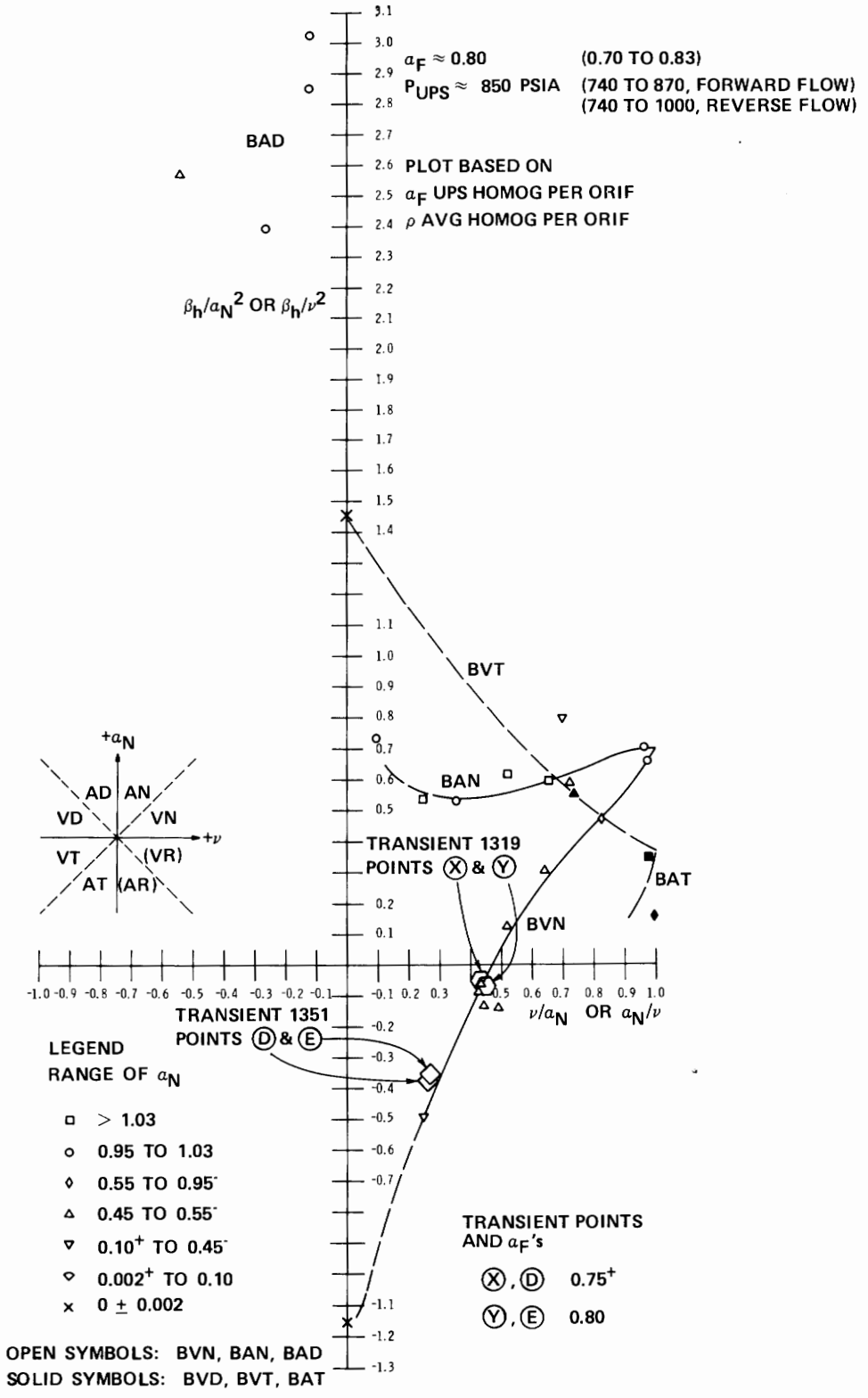

Figure 2-53. Comparison of Transient and Steady-State Performance Data, Homologous Torque for Two-Phase, α_F = 0.80

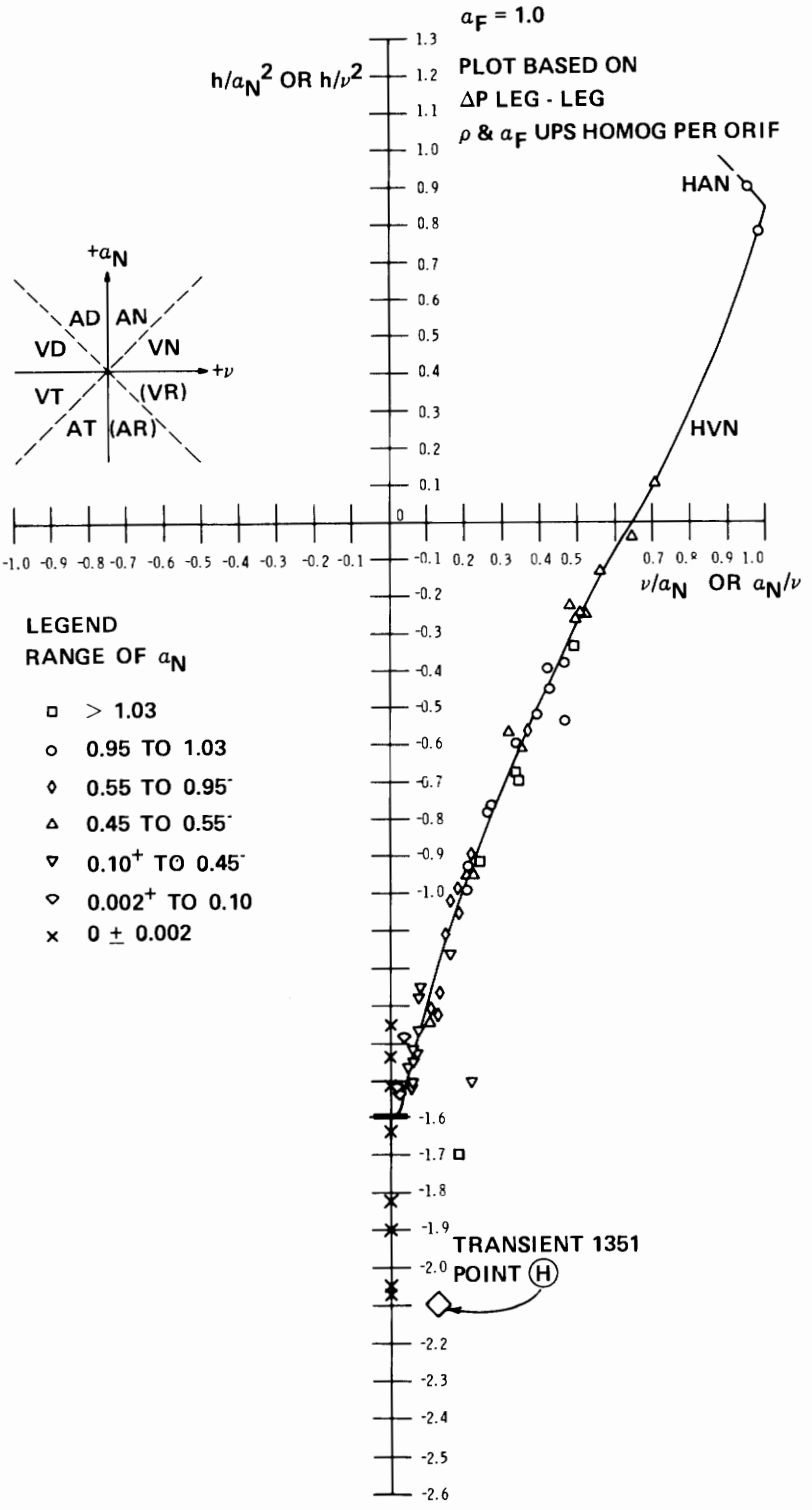

Figure 2-54. Comparison of Transient and Steady-State Performance Data, Homologous Head for Single-Phase Steam

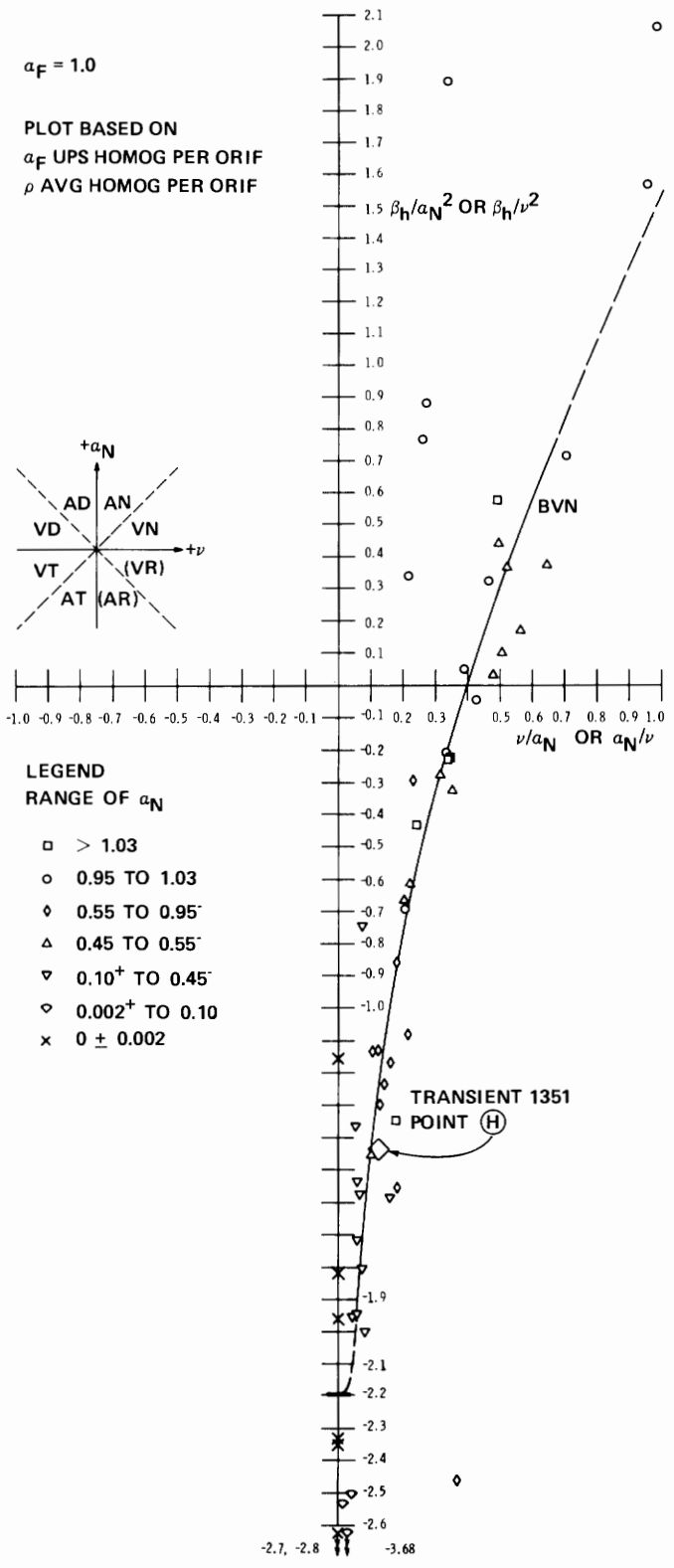

Figure 2-55. Comparison of Transient and Steady-State Performance Data, Homologous Torque for Single-Phase Steam

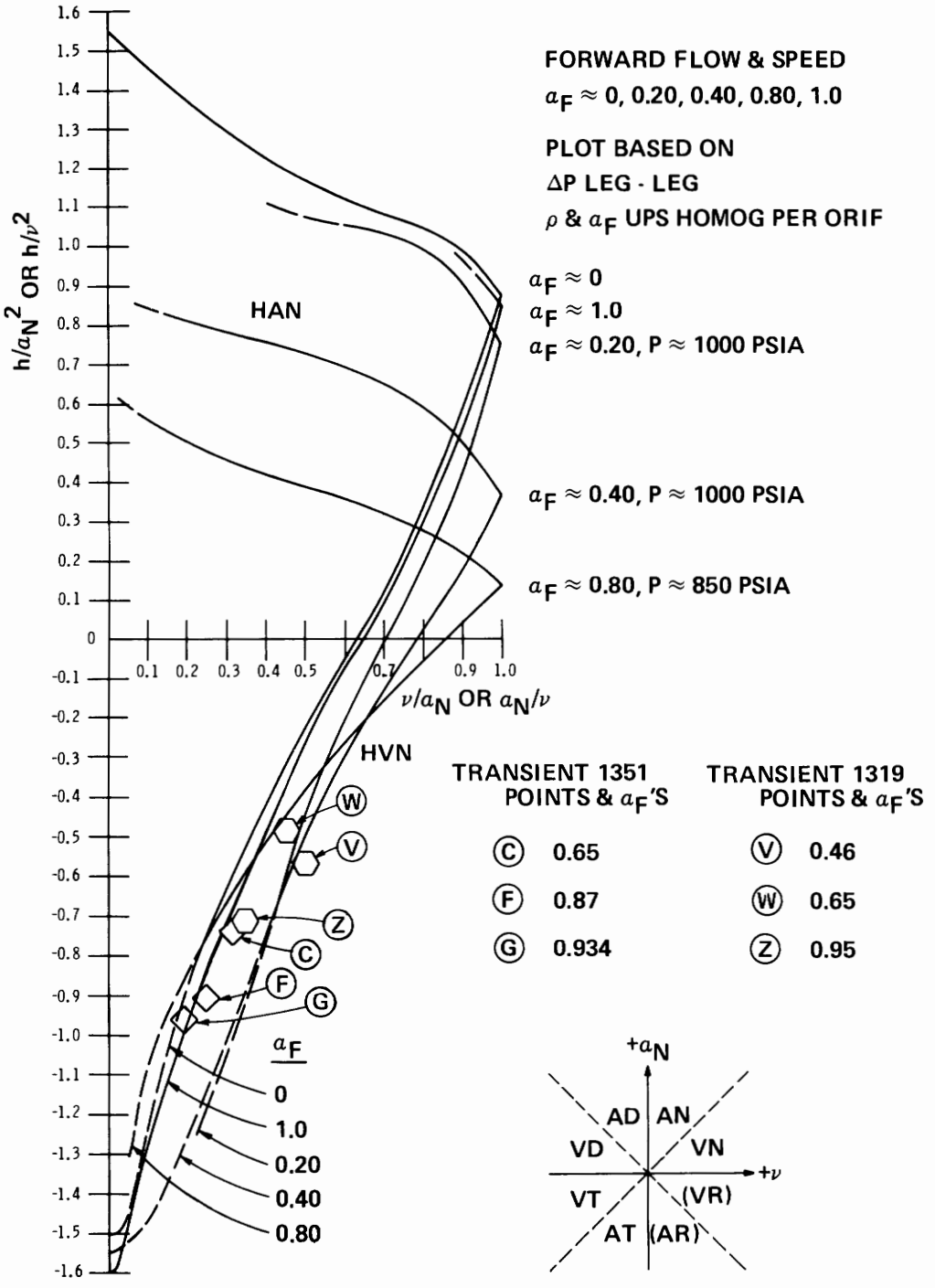

Figure 2-56. Comparison of Transient and Steady-State Performance Data, Homologous Head for Two-Phase, Intermediate α_F's

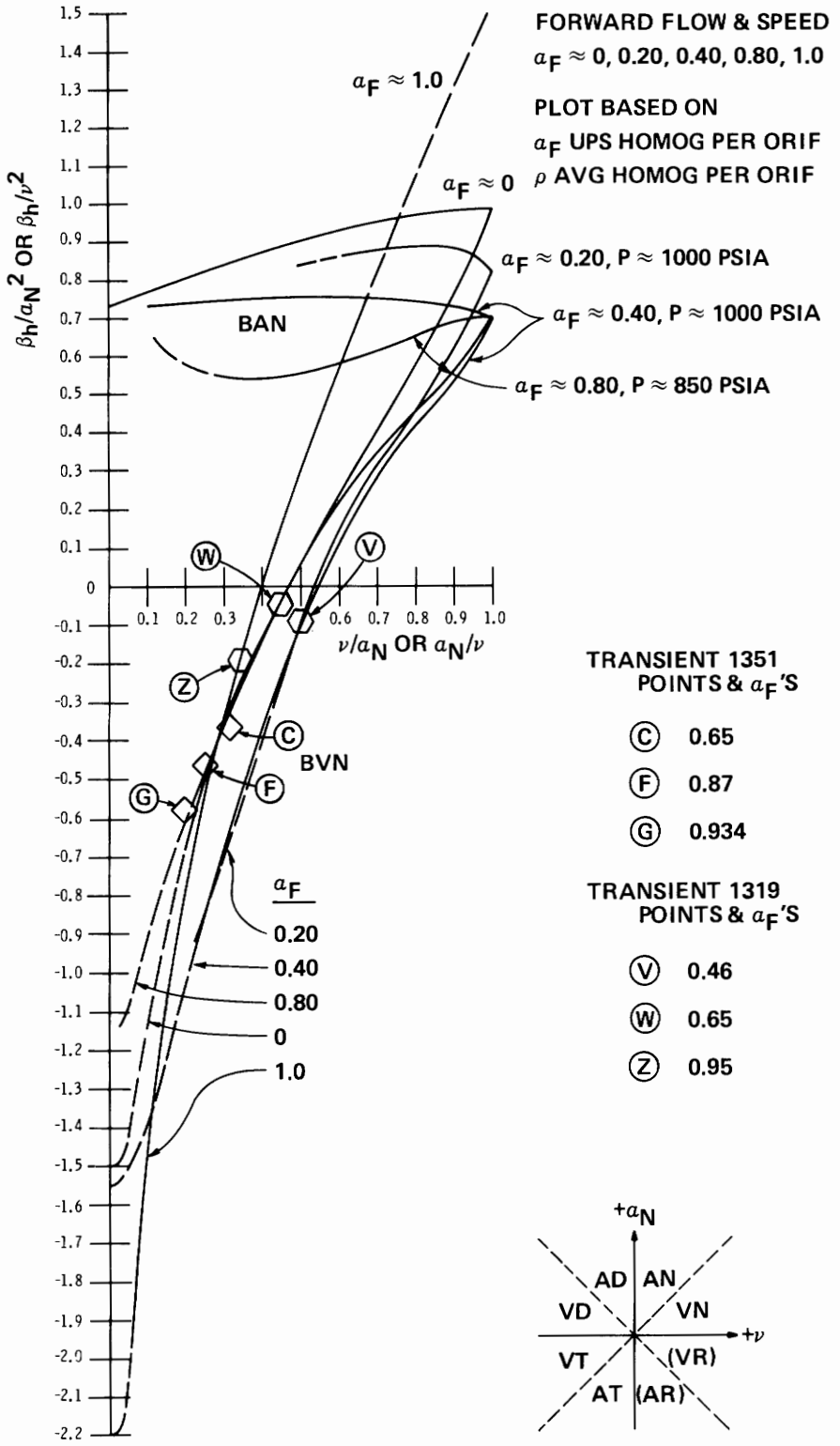

Figure 2-57. Comparison of Transient and Steady-State Performance Data, Homologous Torque for Two-Phase, Intermediate α_F's

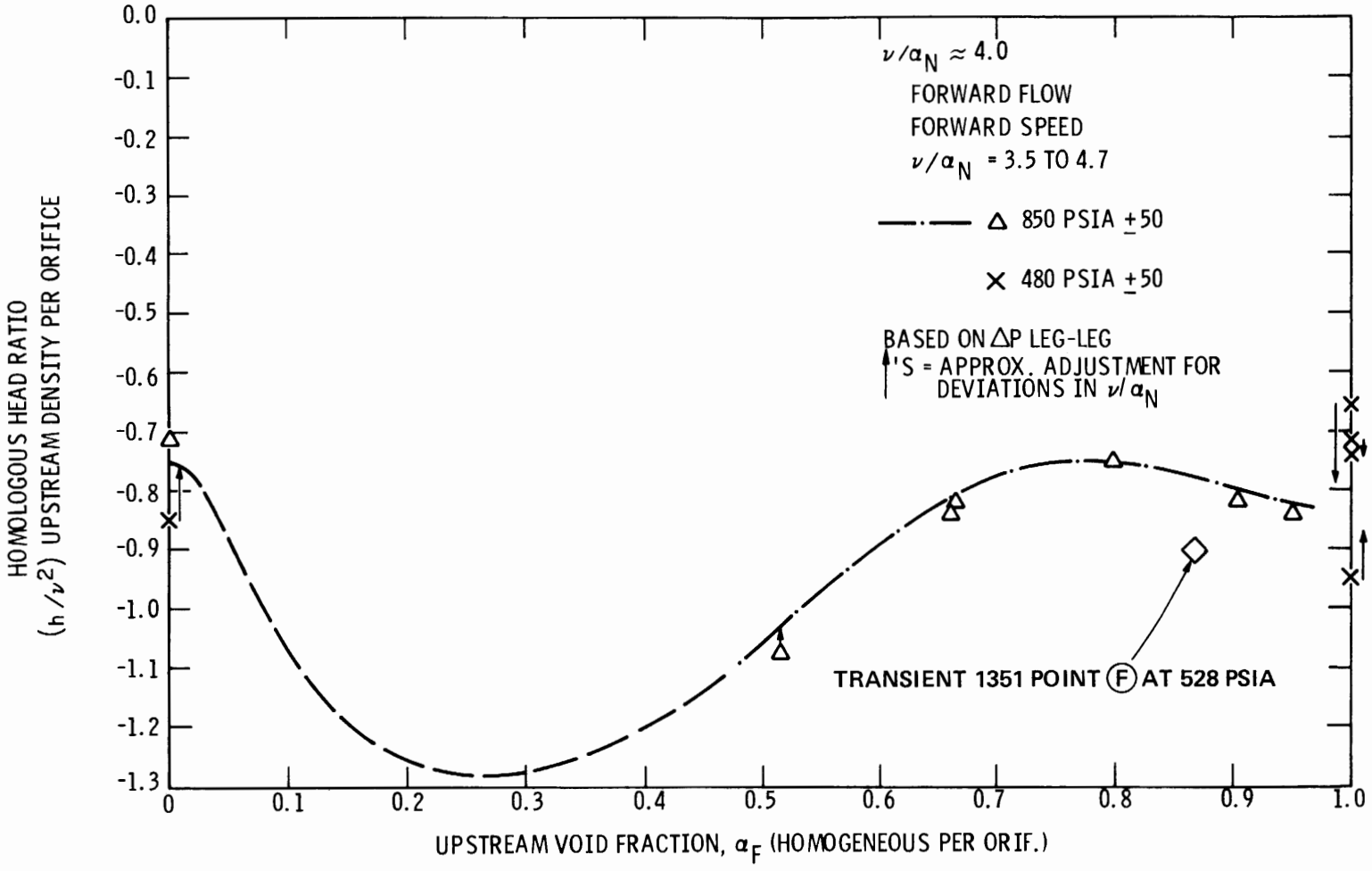

Figure 2-58. Comparison of Transient and Steady-State Performance Data, Effect of Void Fraction on Homologous Head Ratio, $\nu/\alpha_N \approx 4.0$

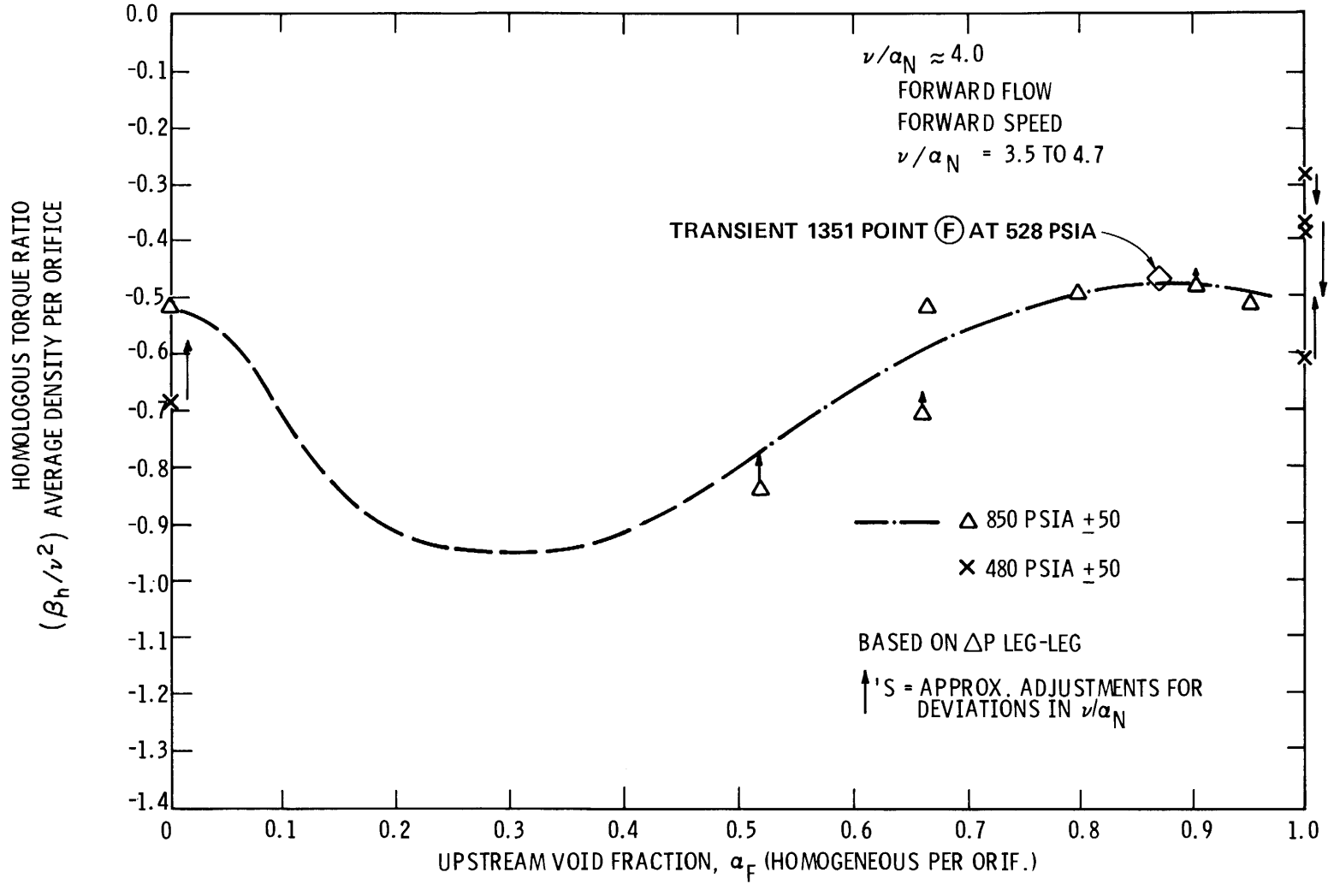

Figure 2-59. Comparison of Transient and Steady-State Performance Data, Effect of Void Fraction on Homologous Torque Ratio, $\nu/\alpha_N \approx 4.0$

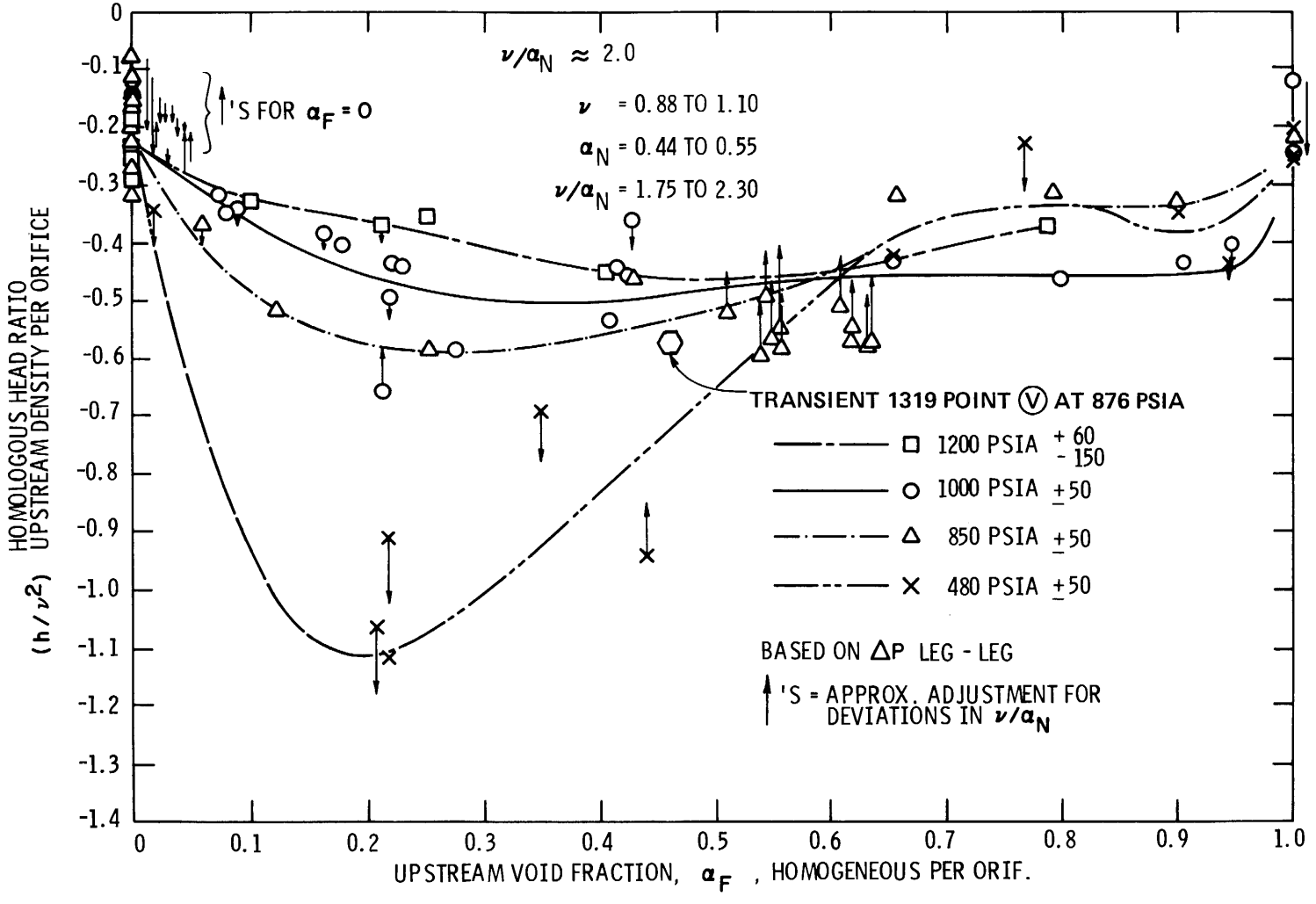

Figure 2-60. Comparison of Transient and Steady-State Performance Data, Effect of Void Fraction on Homologous Head Ratio, $\nu/\alpha_N \approx 2.0$

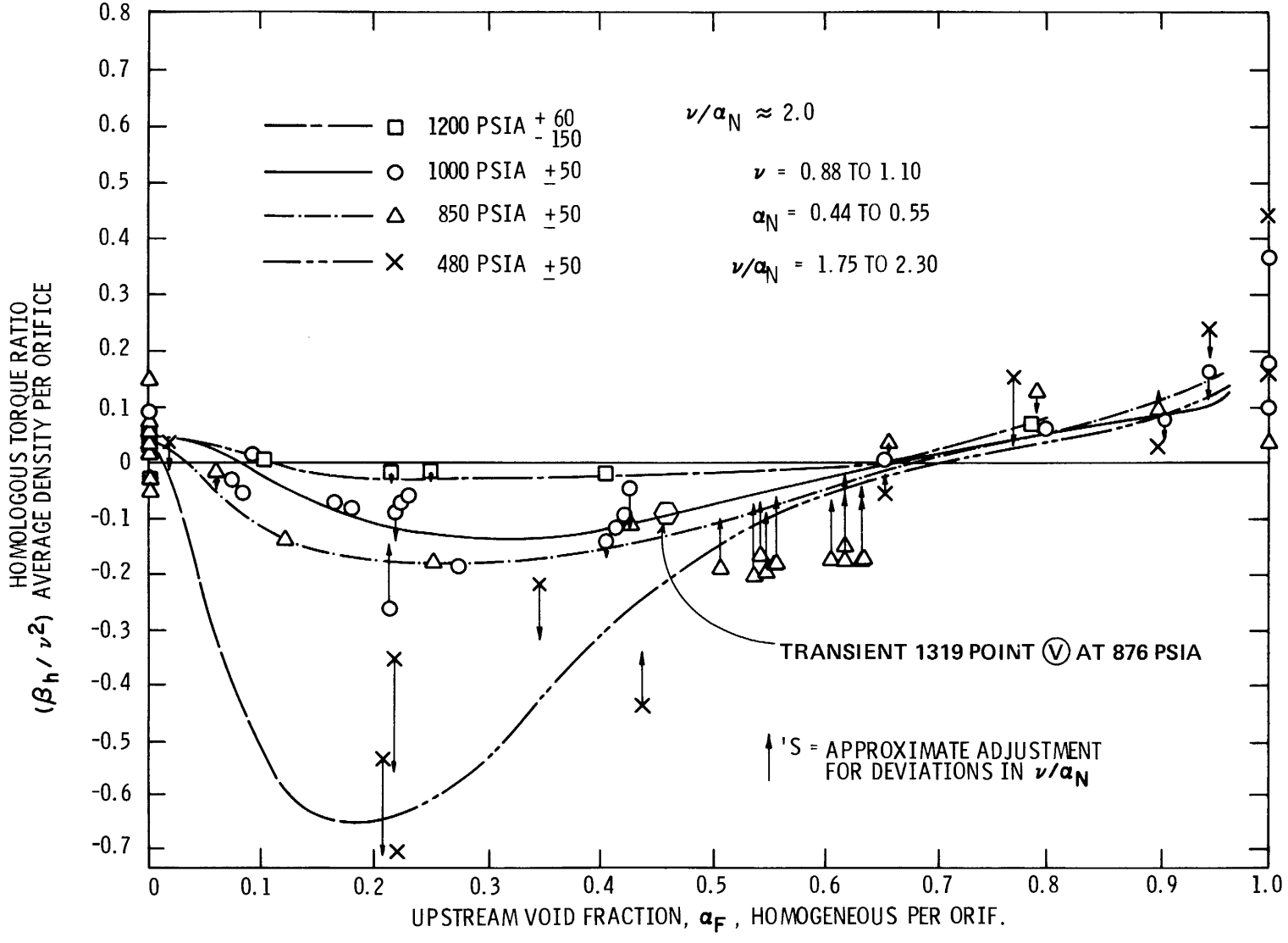

Figure 2-61. Comparison of Transient and Steady-State Performance Data, Effect of Void Fraction on Homologous Torque Ratio, $\nu/\alpha_N \simeq 2.0$

Section 3

SPECIAL TOPICS

Consideration was given as to whether similarity scaling or flow regime effects complicate the comparison of transient data for Tests 1319 and 1351 with steady-state performance data. For the reasons described here, no significant complications are expected from such effects.

Although both Tests 1319 and 1351 employed full-sized breaks and achieved flows beyond the capacity of the steady-state tests, the pertinent steady-state tests minimized these differences by including maximum flow settings (see Steady-State Matrix in Volume II Table 3-1). Thus the transient flows were essentially matched by the steady-state flows up to a void fraction of 0.40, and at higher void fractions the ratio of transient to steady-state flow was held to 2.5 or less. The steady-state speeds were ratioed lower by the same amounts to maintain the ν/α_N ratio appropriate for a given blowdown void fraction. As discussed in Volume II, Section 5.4, good similarity scaling over a range of 2 or 2.5 to 1 is demonstrated extensively in the steady-state performance curves by the common juxtaposition of plot symbols indicating speeds differing from each other by factors of 2 or more (see Figures 2-48 to 2-55). The higher range flow rates also have been observed to favor good similarity scaling (Volume II, Section 5.4).

Regarding flow regimes the flow velocities both in the transient Tests 1319 and 1351 and in the pertinent steady-state tests were generally high enough to promote good mixing of the phases in suction and discharge instrument spools (SIS and DIS), where fluid conditions were measured. This is borne out by the near coincidence of the void fraction and density curves for the gamma densitometer beams in the suction and discharge legs for these transient tests. (See Volume III, Sections 5.2 and 5.5.) Also, the SIS and DIS gamma densitometer readings in steady-state tests did not indicate any strong segregation of the phases. In the steady-state tests the SIS superficial water and steam velocities

Section 4

ASSESSMENT OF COMPARISON RESULTS

4.1 OVERALL AGREEMENT

Inspection of the comparisons of the transient data for Tests 1319 and 1351 with steady-state pump performance in Figures 2-48 to 2-61 above shows that the overall agreement is quite good. The numerical differences are nearly all small fractions of normal rated values and are comparable to the scatter in the steady-state points.

4.2 DISCUSSION OF LOCAL DIFFERENCES

More variation from the steady-state curves appears for point H at 73.6 seconds, when the void fraction was very close to 1, i.e. nearly all steam. The homologous torque appears close to the steady-state curve in Figure 2-55, but the head is quite low in Figure 2-54. Both the homologous torque and head are inversely proportional to fluid density, and there is considerable uncertainty in the gamma densitometer measurement of density close to the all steam condition. A difference of 1 percent by volume of water in the fluid (α_F from 1 to 0.99) affects the attenuation of the gamma densitometer beam very little because when the fluid density is low, most of the attenuation is in the thick steel pipe walls. There is ordinarily this much uncertainty in the gamma densitometer measurement (Volume VIII). The corresponding fluid density change would be an increase by a large ratio. For point H, at a pressure of 190 psia, the density for saturated steam is 0.42 lbm/ft^3 and for 1 percent water it is 0.97 lbm/ft^3, an increase by a factor of 2.3. This would bring the head point up to -0.91 and torque to -0.63.

The gamma densitometer calibration procedures used in conjunction with Phase II transient tests minimized the uncertainty at the steam end of the range by factoring in a steam-density reading at the end of each blowdown (see Volume VIII). However, it is possible that the pipe and fluid were not completely

dry, and the actual condition could have been a water fraction of the order of 1 percent. Thus, the fluid density would be underestimated by a factor of the order of 2. Evidence of such an underestimate seems to be present in the GD/DD volumetric flow rates shown in Figures 2-24 and 2-25, and averaged in Figure 2-5. When these are compared to the turbine meter volumetric flow rates, as in Figure 2-23, the GD/DD flowrates seem to be climbing excessively as the GD void fraction rises to 1. These GD/DD flow rates would be too high if the GD density were too low, because they were derived from

$$\nu_{GD/DD} \sim V_{GD/DD} = \sqrt{\frac{(\rho V^2)_{DD}}{\rho_{GD2}}} \tag{4-1}$$

On the other hand, the turbine meter flows were derived from

$$\nu_{TM} \sim V_{TM} \tag{4-2}$$

directly, without involving fluid density. If the excess of $\nu_{GD/DD\ AVG}$ over $\nu_{TM\ AVG}$ for point H at 73.6 seconds in Figure 2-23 is all ascribed to ρ_{GD} being too low, an adjusted density corresponding to the turbine meter velocity can be calculated by setting

$$(V_{GD/DD})_{adjusted} = \sqrt{\frac{(\rho V^2)_{DD}}{(\rho_{GD})_{adjusted}}} = V_{TM} \tag{4-3}$$

from which

$$(\rho_{GD})\ adjusted = \frac{(\rho V^2)_{DD}}{V_{TM}^2} \tag{4-4}$$

Then combining with equations 4-1 and 4-2,

$$\frac{(\rho_{GD})_{adjusted}}{\rho_{GD}} = \frac{(\rho V^2)_{DD}/V_{TM}^2}{(\rho V^2)_{DD}/V_{GD/DD}^2} = \left[\frac{\nu_{GD/DD}}{\nu_{TM}}\right]^2 \tag{4-5}$$

Using values from Figure 2-23 at 73.6 seconds, for point H

$$\frac{(\rho_{GD})_{adjusted}}{\rho_{GD}} \simeq \left(\frac{8.0}{6.16}\right)^2 \simeq 1.7 \qquad (4\text{-}6)$$

This density adjustment would bring the point H homologous head ratio in Figure 2-54 to -1.23 and the torque value in Figure 2-55 to -0.85, more in line with steady-state head data and still close to steady-state torque data.

This discussion of density effects near $\alpha_F = 1$ is not purported to define specific adjustments to be made to point H, but serves to indicate the nature of the uncertainties, the expected direction and general magnitude of deviations, and the range of resulting shifts in the plotted performance. It is shown that the difference between the plotted transient and steady state performance for point H falls within the likely range of these effects.

Similar remarks are applicable to the transient vs. steady-state comparison of point Z at 48.2 seconds, when the void fraction reached a value of 0.95 for Test 1319. For this point also, the homologous torque falls very close to the steady-state curve of Figure 2-57, but the head is somewhat lower than the steady-state value as shown in Figure 2-56. Again, the uncertainty in the gamma densitometer measurements at higher void fractions may explain the lack of excellent agreement between the transient and the steady-state homologous head in Figure 2-56. Adjustment to the gamma densitometer-measured density as indicated by Equation (4-5) above would be expected to reduce the difference between the transient and steady-state performance for point Z.

4.3 ASSESSMENT OF AGREEMENT

As described above, the overall agreement between the transient performances in full-size 6-inch pipe diameter blowdown tests 1319 and 1351 and steady-state curves is quite good, and encompassed periods of rapid changes of operating conditions, including the two-phase index $d\alpha_F/dt$. Performance variations as α_F approaches 1 are considerably larger but within likely uncertainties in flow and density measurements near all-steam conditions. Some reduction in deviations of the near-steam transient values may be possible with further analysis. Otherwise, the differences between the plotted transient and steady-state

performance are comparable to the scatter in the steady-state points. This steady-state data coherence is regarded as good, and this amount of variation is considered acceptable for LOCA analysis. On the basis of the comparisons made, the steady state performance plots appear appropriate as a source of information on pump two-phase performance for modeling pump behavior in transient analysis, provided allowance is made for more uncertainties near $\alpha_F = 1$.

Section 5

REFERENCES

1. J.M. Mandhave, G.A. Gregory, and K. Aziz. "A Flow Pattern for Gas-Liquid Flow in Horizontal Pipes." International Journal of Multi-Phase Flow, Vol. I, No. 4, October 30, 1974.